ARPA ORDER NO. 189-1

R-760-ARPA

May 1971

EFFECTS OF STRONG EXPLOSIONS

Simon Kassel

A Report prepared for

ADVANCED RESEARCH PROJECTS AGENCY

Rand
SANTA MONICA, CA 90406

This research is supported by the Advanced Research Projects Agency under Contract No. DAHC15 67 C 0141. Views or conclusions contained in this study should not be interpreted as representing the official opinion or policy of Rand or of ARPA.

DOCUMENT CONTROL DATA

1. ORIGINATING ACTIVITY The Rand Corporation	2a. REPORT SECURITY CLASSIFICATION UNCLASSIFIED 2b. GROUP ---

3. REPORT TITLE

EFFECTS OF STRONG EXPLOSIONS

4. AUTHOR(S) (Last name, first name, initial)

Simon Kassel

5. REPORT DATE	6a. TOTAL NO. OF PAGES	6b. NO. OF REFS.
May 1971	116	3

7. CONTRACT OR GRANT NO.	8. ORIGINATOR'S REPORT NO.
DAHC-15-67-C-0141	R-760-ARPA

9a. AVAILABILITY/LIMITATION NOTICES	9b. SPONSORING AGENCY
DDC-1	Advanced Research Projects Agency

10. ABSTRACT

The report contains English-language abstracts and reviews of 1969 and 1970 articles from the open Soviet technical literature relevant to explosions, soil mechanics, laser and particle beams, thermodynamics, and reentry problems. The abstracts, prepared by Stuart Hibben and Andrey Polushkin of Informatics-Tisco, Inc., vary in length according to the importance assigned to the original paper. They are grouped under the following general headings: nuclear explosions; shock waves and explosions in gases; shock waves in solids; interaction of shock waves with solids; plasma dynamics; plasma-induced surface effects; laser simulation and related effects; deformation of materials; high-pressure research; soil mechanics; particle beams; and miscellaneous, including equations of state, sound and laser wave propagation underwater, and laser beam attenuation by fog. Longer articles by Polushkin review the literature of hypersonic gas flow around a blunt body and electrical explosions in a vacuum. This is part of a continuing project that monitors the Soviet literature.

11. KEY WORDS

Physics
Lasers
USSR--Science
Gas Dynamics
Bibliography
Nuclear Explosions
Thermodynamics

ARPA ORDER NO. 189-1

R-760-ARPA

May 1971

EFFECTS OF STRONG EXPLOSIONS

Simon Kassel

A Report prepared for

ADVANCED RESEARCH PROJECTS AGENCY

Rand
SANTA MONICA, CA. 90406

Rand maintains a number of special subject bibliographies containing abstracts of Rand publications in fields of wide current interest. The following bibliographies are available upon request:

Africa • Arms Control • Civil Defense • Combinatorics
Communication Satellites • Communication Systems • Communist China
Computing Technology • Decisionmaking • Delphi • East-West Trade
Education • Foreign Aid • Foreign Policy Issues • Game Theory
Health-related Research • Latin America • Linguistics • Maintenance
Mathematical Modeling of Physiological Processes • Middle East
Policy Sciences • Pollution • Program Budgeting
SIMSCRIPT and Its Applications • Southeast Asia • Systems Analysis
Television • Transportation • Urban Problems • USSR/East Europe
Water Resources • Weapon Systems Acquisition
Weather Forecasting and Control

To obtain copies of these bibliographies, and to receive information on how to obtain copies of individual publications, write to: Communications Department, Rand, 1700 Main Street, Santa Monica, California 90406.

Published by The Rand Corporation

PREFACE

The present report is prepared as part of a continuing study of selected areas of Soviet science and technology within the Advanced Research Projects Agency sponsored Rand Project--Soviet Literature Exploitation. The material in this report is based exclusively on Soviet open-source technical literature published for the most part in 1969 and early 1970.

The English-language abstracts have been prepared by Stuart Hibben and Andrey Polushkin of Informatics-Tisco, Inc. The studies are due to Andrey Polushkin.

BLANK PAGE

CONTENTS

I. INTRODUCTION

The effects of interactions of explosions with the ground, the atmosphere, and materials have broad research ramifications and significance, especially in the case of nuclear explosions. The pertinent topics include simulation studies, effects of high pressures and temperatures on materials, reentry problems, radiation effects, electromagnetic phenomena, etc. It is hoped that in the course of this study most of these topics will be explored in this and future reports based on the current Soviet scientific and technical literature.

This report is one of a series intended to provide a preliminary approach to Soviet research activities in the form of a wide-range review of their current pertinent research papers. The preliminary approach will subsequently be followed by analytic studies of specialized topics selected from the reviewed material.

The material is divided into two parts. Part A presents a series of abstracts of the original Soviet research papers arranged according to fairly general subject areas. The abstracts vary in length depending on the degree of pertinence and significance of the individual papers. Their purpose is primarily to call attention to the work being done in the USSR on the given subject. Part B combines studies on more specialized topics, each based on a number of closely related papers and intended as a preliminary outline of the development of a specific research effort. This part thus can be regarded as a nucleus of possible analytic studies in depth mentioned above. Neither part purports to have exhausted the source material in the subject areas treated in this report. The completeness of coverage ultimately depends on the steady application of this review effort through subsequent reports of this series and the development of analytic studies.

II. ABSTRACTS

NUCLEAR EXPLOSIONS

Yerokhin, Yu. G.; and O. P. Larionenko. Effects of the U. S. Starfish explosion on the ionosphere as observed in Central Kazakhstan. Kosmicheskiye issledovaniya, v. 7, no. 4, 1969, 580-583.

Ionospheric sounding data obtained during 4 July-13 July, 1962 by the automatic ionospheric station in Central Kazakhstan are analyzed. This period includes the time of the Starfish explosion, which occurred on July 9 at 1500 hours local time (used as time reference in the paper). Figures 1-3 show the time variation of critical frequencies (f_{OF2}, f_{OE}) minimum effective heights (h') of the E and F layers, and the minimum observable frequency, f_{min} immediately preceding the explosion.

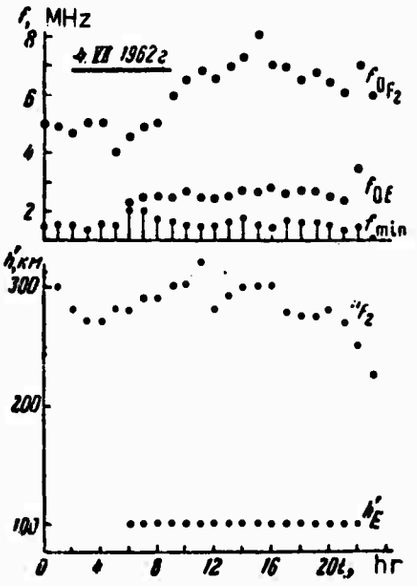

Fig. 1

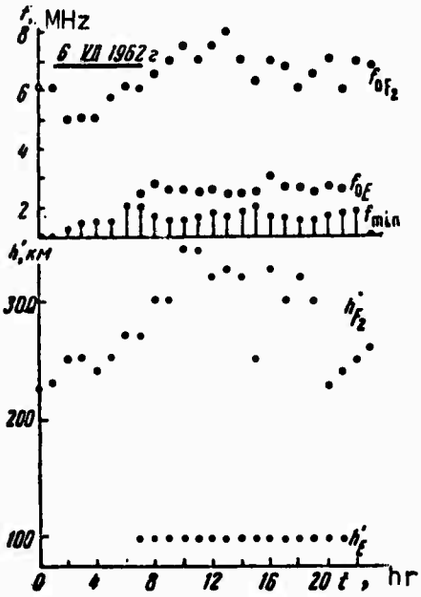

Fig. 2

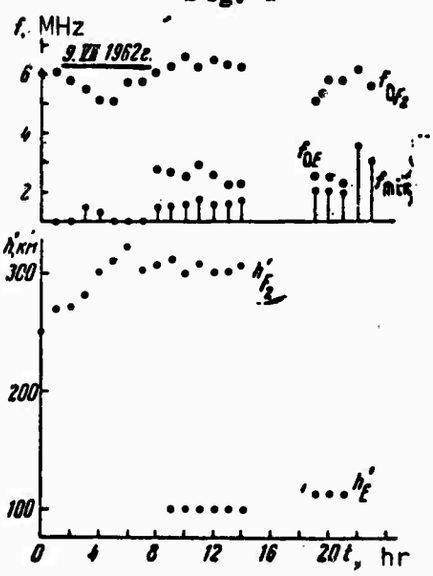

Fig. 3

Similar data acquired after the explosion are given in Figures 4 through 7.

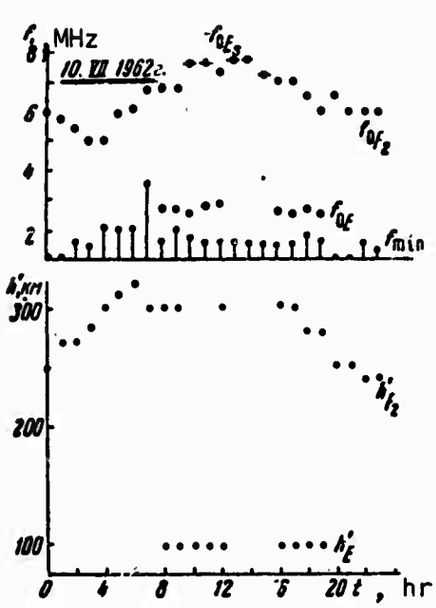

Fig. 4

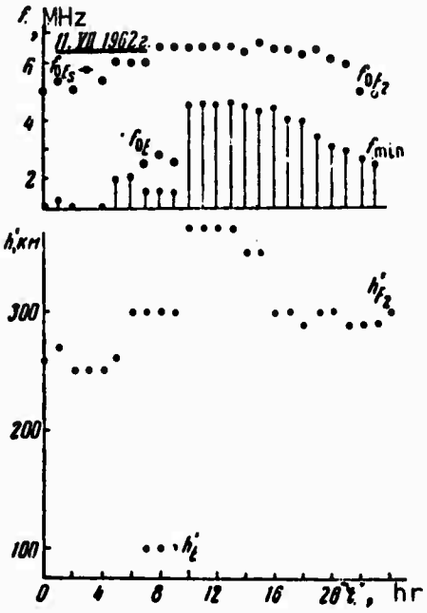

Fig. 5

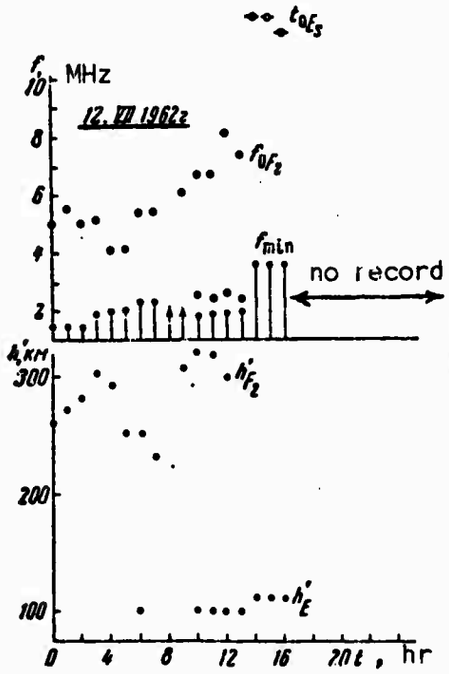

Fig. 6

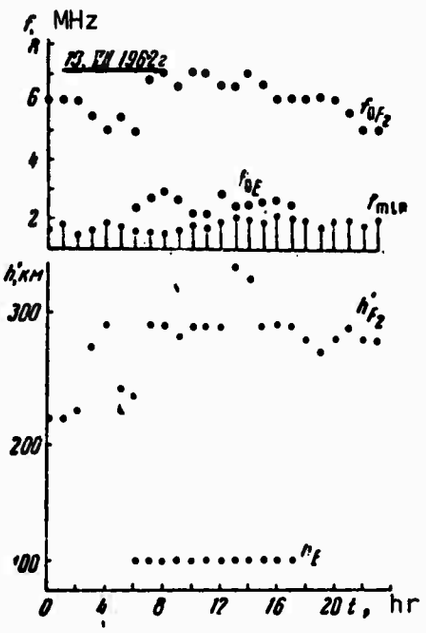

Fig. 7

The paper also presents 14 photographic reproductions of the recorded ionograms. The authors' interpretation of the events taking place is as follows:

1530 hours — Ordinary and extraordinary components of the F_2 layer diverged noticeably, and the sporadic E_s layer with a critical frequency of 6.3 MHz started to emerge. The minimum observable frequency increased to 3.9 MHz and weak reflections from the F_1 layer appeared;

1542 hours — The E_s layer broadened somewhat along the vertical and ionization began to increase from this point on;

1547 hours — Multiple reflections from the F_2 layer appeared and the E_s layer continued broadening;

1600 hours — The electron concentration in the E_s layer increased sharply (f_{oe2} over 8 MHz), shielding the upper layer sufficiently that the low-frequency part of the F_2 layer was not noticeable. Multiple reflections appeared from the E_s layer. Minimum observable frequency increased to 4.3 MHz and considerable stratification could be seen in the high-frequency part of the E_s layer;

1610 hours — Critical frequency of the E_s layer increased to 9 MHz and multiple reflections became clearer;

1620 hours — The critical frequency of the shielding sporadic E_s layer reached 9.5 MHz;

1700 hours — Toward 1700 hours the critical frequency of the E_s layer dropped to 7 MHz and E and F_2 layers were clearly seen. In subsequent ionograms the critical frequency of the E_s layer diminished rapidly;

1800 hours — A sudden complete absorption occurred and continued for about 20 minutes;

1830 hours — The E and E_s layers were determined to be at 120 km altitude; this was typical for all subsequent ionograms, in which time the electron concentration also increased steadily;

1900 hours Reflections were observed from the region at an altitude of 500-600 km in the frequency range of 4.5-5.1 MHz; their nature could not be explained;

1930 hours E, E_s, and F_2 layers were observed. Further changes of ionospheric parameters during July 9 are given in Fig. 3. They indicate that the ionosphere was returning to a normal state.

Strong absorption occurred at 0700 hours on July 10, 1962 (Fig. 4) and the sporadic E_s layer twice shielded the higher layers (at 0911 hours and from 1300 hours to 1500 hours). On July 11 (Fig. 5), sporadic shielding by the E_s layer was observed from 0200 hours to 0400 hours. From 1000 hours to 2400 hours the high frequency characteristics of the E layer could not be observed and the minimum detectible frequency reached the value of 4.5MHz, beginning to decrease only at 1800 hours to reach its normal value (1.5 MHz)at 2400 hours. The increase in the minimum detectible frequency was accompanied by an increase of the minimum effective height of the F_2 layer from 300 to 370 km. On July 12 (Fig. 6) the shielding sporadic E_s layer appeared between 0700 hours and 0900 hours and again between 1416 hours and 1600 hours at 100 km altitude. Finally, on July 13, the fourth day after explosion, (Fig. 7), no deviations from the normal quiet state of the ionosphere were observed.

Shafer, Yu. G.; Yu. N. Gal'perin; A. G. Kulagin; and A. D. Bolyunova. Radioactivity of Kosmos-6 satellite and assumed collection sites of radioactive debris at a height of 300-350 km. Geomagnetizm i aeronomiya, v. 9, no. 4, 1969, 608-612.

The Kosmos-6 satellite which was launched on June 30, 1962, contained an ionization chamber programmed by a gas-discharge counter, and a circular counter assembly. Radiation data obtained with STS-5 isolated counters (shielded by $\sim 16 g/cm^2$ W and by $\sim 2.56 g/cm^2$ Al) are analyzed in this paper. At the time of the explosion over Johnston Island, Kosmos-6 was in a near circular, northeasterly orbit (apogee of 345km, perigee of 274 km), in its 140th revolution. At the explosion, Kosmos 6 began transmission over the USSR. Within 10 minutes of the first transmission period, radiation flux had increased by a factor of 3. For a period of $\sim 10^6$ sec after the explosion the radiation level varied significantly from revolution to revolution.

The Kosmos-6 orbital trajectories during which it collected radioactive debris are shown by solid lines in Fig. 1. Dashed lines indicate the revolutions during which no debris was collected. The Brazil and Capetown anomalies are shown by dot-dash lines; the explosion site is indicated by a star and its conjugate point by a dot.

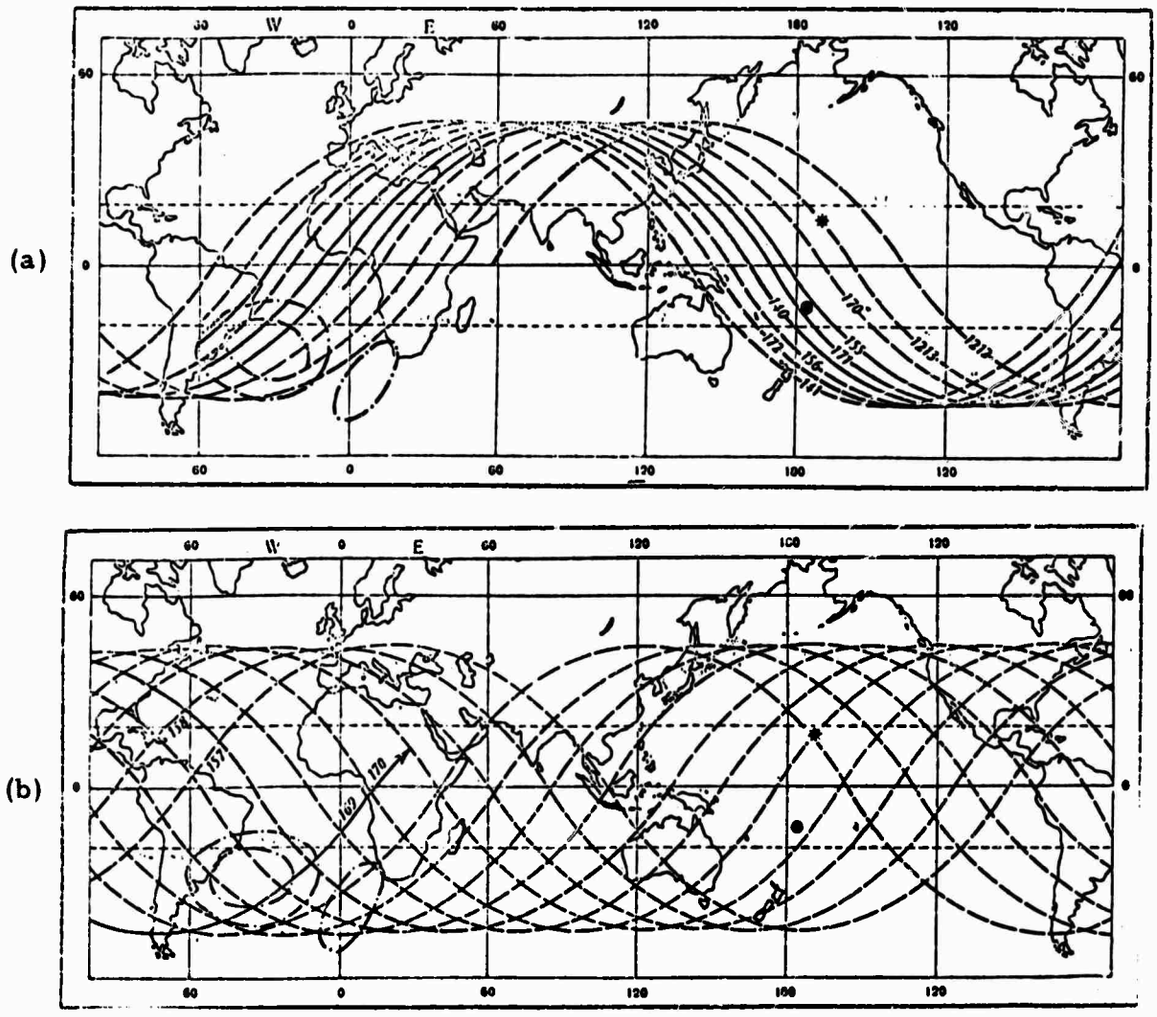

Fig. 1. Trajectory of Kosmos-3 (a) and Kosmos-6 (b).

The fact that no radioactive debris was collected by Kosmos-6 in the explosion area was confirmed by data from Kosmos-3, which also reported no radioactive debris on its 1212th and 1213th revolutions (Fig. 1a). The approximate distribution and duration of radioactive regions as determined from accumulated data was used to postulate the following model for the explosion effects: at the time of explosion about half of the radioactive debris was propelled along a force tube to its magnetic conjugate point. The remainder was scattered in all directions, with ascending debris being captured and confined by the Earth's magnetic field.

Cherkas, V. I. Long-term disturbances of the ionosphere from the effect of high-altitude thermonuclear explosions. Kosmicheskiye issledovaniya, v. 7, no. 3, 1969, 429-435.

The scintillation of short wave radio signals from earth satellites has been statistically analyzed in order to establish behavior in the distribution of small-scale inhomogeneities of electron density, in the undisturbed ionosphere and after its excitation by the Starfish high altitude thermonuclear burst. The analysis was made from tape recordings of the short-wave signals from ten earth satellites (Kosmos-1, 2 and 4 through 11) over the period from March to October 1962, which were received at sixteen ground stations in the USSR. These data provided the scintillation character of the signal and the time of its reception, while the transmitter coordinates were computed from orbital data catalogs. The degree of ionospheric disturbance along the propagation path was measured by the reception probability of a scintillating signal

$$P_{B,T} = \sum_{i=1}^{k} \frac{n_{B,T}}{N_{B,T}}$$

where $n_{B,T}$ is the number of scintillating receptions for any given latitude B and any local time T; $N_{B,T}$ is the total number of the satellite signals received for the same B or T; and k is the total number of revolutions summed over the time interval under consideration. Observational data are presented as curves showing the probability of scintillating signal reception as functions of latitude or local time, and comparing data for the periods May 28 to July 9, 1962 and July 9 to September 9, 1962. It is found that a persistent intensive maximum of ionospheric disturbance appeared in the middle latitudes as a result of the Starfish burst. Four months after the burst it had not shown any tendency to decrease. The correlation between the terrestrial magnetic field disturbance created by the burst and particle intensity in the outer and inner radiation belts is also discussed. The observational data appear to confirm the assumption that the formation of ionospheric inhomogeneities on a planetary scale is associated with processes occurring in the Earth's radiation belts.

Kozlov, S. I. Electron density decrease in the F_2 region after the American high altitude burst of July 9, 1962. Kosmicheskiye issledovaniya, v. 7, no. 4, 1969, 584-591.

This paper disputes some assumptions and conclusions of Whitten and Dalgarno (Planet. Space Sci., v. 15, 1967, no. 9, 1419) about the cause of the electron density in the F_2 region of the ionosphere, detected experimentally after the Starfish burst. The latter assumed that the principal "heating" agents are the primary fast photoelectrons produced by air absorption of soft x-rays from the burst radiation. After the initial energy loss down to ~ 20 ev upon excitation and ionization of air components, a further energy loss occurs because of elastic collisions with atmospheric electrons, leading to a rapid increase of their temperature up to 10^4 °K and higher. These hot electrons excite molecular nitrogen N_2 sufficiently to increase the rate of the ion-molecular reaction

$$N_2 + O^+ \rightarrow NO^+ + N, \qquad (1)$$

which controls the electron density because of its substantially lower rate compared with the rate of the dissociative recombination

$$NO^+ + e \rightarrow N + O. \qquad (2)$$

Expressions are derived for electron concentrations for cases when either (1) or (2) is the dominant process, and for one critical value of electron concentration when the rates of both processes are equal. Calculations based on these equations indicate that with increasing temperature of the electron gas the contribution of Eq. (2) as a process controlling electron concentration in the F_2 region significantly increases -a fact overlooked by Whitten and Dalgarno. The possibility of substantial heating (up to 10^4 °K and higher) of the electron gas by primary photoelectrons produced by air absorption of the soft x-rays from the burst radiation is thoroughly investigated. The author concludes that, excluding a small atmospheric region immediately adjacent to the point of burst, such a heating of the electron gas at heights in the F_2 region is fundamentally impossible. However, under conditions of "cold" electron gas, the reaction rate of Eq. (1) may rise with the increase in concentrations of molecular nitrogen in a state of vibrational excitation. Therefore, other excitation mechanisms not associated with high temperature of the electron gas should be considered.

SHOCK WAVES AND EXPLOSIONS IN GASES

Losev, S. A., and V. A. Polyanskiy. On the extent of the relaxation ionization region behind a strong shock wavefront in air. IN: AN SSSR. Doklady, v. 182, no. 1, 1968. 75-76.

The authors report a theoretical study of ionization phenomena occurring behind a strong shock wave propagating in air. Attention is centered on the anomalously wide ionization region that occurs at propagation velocities near V=10m/sec. It is assumed that when V>10m/sec, limiting molecular dissociation is reached, while for lower velocities ionization is not a major factor. Calculations show that an electron density maximum will occur near the wavefront at about V=9 m/sec; with an increase to 9.5 m/sec this peak disappears while the ionization region abruptly broadens. A mechanism for this phenomenon is suggested in terms of relative associative and dissociative rates of N_2 and NO; the ion contribution of oxygen alone is considered to be negligible. Results suggest that in the velocity range in question a sharp temperature drop occurs behind the shock wave, in which case the dissociation rate decreases by several orders of magnitude. The corresponding increase in ionization is then accounted for mainly by associative molecular ionization. The findings are compared with some theoretical and experimental data from similar previous studies.

Arutyunyan, T. M., V. A. Belokon', and L. V. Karchevskiy. The effect of adiabatic exponent on reflection of shock waves. Zhurnal prikladnoy mekhaniki i tekhnicheskoy fiziki, no. 1, 1970, 62-66.

The conditions which govern the reflection of a shock wave in gas from a confining surface, or from another shock wave, are analyzed. In particular the effect of adiabatic exponent γ on other critical reflection parameters is investigated. The problem is simplified to the extent that a reflection is assumed to be instantaneous, and also that actual gas parameters such as viscosity and thermal conductivity are ignored. The general case of an obliquely incident shock wave is assumed, for which a critical angle of incidence α_* exists above which regular reflections cannot occur. Expressions are

derived for determining α_* as a function of γ and gas pressures in incident and reflected waves. Graphical solutions obtained by computer are also given for nine discrete values of γ between 1 and 3. It is further shown that for sufficiently weak shock waves the critical angle becomes practically independent of γ .

Dzhusupov, K., and K. P. Stanyukovich. Reflection of a one-dimensional rarefaction wave in a constant gravitational field. IN: AN SSSR. Doklady, v. 190, no. 3, 1970, 545-548.

Expressions are derived which define the motion of a plane rarefaction wave after its reflection from a boundary wall. Proceeding from gasdynamic equations for the general case of wave motion, the authors assume linear motion of the incident wave along the x-axis of an arbitrary rectangular coordinate system. The travel time of the wave from point of origin through a distance l to the wall is then given by

$$t = t_l = \frac{2}{(k-1)a}\left[\sqrt{c_н^2 + (k-1)al} - c_н\right]$$

where a = acceleration of gravity; C_H is initial sonic velocity at the point of origin; and $k \equiv 2n+3/2n+1$, n=0, 1, 2..... From this the equation of motion for the reflected wave is derived and a sample theoretical solution is obtained for the case of n=0. Solutions for increasing values of n involve higher order algebraic equations whose exact solutions are tedious. Substitutions of simplified approximate expressions for these cases are therefore suggested.

Popov, Ye. G., and M. A. Tsikulin. Spectral brightness of shock waves in air. Zhurnal eksperimental'noy i teoreticheskoy fiziki, v. 56, no. 2, 1969, 522-525.

Studies of emission spectra from shock waves in the 9-14 km/sec velocity range are reported. A spectrophotochronograph array was used which covered the spectrum from 220 to 800 nm; spectral resolution was 0.07 nm, and time resolution was 0.1 μsec. Spectral linesdown to 2% brightness differential from background were detectible. Shock waves were generated by shaped explosive charges. Examples of emission spectra are shown for varying wave velocities and applied filters. The relaxation layer

preceding the shock wave has a negligible effect on emission at visible and shorter wavelengths, but causes a significant absorption of emission in the infrared range. The width of the relaxation layer is estimated to be 10^{-4}—10^{-5} cm for the velocity range observed. The spectral measurements agree with calculated temperature values for a shock-heated gas, increasing from 12,000°K at 9 km/sec to 25,000°K at 14 km/sec.

Bochkarev, A. A.; Rebrov, A. K.; and Chekmarev, S. F. Supersonic spherical expansion of a gas having a stationary shock wave. Zhurnal prikladnoy mekhaniki i tekhnicheskoy fiziki, no. 5, 1969, 62-67.

An experiment is described in which a spherical gas volume was expanded into a surrounding vacuum chamber at supersonic velocities, which subsequently decreased to subsonic. The conditions in the vicinity of the resultant shock wave were observed and analyzed. The gasdynamic source was a spherical shell 1.6 meters in diameter with a uniform hole pattern drilled over its surface. Gas was supplied at a constant rate and at a static pressure of several mm Hg; the surrounding chamber was held to the order of 10^{-2} torr. Test gases included N_2, He, Ar, and He-Ar mixtures. The shock wave region was analyzed qualitatively by exciting a glow discharge in the gas with an electron beam, and photometrically recording the discharge parameters. Data given include molecular densities in the shock wave region for various test conditions.

Shurshalov, L. V. On the problem of a strong explosion at the boundary of a gas-filled half-space. Prikladnaya matematika i mekhanika, no. 2, 1969. 358-363.

The problem is examined of a point explosion at the boundary of a half space assumed to be filled with a gas having some arbitrary adiabatic exponent γ. The wave motion is analyzed on the basis of a shock wave generated by high kinetic energy propagation of explosion products; the work is specifically presented as a refinement of the treatment given by Collins and Holt (Phys. Fluids, v. 11, no. 4, 1968) on intense explosions at an ocean surface. Using the governing physical parameters and a variable system of spherical coordinates, the author derives a set of expressions defining wave motion at the assumed surface. The two general cases considered are for "regular"

reflections, in which rarefaction waves lag the shock wave, and "irregular" reflections, in which the rarefaction waves overtake the shock wavefront. In the latter case, the reflected wavefront at the boundary surface becomes indeterminate.

Kestenboym, Kh. S.; Turetskaya, F. D.; and Chudov, L. A. A point explosion in a nonhomogenous atmosphere. Zhurnal prikladnoy mekhaniki i tekhnicheskoy fiziki, no. 5, 1969, 26-28.

A model of a point explosion in a nonhomogenous atmosphere is postulated and solutions for shock wave propagation and other parameters are obtained. The atmosphere is assumed to have an exponentially decreasing density with altitude; otherwise, actual atmospheric conditions are not taken into account. Gas-dynamic expressions are derived which define wave motion from the initial through final phases of the explosion. This treatment extends earlier analyses of the problem, which dealt rigorously only with initial stages of an explosion when inhomogenity is relatively small, or else used approximations throughout. The assumed geometry and coordinate systems are defined, and calculated theoretical values of pressure and density are given as functions of several variables. Some discrepancies between this and previous analyses are discussed.

SHOCK WAVES IN SOLIDS

Nigmatulin, R. I. A model for motion and shock waves occurring in two-phase solids with phase transitions. Zhurnal prikladnoy mekhaniki i tekhnicheskoy fiziki, no. 1, 1970, 88-95.

A theoretical analysis is made of a fixed-temperature and fixed-velocity model of impact motion in a two-phase solid for the case where each phase occupies a certain portion of the total volume. The study is developed using Lagrange variables and divides the stress tensor in the mixture into two parts: a hydrostatic pressure common to both phases, and a stress deviator which is variable up to some limit, beyond which it remains constant. Relations are derived for the kinetics of phase transitions, which are functions of characteristic times in the reaction. An example is given for an assumed one-dimensional nonstationary impact between a steel projectile and a steel plate strong enough to induce the phase transitions $Fe^{\varepsilon} \rightleftarrows Fe^{\alpha}$ behind the resultant shock wave. Stress diagrams are given which are based on typical parameters for steel and an assumed relative impact velocity of 1325 m/sec. The applicability of the analysis to shock hardening is briefly discussed.

Chernyshov, A. D. Propagation of shock waves in an elastoplastic medium. Prikladnaya matematika i mekhanika, no. 1, 1969, 143-147.

In the general case of shock wave interaction with an elastoplastic medium, it is not possible to write rigorous expressions directly without knowing the effect of discontinuities on the shock wave. The author attacks the problem by assuming the discontinuity boundary to be replaced by a continuous transition layer of arbitrary thickness. The problem then reduces to determining simultaneous expressions for shock wave structure and shock wave propagation through the assumed layer. An analysis is made on this model, further assuming that flow outside the transitional boundary layer of the elasto-plastic medium satisfies the determining equations of Prandtl-Reuss, together with the plasticity criterion of Mises. The physical rationale for using a transition layer is that additional variables affecting the incident shock wave become significant here, for example, viscosity. The approach suggested is more accurate when the shock wave configuration is known; it can also be extended for study of shock wave propagation in other complex media.

Kondrat'yev, V. N., I. V. Nemchinov, and B. D. Khristoforov. Attenuation of plane explosive shock waves in solids. Zhurnal prikladnoy mekhaniki i tekhnicheskoy fiziki, no. 4, 1968, 61-65.

Theoretical and experimental data are presented for determining attenuation of explosion-induced shock waves in solids. The incident wave is assumed to be planar, generated by a charge detonated at or near the target surface. The target material is treated as ideal to the extent that viscosity, thermal conductivity and hardness are neglected; in shock loading this remains a valid assumption even when the material yield point is exceeded. Entropy increase in the detonation wavefront reflected from the target-explosive interface is also neglected. From the derived equations of motion, numerical results are calculated for types AD-1 aluminum and L-59 brass targets subjected to explosive charges from a TNT compound. Velocity data from calculated and experimental figures are compared for explosive charge thicknesses from 2 to 50 mm. Although discrepancies up to 10% between theoretical and experimental results were noted in aluminum, the hydrodynamic approximation proposed is considered precise enough for the present problem. In addition to determining the motion caused by shock loading, it can be extended to analyze the subsequent unloading phase.

Rusakov, M. M. Experimental study of the dispersion of material after being traversed by a powerful shock wave. Zhurnal prikladnoy mekhaniki i tekhnicheskoy fiziki, no. 2, 1969, 77-78.

Experimental data are reported on the dispersion of matter from the exit surface of a solid after passage of a high-velocity shock wave through it. The laser-generated shock wave was induced axially in a cylindrical paraffin plug and was recorded to have a mean velocity of 33 km/sec during five successive tests. The rms error in velocity measurement was 0.85 km/sec, and within measurement limits velocity was found to be constant during traversal of the specimen. The discharged matter following the shock wave was confined to a cylindrical tube having the same diameter as the paraffin plug, and with ambient pressures of 0.1, 85, and 100 torr. From the equation of state the author constructs curves for expansion of the discharged matter as shown in Figure 1 for isentropic indices of 3 and 1.3. It is seen that the experimental

value (point 2) lies very close to the theoretical curve for $\gamma = 3$. Calculated paraffin density at this point was about 0.3 g/cm^3. Calculations indicate that further expansion of the discharge material is accompanied by a drop in γ (points 3 and 4), contrasting with cited earlier reports in which γ is assumed to remain constant during the expansion process. The author's results are analogous to other cited studies in which particle velocities from mass impact attained 68 km/sec.

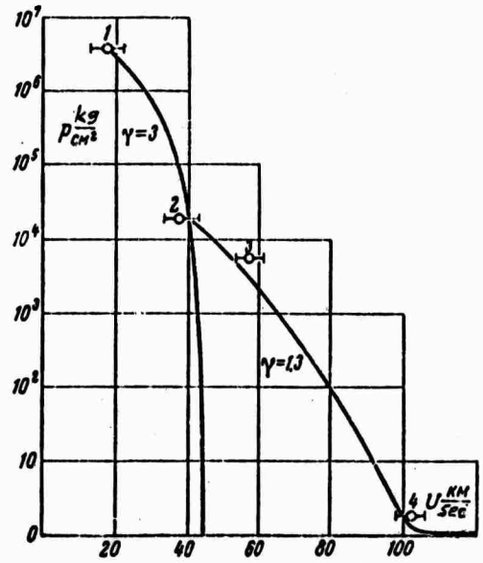

Fig. 1. Discharge particle pressure vs. velocity

Stepanov, G. P. On the reaction impulse from impact of spherical particles with a target. Kosmicheskiye issledovaniye, no. 4, 1969, 602-606.

The kinematics of material dispersion from a cratering impact of a projectile on a solid target are briefly reviewed, followed by experimental data from impacts of steel and lead pellets on lead targets. Impact velocities from 0.6 to 2,4 km/sec were used. High-speed photo sequences for two tests are presented, both using steel pellets at 2km/sec on lead targets, with one impact direction normal to the surface, and the second inclined at 60° to it. In the first case, the ejected material began to appear about 5 μ sec after impact, in a generally disc-shaped pattern, and dispersing at close to impact velocity. Local jet flow in the crater was simultaneously observed, which converted to discrete particle ejection moving at about 5% of impact velocity. For inclined impacts an initial tangential ejection velocity component is present, followed by particle ejection

in a normal direction. Generally for the inclined impact case at higher velocities there was no evidence of jet flow in the impact crater, which apparently was obscured by simultaneously ejected dispersion matter. Sample data on the amount of ejecta and the values of reactive impulse as functions of impact velocities are shown in Figures 1 and 2 respectively.

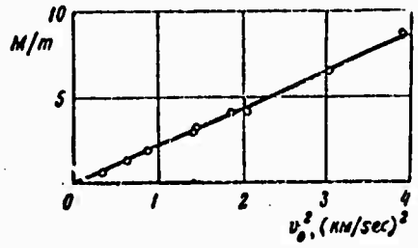

Fig. 1. Ejected mass vs. (velocity)^2, lead on lead.

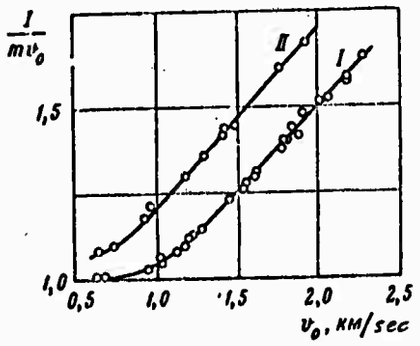

Fig. 2. Impulse vs. pellet velocity.
I=Steel; II=Lead.

Titov, V. M., Yu. I. Fadeyenko, and N. S. Titova. Acceleration of solid particles by a cumulative explosion. IN: AN SSSR. Doklady, v. 180, no. 5, 1968, 1051-1052.

Optimum conditions are discussed for the size and configuration required for cylindrical explosive charges used for particle acceleration. In the general case, the ejected jet stream of detonation products will appreciably exceed the detonation rate. For optimum acceleration of the target material, Eq. 1 should be satisfied, in which l = jet stream length; ρ = jet density; ρ_1 = target material density; and r = nominal per unit radius of the target material.

$$l\rho / r\rho_1 \geqslant 1 \qquad (1)$$

One requirement for achieving this is that the discharge tube length should be twenty-five to thirty times its diameter. Another criterion is that the detonation jet density be limited to a value that will not cause destruction of the target material, i. e., the conditions $\rho v^2 \leqslant H$ must be met, where ρv^2 is jet dynamic pressure and H

is target hardness. Examples of discharge tubes are shown which were used to accelerate specimen charges of metal, glass and ceramic pellets. The highest target velocity obtained was 14km/sec in vacuo with 80-100μ nichrome pellets, using a 200g explosive charge. Considerable ablative loss occurred in the cited example, detection methods for which are also discussed.

Pryakhin, G. V., and V. M. Titov. Shock impact of a high velocity body on light porous material. Zhurnal prikladnoy mekhaniki i tekhnicheskoy fiziki, no. 5, 1969, 110-112.

Experimental studies are described on penetration effects of high-velocity steel pellets into light porous materials. Targets tested included several foam plastics of the polyurethane type, and fibrous materials, with densities in the range of 0.06-0.35g/cm^3. The projectiles were steel pellets several millimeters in diameter, accelerated up to 10km/sec by explosive charges; pore dimensions in the target materials were substantially less than pellet diameters. Penetration depths are shown as a function of increased impact velocity for three general cases: no target damage sustained; physical damage sustained; and local flow of target material induced. Sample graphical data for one type of foam plastic shows that maximum penetration does not increase monotonically with pellet velocity, but peaks in the vicinity of 5km/sec.

Deribas, A. A., and G. Ye. Kuz'min. Impelling a plate by a glancing detonation wave, treated as a two-dimensional problem Zhurnal prikladnoy mekhaniki i tekhnicheskoy fiziki, no. 1, 1970, 177-180.

A theoretical analysis is given for the dispersion motion of explosion products, for the case where the latter are bounded on one surface by an angled plate of arbitrary geometry. The actual three-dimensional problem is reduced as a first approximation to two-dimensional, on the assumption that the length and width of the explosive charge are large compared to its depth. The mathematical model is based on the configuration shown in Figure 1, in which

region 1 is unexploded charge, and region 2 represents the diverging explosion products. For convenience, a rectangular coordinate system is assumed whose origin moves from left to right with sonic line AB. The problem is shown to reduce to a plane stationary supersonic motion of the product gases, expressions for which are derived. Solutions in terms of the assigned geometry and gas parameters were obtained by computer; samples of graphical results are included.

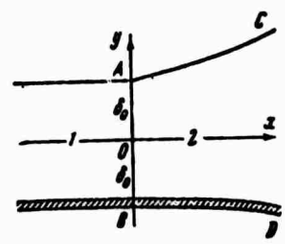

Fig. 1. Model for dispersion of explosion products.
1-undetonated charge;
2-dispersion region;
A, B-sonic line

INTERACTION OF SHOCK WAVES WITH SOLIDS

Shifrin, E. G. On the form of a detached shock wave from flow around a profile. Prikladnaya matematika i mekhanika, no. 5, 1969, 891-895.

The author gives an analysis of detached shock wave formation occurring from flow around a convex profile. The work is a continuation of an earlier paper (Shifrin, Prikladnaya matematika i mekhanika, no. 1, 1969) where a pronounced convex profile was treated; in the present case the analysis is extended to the general problem of a shallow convex profile. In the former case, it is shown that over a range of slightly supersonic approach velocities a segment of the generated shock wave will be convex in the direction of the arriving gas. The same velocity range is treated in the present case, namely a narrow supersonic range over which any entropy change in the shock wave can be neglected. The geometry of the subsonic flow region Q in the vicinity of the obstacle is defined as the only region of subsonic velocity following the shock wave. Other idealized conditions assumed are that the shock wave has a smooth contour, and that secondary compression shock waves are not present at the boundary of Q. The analysis verifies that the shock wave in the investigated region is continuously convex in the direction of incident gas flow.

Larina, I. N. Flow of a rarefied gas around a sphere. Prikladnaya matematika i mekhanika, no. 5, 1969, 895-898.

Expressions are derived for determining parameters of rarefied gas flow around a sphere. The analysis is based on Krook's equation, which in the present case is solved by the method of iterative integrations. A general dimensionless equation for flow velocity, together with two expressions for boundary conditions, are shown to be necessary and sufficient for determining flow through any point of a sectional field in the vicinity of the sphere. The problem reduces to solution of a quadruple integral for the desired point; this was done on a BESM-6 computer, using a field with 1,000 random points. The velocity and temperature values thus arrived at are considered to be accurate within 2% and 3% respectively. Sample results for gas density and temperature values before and after passing the sphere are shown in Figure 1, relative to initial upstream conditions. The dashed lines in the figure indicate idealized results for free-molecular gas flow; for the conditions assumed, shock waves were not present.

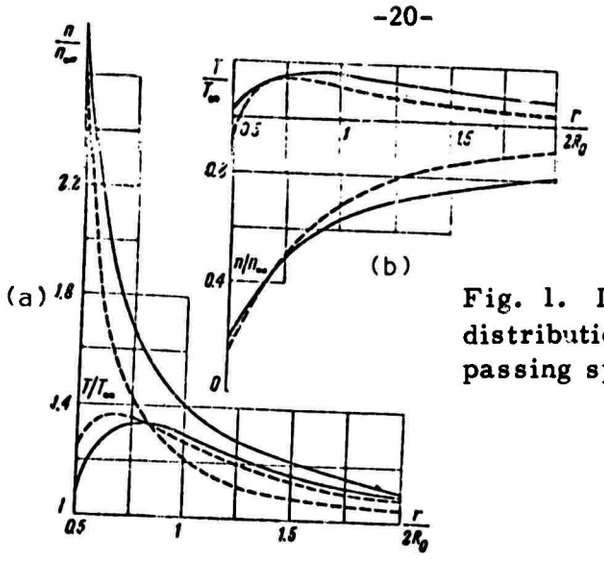

Fig. 1. Density and temperature distribution before (a) and after (b) passing sphere. R_0 =sphere radius.

Voytenko, D. M. Interaction of a shock wave with a penetrable barrier. IN: Moscow Universitet. Vestnik. Seriya matematika, mekhanika, no. 3, 1969, 118-122.

A detailed theoretical analysis is presented on the interaction of a gaseous shock wave with a penetrable barrier, e.g., a grid of steel wires, for which no rigorous theory has so far been advanced. A plane incident shock wave is assumed to arrive in a direction normal to the grid as shown in Figure 1. Intersection of incident wave U_1 with the grid causes an arbitrary discontinuity resulting in a reflected shock wave U_r; contact surface C, and a continuing altered wave U_t. It is assumed that the incident shock wave is inherently stable, so that it resumes its planar front shortly after a brief re-forming interval beyond the grid; for present analytical purposes this interval is neglected. Figure 2 shows calculated exit shock wave velocity as a function of grid characteristic η, where $\eta \equiv$ active grid area/total grid area.

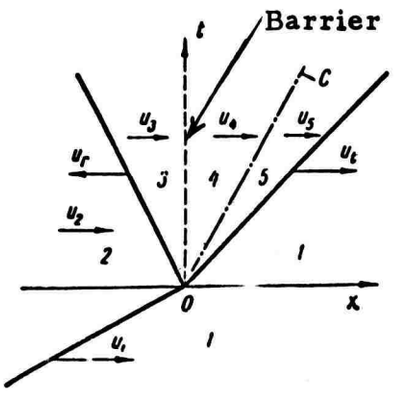

Fig. 1. Model for shock wave intersecting a penetrable barrier.

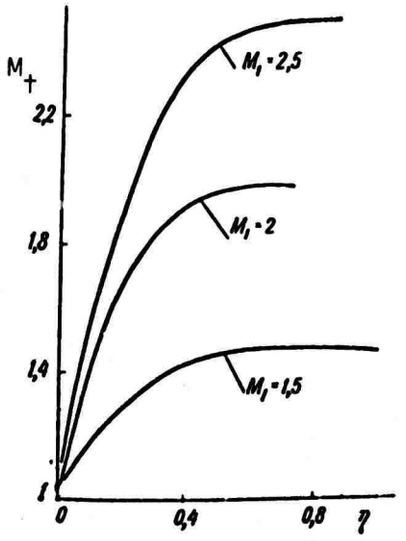

Fig. 2. Exit wave velocity vs. grid configuration. M = Mach no.; M_1 = approach velocity.

Ivanov, A. N., and S. Yu. Chernyavskiy. Interaction of spherical shock waves with solids. Zhurnal prikladnoy mekhaniki i tekhnicheskoy fiziki, no. 6, 1969, 115-119.

Two sets of experiments are described to observe interaction of a spherical shock wave with a solid object. In both cases the objects were foam polyurethane cylinders of varying diameters; in one case the cylinder was suspended in the shock wave path, while in the second case it was propelled axially to meet the wave. In the stationary test specimens were suspended approximately 5m from an explosive source. Shock impulse duration and wave form were registered both by piezoelectric accelerometers fixed to the specimen and by the e.m.f. generated when the specimen was propelled by the shock wave through a d-c magnetic field; measurement error for either method was not over 10%. Figure 1 shows examples of impulse waveform, together with the increase in static pressure, measured at the impact surface. In the second part of the test, plastic rods with hemispherical ends were accelerated axially in a light gas gun up to a speed of Mach 0.82 prior to meeting the arriving detonation wave. The interaction interval was photographed with an IAB-451 high-speed Toepler shadowgraph. Sample photos are presented which clearly show development of a bow wave following penetration of the shock wave front. The formation of the bow wave can be roughly divided into an initial stationary interval, followed by a terminating quasistationary interval.

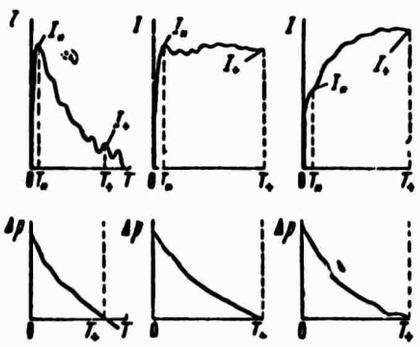

Fig. 1. Shock impulse and static pressure vs. time, stationary target.

Apshteyn, E. Z. Destruction of a vitreous body in a hypersonic gas flow taking internal radiative energy transfer into account. Inzhenerno-fizicheskiy zhurnal, v. 17, no. 1, 1969, 150-154.

The radiative energy transfer within an ablating body is incorporated into an earlier solution of the glassy body ablation problem (Tirskiy, G. A., PMTF, no. 6, 1961) by inclusion of the term $\partial H_y / \partial y$ into the energy equation. Here H_y is the flow of radiant energy along the y - axis (normal to the surface), approximated by

$$H_y = -\frac{16}{3}\frac{\sigma_r T_1^3}{\rho_1 \alpha_r}\frac{dT_1}{dy} = -\frac{16}{3} l_r \sigma_r T_1^3 \frac{dT_1}{dy}. \qquad (1)$$

where σ_r - Stefan-Boltzmann constant,
ρ_1 - density of a liquid film,
α_r - absorption factor,
l_r - mean free path of radiation.

It is assumed that the viscosity of the vitreous body has the following temperature dependence:

$$\mu_1 = \mu^* \exp(T^*/T_1) \text{ at } T_1 > T^{**}$$
$$\mu_1 = \infty \text{ at } T_1 \leqslant T^{**}$$

i.e. at T** the glass is a solid, μ^*, T*, and T** are constants. This yields the following dimensionless motion equations for the liquid film:

$$\frac{d^2\varphi_1}{d\eta_1^2} = -(\tau_0 + \eta_1)\exp\left(-\frac{1}{\theta_1}\right),$$
$$\frac{d}{d\eta_1}\left[(1 + \lambda_R \theta_1^3)\frac{d\theta_1}{d\eta_1}\right] + \varphi_1 \frac{d\theta_1}{d\eta_1} = 0 \qquad (2)$$

with the boundary conditions

$$\varphi_1(0) = \alpha_1, \quad \theta_1(0) = \theta_0 = T_\omega/T^*,$$
$$\frac{d\varphi_1(\infty)}{d\eta_1} = 0, \quad \theta_1(\infty) = \theta_T = T_T/T^*, \qquad (3)$$

where $\lambda_R = \frac{16}{3}\sigma_r T^{*3}/\lambda_1 \rho_1 \alpha_r$ is a dimensionless parameter, depending on the absorption factor;

Φ_1 - dimensionless flow function;
γ_0 - dimensionless friction on the surface;
η_1 - dimensionless coordinate normal to surface of body;
θ_1 - T_1/T^* - dimensionless temperature;
θ_0 - T_ω/T^*, T_ω - temperature on film surface;
θ_T - T_T/T^*, T_T - temperature in the depth of a body.

An approximate solution is offered and compared with the exact computer solution in the enclosed figure. Solid lines represent computer calculations, while dashed lines designate approximate calculations. Curves 1, 2, and 3 are for $\lambda_R = 10^5$, 10^4, and 0 respectively. Applicability limits of accepted approximations are discussed.

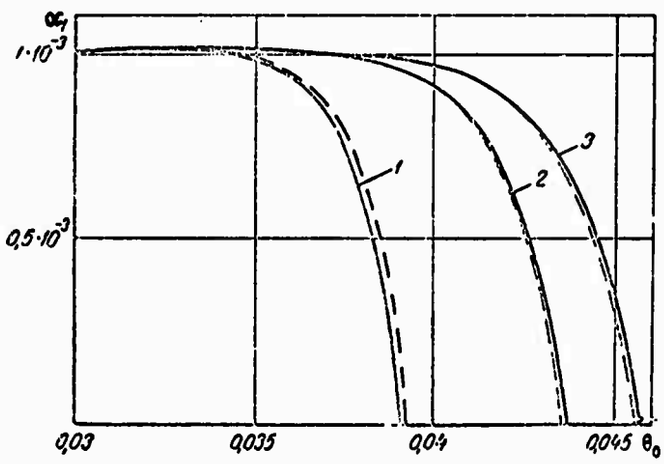

Fig. 1. Dimensionless removal rate in a gaseous phase α_1 as a function of dimensionless temperature.

Bud'ko, N. I. Perturbation of nonisothermal plasma by a body moving at supersonic velocity. Zhurnal eksperimental'noy i teoreticheskoy fiziki, vo. 57, no. 2, 1969, 686-697.

The structure of a perturbed region is considered as a function of plasma nonisothermality (characterized by the parameter $\eta = T_e/T_i$) at large distances from a rapidly moving body with a metal surface. The Fourier components of ion and electron density perturbations are obtained by a method somewhat different from the usual in order to render the effect of Čerenkov

excitation of ionic acoustic waves more explicit. The mathematical exposition commences with the description of particle distribution by a collisionless kinetic equation that accounts for particle absorption by the metal surface. An inverse Fourier transform is used to determine the perturbation of particle density. In a spherical system of coordinates with the axis along the vector $\vec{V}_0$ (= velocity of a moving body) the perturbation of the particle density is found to be

$$\delta N(r, 0) = -\frac{SN_0a_0}{(2\pi)^2}\int_0^\infty k\,dk \int_0^\pi \sin\chi\, d\chi\, B(z)\, e^{ikr\cos\theta\cos\chi} J_0(kr\sin\theta\sin\chi) \tag{1}$$

where S is the area of the body projection onto the plane perpendicular to the motion direction;

$$B(z) = \sqrt{\pi}\, W(z)\left[1 + \frac{T_e}{T_i}(1 + i\sqrt{\pi}\, zW(z))\right]^{-1}, \quad z = a_0\cos\chi. \tag{2}$$

and

$$W(z) = e^{-z^2}\left\{1 + \frac{2i}{\sqrt{\pi}}\int_0^z e^{u^2}du\right\}. \tag{3}$$

This is further transformed into

$$\delta N(r, \alpha) = \frac{SN_0a_0\cos\alpha}{(2\pi)^2 r^2}\int_{-1}^{1} B(a_0t)\frac{t\,dt}{(t^2 - \sin^2\alpha - 2it\,\mathrm{sign}\cos\alpha)^{3/2}}, \tag{4}$$

in which α is the angle of vector $\vec{r}$ with axis $(-\vec{V}_0)$, so that behind the body $\cos\alpha > 0$ and in front of the body $\cos\alpha < 0$. The integral in Eq. 4 has been numerically tabulated elsewhere for the case of an isothermal plasma (Geomagnetizm i aeronomiya, v. 4, 1964, 256). Eq. 4 is approximated by

$$\delta N(r, \alpha) = -N_0\frac{Sa_0^2}{\pi r^2}\cos\alpha F(a_0\sin\alpha), \tag{5}$$

$$F(a) = -\frac{1}{4\pi}\int_L \frac{B(z)z}{(z^2 - a^2)^{3/2}}dz, \tag{6}$$

and the integration contour L for $\cos\alpha > 0$ is shown in Figure 1.

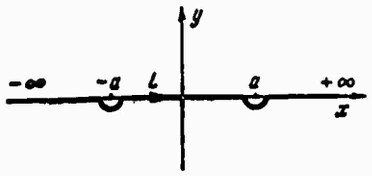

Fig. 1. Integration contour L.

F(a) is a universal curve for the problem parameters and depends on $a = a_0 \sin\alpha$. Positive F(a) values correspond to decreased particle density, negative values to increased density. It is shown that F(a) has the property

$$\int_0^{a_0} aF(a)\,da = \frac{1}{2}. \tag{7}$$

At $\cos\alpha > 0$, B(z) has poles for zero values of its denominator. The values of the first three B(z) poles have been calculated for the two values of $\eta = T_e/T_i$:

	z_0	z_1	z_2
$\eta = 1$:	$1{,}48 - i\ 0{,}58$	$2{,}36 - i\ 1{,}85$	$3{,}00 - i\ 2{,}49$
$\eta = 4$:	$2{,}05 - i\ 0{,}21$	$2{,}57 - i\ 1{,}56$	$3{,}26 - i\ 2{,}13$

Universal functions F(a) for $\eta = 1$ and $\eta = 4$ are presented in Fig. 2, with the dashed curve indicating the first pole contribution. Angular dependence of density perturbations $\Phi(a_0, \alpha) = \cos\alpha\, F(a_0 \sin\alpha)$ constructed by these universal functions for various a_0 values are presented in Fig. 3.

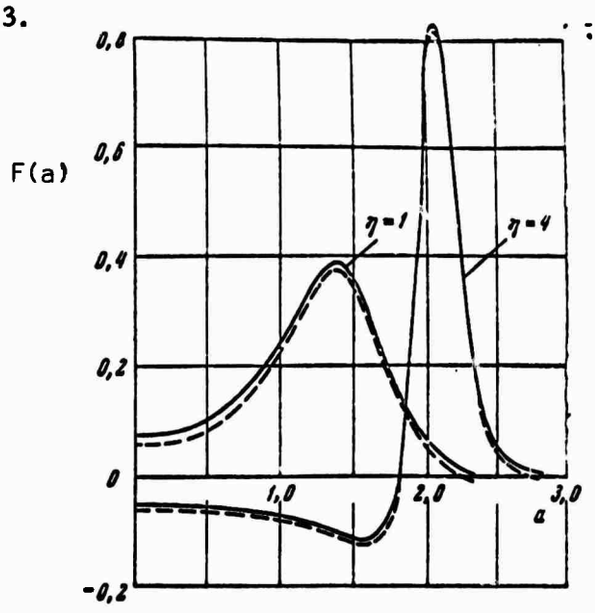

Figure 2.
F(a) for $\eta = 1$ and 4

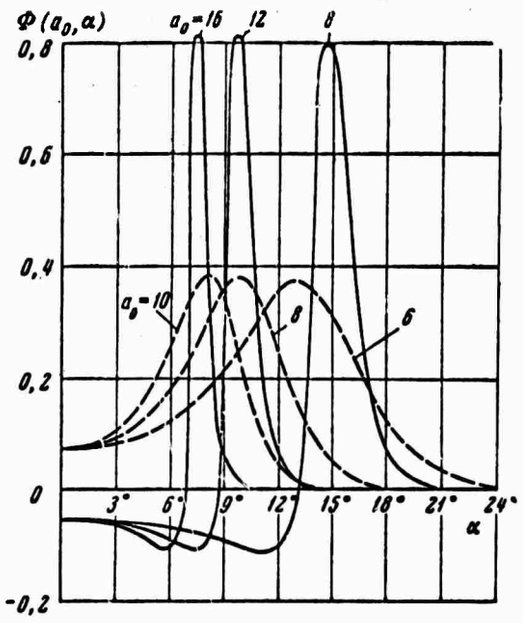

Fig. 3. $\Phi(a_0, \alpha)$ vs. α. Solid lines are for $\eta = 4$, dashed lines are for $\eta = 1$.

The analysis yields the following conclusions: in an isothermal plasma ($\eta = T_e/T_i = 1$) a rarefaction exists behind the body; for $T_e/T_i < 0.23$, maximum rarefaction is on the axis, and at $T_e/T_i > 0.23$ it is on the surface of a maximum rarefaction cone analogous to the Mach cone. In the region $1.76 < T_e/T_i < 2.43$ both rarefaction and compression exist with maximum compression on the axis. At $T_e/T_i > 2.43$ maximum compression is on the conical surface inserted into the cone of maximum rarefaction.

Stanyukovich, A. K. Approximate determination of shock adiabatic exponent for the motion of large meteors in the atmosphere. Zhurnal prikladnoy mekhaniki i tekhnicheskoy fiziki, no. 2, 1969, 104-105.

An approximate formula is derived for the effective value of the air adiabatic exponent k* in the shock wave formed during the hypersonic motion of a meteor in the atmosphere:

$$k^* = \frac{1}{\rho_2^*/\rho_1 - 1}\left[\frac{\rho_2^*}{\rho_1}\left(1 + \frac{2}{M_1^2}\right) + 1\right] \qquad (1)$$

where ρ_2^* = density behind the shock wave in the presence of dissociation and ionization;
ρ_1 = density in front of the shock wave; and
M_1 = Mach member.

For the practical determination of the effective adiabatic exponent k* the use of Rozhdestvenskiy curves is recommended (Rozhdestvenskiy, I. B. Thermodynamic and gasdynamic properties of air flow behind a shock wave with dissociation and ionization taken into account. IN: AN SSSR, Physical Gas Dynamics. Moscow, 1959). The following k* values are calculated using these curves for altitudes of 80 - 100 km, where the pressure value is accepted to be $\sim 10^{-4}$ atm.

M_1	25	30	35	40
ρ_2^*/ρ_1	18.5	17.8	18.5	19.9
k*	1.130	1.120	1.116	1.111

The given formula may be further simplified for extreme hypersonic velocities ($M_1 > 30$) when the term $2/M_1^2$ may be neglected, thus reducing k* to

$$k^* = \frac{\rho_2^*/\rho_1 + 1}{\rho_2^*/\rho_1 - 1}. \qquad (2)$$

Finkel', V. M.; V. N. Gurariy; and N. I. Alyushina. Kinetics of a thermal shock fracture. IN: AN SSSR. Doklady, v. 188, no. 3, 1969, 567-570.

Some kinetic aspects of the thermal shock fracture type, manifested by surface layer fragmentation into a dense network of cracks, are experimentally investigated. The experimental arrangement is shown in Fig. 1. The thermal shock was created by exposing an LiF crystal tc a plasma beam of $\sim 10^{-5}$ g/cm^3 density and wavefront velocity over 30 km/sec. The fragmentation process was recorded by a SKS ultra high-speed camera. The plasma beam was produced by

exploding a thin foil inside a small chamber at a distance of 15 - 20 mm from the crystal surface by a 6 μsec discharge of a capacitor bank. The thermal energy delivered to the target during an impact time interval ~ 10^{-5} sec, as determined by a SFR streak camera, was about 2 joules/cm^2. Micrographic investigations indicated that cracks penetrate to a depth of 100 - 400 μ, are located in cleavage planes, and produce fragments averaging about 200 μ in size. Crack propagation was observed with a motion-picture camera, and was calculated from the tensile stresses arising during cooling. Both results are presented in Fig. 2. Dependence of crack velocity on its size is also calculated and results are compared with experimental data in Fig. 3. The noncoincidence regions are discussed and explained.

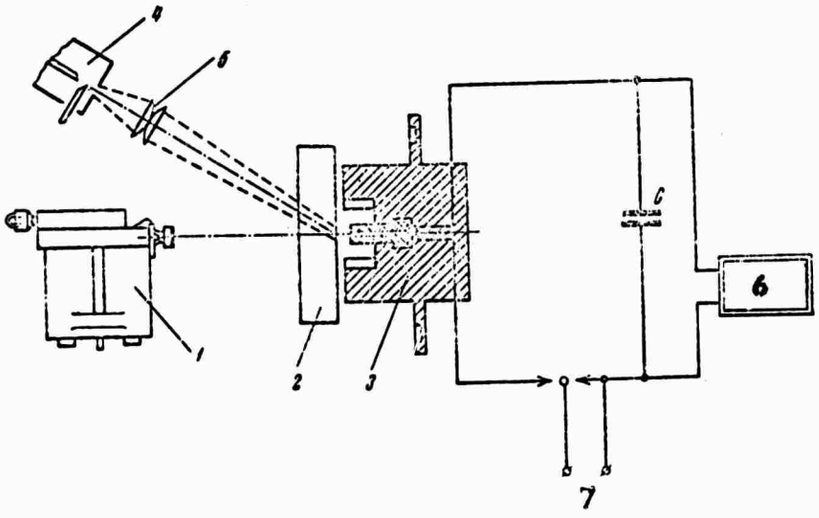

Fig. 1. Thermal shock test apparatus

1 - SKS movie camera with velocity of 4200 frames per second; 2 - LiF crystal sample 15-20 mm thick with an impact surface area of 40 x 40 mm^2; 3 - shut-off device; 4 - arc light source; 5 - condensing lens; 6 - charging power supply; 7 - trigger; c - 13.6 μf capacitor bank at 30kv.

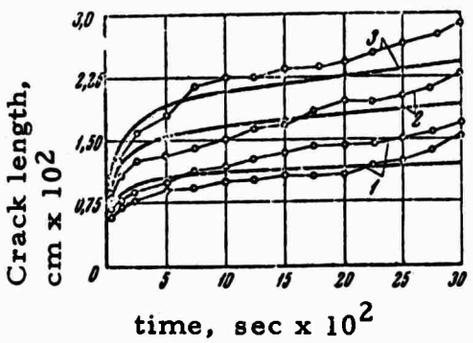

Fig. 2. Experimental (broken) and calculated (smooth) motion curves of separate cracks for fragment dimensions of 100μ(1), 200μ(2), and 300μ(3).

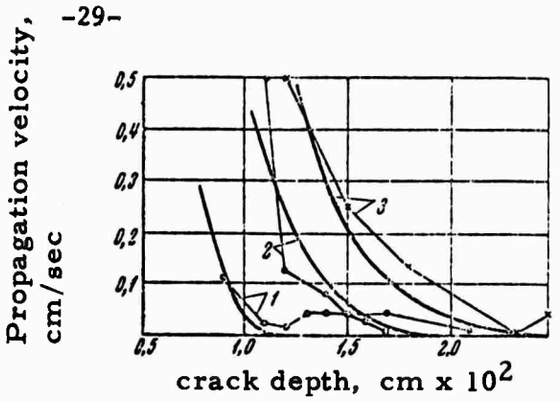

Fig. 3. Experimental and theoretical curves of crack propagation velocities (notations are the same as in Fig. 2.).

Gurariy, V. N.; V. P. Ivanov; V. K. Karelin; P. S. Nosov; and V. M. Finkel'. Impact effects of fast plasma beams on LiF crystals. Fizika i khimiya obrabotki materialov, no. 4, 1969, 19-26.

The nature of impact damage to the surface of LiF crystals caused by plasma beams at velocities up to 35 km/sec is experimentally investigated. The experimental setup is similar to that described by V. E. Sherrer (An exploding wire hypervelocity projector, in "Exploding Wires", vol. 2, Plenum Press, New York, 1962, 235-244). A SFR-1 streak camera with a mirror rotation rate of 60,000 rpm was used to determine plasma velocity. The relative error of velocity measurements, depending on the accuracy of length measurements, was 8-10% for a plasma front velocity of 30-35 km/sec. The energy storage parameters were: capacitor bank - 13.5 μf and 6000 j; discharge period - 10 μsec, and discharge power - 1.2×10^9 watts. The explosion temperature of the foil before expansion was calculated to be 1.1×10^5 °K at U max = 30 km/sec. The plasma density ρ on the target surface at a distance h from the end of the capillary tube was calculated by:

$$\rho = \frac{m(U_1 + U_2)}{2\pi(U_1 - U_2)x(r + h\,\mathrm{tg}\,\alpha/2)^2}$$

where m is the mass of the exploded foil (0.23 mg), U_1 and U_2 are front and rear velocities of the plasma bunch respectively, $x = l + h$, where l = 3 cm is the length of the capillary and α is the mean divergence ($\approx 40^\circ$) of the beam. With a known beam density ρ the pressure on the crystal is determined from $P = \rho U^2$. The beam kinetic energy during these experiments was 20 joules. The following

table shows the crystal damage produced by beams of varying density:

h, cm	Average beam density, g/cm^3	Average pressure on crystal, atm.	Impact duration sec	Impact surface, cm^2	Type of damage
0.02	$4 \cdot 10^{-3}$	$2.0 \cdot 10^4$	10.0	0.01	crater
0.3	$6 \cdot 10^{-4}$	$2.5 \cdot 10^3$	10.0	0.08	
0.4	$4.0 \cdot 10^{-4}$	$1.6 \cdot 10^3$	11.0	0.12	
1.0	$1.0 \cdot 10^{-4}$	$4.0 \cdot 10^2$	13.0	0.54	surface
2.0	$1.5 \cdot 10^{-5}$	60.0	16.0	1.70	splitting
6.0	$3.0 \cdot 10^{-6}$	12.0	30.0	15.70	dislocated
12.0	$8.5 \cdot 10^{-7}$	3.5	50.0	—	lattice

At lower plasma densities the compressive thermal stress is much higher than the gas dynamic pressure, causing damage of the dislocation grid or surface splitting type. Cratering occurs at higher plasma densities when the thermal and mechanical damage mechanisms are equally effective. The penetration depth of plastic deformation and slippage is calculated for the case when surface temperature reaches the melting point. It coincides with the experimentally observed depth of surface splitting, i.e. for beam densities of 10^{-4} - 10^{-5} g/cm^3. The slippage type depends on indices of the affected crystallographic plane; when a (100) plane is the target, dislocations are aligned along the (100) directions and form a dense orthogonal grid. The irreversible deformation in the slope of an expanding heated disc in the crystal surface causes tensile stress upon cooling which could reach 200 kg/mm^2 if not for relaxation splitting. The article includes magnified photographs showing this effect, as well as other examples of fracture behavior and crater structure at beam densities of 5 x 10 g/cm^3 or more.

Chekalin, E. K.; and V. S. Shumanov. Radiation of a dense plasma produced by electric explosion in vacuum. Zhurnal tekhnicheskoy fiziki, v. 39, no. 1, 1969, 71-74.

Optical and spectral properties are investigated of an expanding dense plasma, obtained by the explosion of copper and aluminum wires in vacuo. Synchronized fast frame and streak photographic sequences of the exploding wire together with the time scan of the visible emission spectrum, and electrical characteristics are presented in Fig. 2. The maximum time resolution is ~ 0.1 μsec. The experimental arrangement is shown in Fig. 1. Parameters of the discharge circuit are: U_o = 30 kv, C_1 = 41 μf, Lo = 1.3 μH, Imax = 150ka, T/2 = 23 μsec. It is found that the plasma expands in a form of a cylindrical shell with strong flute instabilities in the leading edge. The velocity of plasma expansion is fairly constant up to 20 μsec at 3 km/sec for the 0.31 mm copper wire. A short intense burst of continuous spectrum coinciding with the maximum electrode voltage is typical. Its duration (0.1 to 2.5 μsec) depends on the material and diameter of the wire, as shown in the table:

Material	Copper			Aluminum		
diameter, mm	0.2	0.31	0.62	1.08	0.3	0.5
T, μsec	0.1	0.1-0.2	0.5-1.0	2.5	0.1	0.15

The absorption spectrum of the wire material is detected after the continuous spectrum burst, when the temperature of the plasma bunch is lower at the periphery than at the center. The origin of the continuous spectrum generated in the initial stage of the electric explosion is discussed.

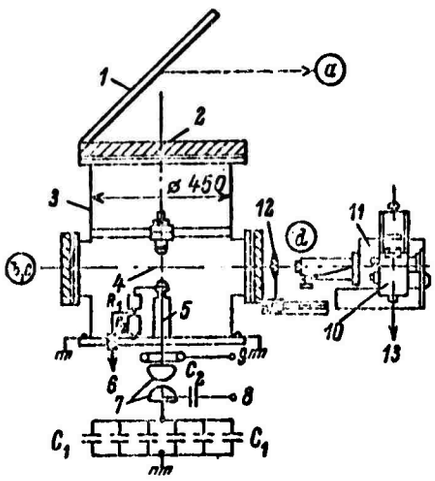

Fig. 1. Schematic diagram of exploding wire plasma experiment.

1 - mirror;
2 - upper plastic window;
3 - vacuum chamber (pressure 3 x 10^{-5} torr);
4 - aluminum or copper wire (length = 100 mm and diameter = 0.2 to 1.0 mm);
5 - high voltage electrode;
6 - signal from voltage divider;
7 - air spark gap;
8 - trigger pulse from control panel of recording camera;
9 - signal from Rogovski belt;
10 - SFR-2M ultra high-speed camera;
11 - ISP-51 spectrograph integrated with SFR camera;
12 - condensing lens (f = 94 mm);
13 - synch pulse to SFR-2M control panel.

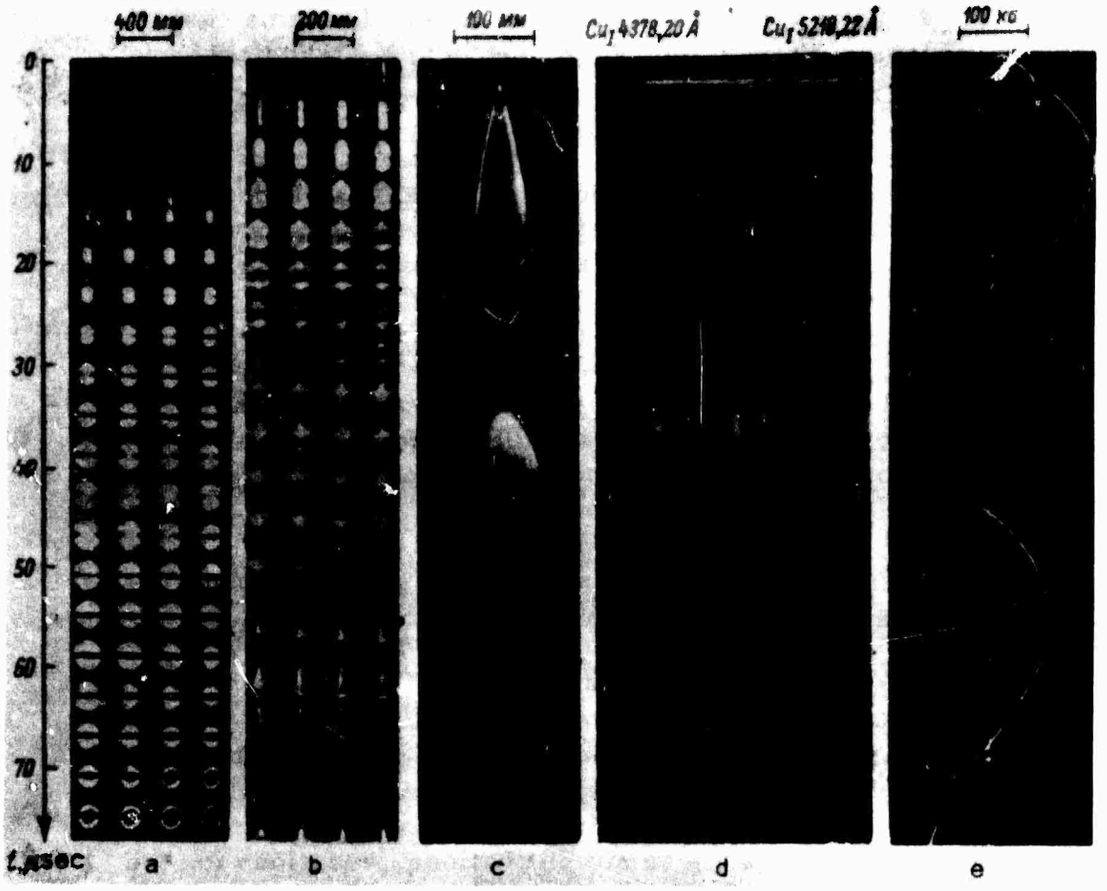

Fig. 2. Time synchronized frame pictures along the wire axis (a) and from the side of the wire (b), streak picture (c), time display of the spectrum (d), and discharge current (ë) during the explosion in a vacuum of a wire 0.31 mm in diameter.

PLASMA DYNAMICS

Gefter, V. M. Expansion into vacuum of rarefied plasma having two types of ions. Zhurnal prikladnoy mekhaniki i tekhnicheskoy fiziki, no. 1, 1970, 32-38.

An analysis is given of the expansion into a vacuum of a uniform temperature plasma consisting of two types of ions. It is assumed that the ions have a Maxwellian velocity distribution, and that a rarefaction wave is propagated at sonic velocity in the plasma. An expression for this velocity is obtained. It is shown that the initial expansion stages can be treated on a self-similar basis. The work is an extension of the method described by Gurvich et al (Zhurnal eksperimental'noy i teoreticheskoy fiziki, v. 49, no. 3, 1965) which treated the simple case of expansion with only electrons and one type of ion present.

Borisov, V. M. On the wavefront structure of nonequilibrium ionization in gas. Zhurnal vychislitel'noy matematiki i matematicheskoy fiziki, v. 10, no. 1, 1970, 252-255.

The structure of ionization wave propagation in a non-equilibrium weakly ionized cold plasma is investigated. It is assumed that only singly-ionized atoms are present, and that the temperature of ions and neutral atoms remains constant during the process. With these simplifications, equations for the structure of the ionization wavefront and its propagation velocity are derived from energy balance considerations, expressed in the form of series with small parameters.

Chutov, Yu. I. Experimental study of shock waves in a partially-ionized gas-discharge plasma. Zhurnal prikladnoy mekhaniki i tekhnicheskoy fiziki, no. 1, 1970, 124-130.

A detailed study is reported on a plasma propagation experiment in argon, in which the shock wave from a pulse-discharge plasma was propagated into an existing argon plasma. Both plasmas were generated by capacitor discharge in a shock tube; however, for the target plasma the discharge rate was enough slower that the latter could be considered quasistationary. An array of probes in the discharge tube were used to record temperature, density, etc. as functions of time during shock wave propagation. Interest is centered on the width of the shock wavefront, which was determined to be considerably larger than mean free path of argon atoms under the test conditions.

Veselovskiy, I. S. Electric field structure in a shock wave propagating through a weakly-ionized gas. Zhurnal tekhnicheskoy fiziki, no. 2, 1970, 387-389.

A brief theoretical analysis is made of the electric field generated near a shock wavefront propagating through an ionized gas. The particular case considered is for a weakly-ionized gas exhibiting the Ramsauer effect, e.g. in argon where $T < 10^5$ deg. K. The electric field arises from charge redistribution caused by the incident shock wave, and decays exponentially with distance normal to either side of the wavefront. With a weak initial ionization assumed, the contribution of existing electrons and ions to the energy balance equations can be neglected, and the shock wave is considered to be propagating through a neutral gas. The extent of the electric field region is shown to be on the order of a Debye wavelength.

Bodulinskiy, V. K., and Yu. A. Medvedev. Electromagnetic excitation generated by the expansion of an ideally conducting sphere in a magnetic field. Zhurnal prikladnoy mekhaniki i tekhnicheskoy fiziki, no. 6, 1969, 103-104.

A rigorous analysis is presented for defining the electromagnetic field generated by expansion of an ideally conducting spherical surface through a uniform magnetic field. It is assumed that the external field is constant, and that the expansion occurs at a linear rate a = vt, where a = spherical radius and v is on the order of light velocity. Starting with the general field equations given by $\text{rot } H = \frac{1}{c}\frac{\partial E}{\partial t}$, $\text{rot } E = -\frac{1}{c}\frac{\partial H}{\partial t}$, $\text{div } H = 0$, the authors assigned convenient coordinates and derived field expressions which include the necessary initial and boundary conditions. A self-similar substitution is used to arrive at a sample solution for some arbitrary time t between start and finish of the expansion process. The treatment is presented as a correction to a previous solution of this problem reported by Krasil'nikov (Sbornik. Problemy difraktsii i rasprostraneniya voln. Izd-vo LGU, no. 4, 1965), which did not properly account for initial conditions in the field equations. The authors' results are specifically applicable to the practical case of rapid shock wave propagation caused by a laser spark in a magnetic field.

Nadezhin, A. D., and Ye. A. Pomishevskiy. Nonequilibrium radiation from a strong shock wave. Zhurnal prikladnoy mekhaniki i tekhnicheskoy fiziki, no. 1, 1969, 27-32.

The principal factors which govern nonequilibrium radiation from a strong shock wave in air are examined. Experimental and theoretical data are cited to show that under certain shock wave conditions a pronounced peaking of radiation occurs, caused mainly by transitions in molecular energy bands of O_2 and N_2, of which N_2^+ is the major contributor. Attention is therefore centered on the radiation associated with the first negative band of N_2^+. It is emphasized that correct evaluation of this problem requires precise knowledge of the excitation mechanism, in addition to evaluation of temperatures and densities behind the shock wave. The two main ionizing mechanisms considered are vibrational excitation of the N_2 molecule and electron impact, for each of which the governing parameters are discussed. Fig. 1 shows theoretical curves comparing radiation intensity peaks for these two cases. Evaluation of derived expressions for two assumed shock wave velocities shows a distinct difference in excitation factors: for $V \leq 6$ km/sec, vibrational excitation predominates, since electron concentration remains low; on increasing to V=8 km/sec or higher, electron density rises sufficiently to make electron impact the predominant ionization mechanism. The theoretical conclusions presented are claimed to be in good agreement with experimental data of other authors.

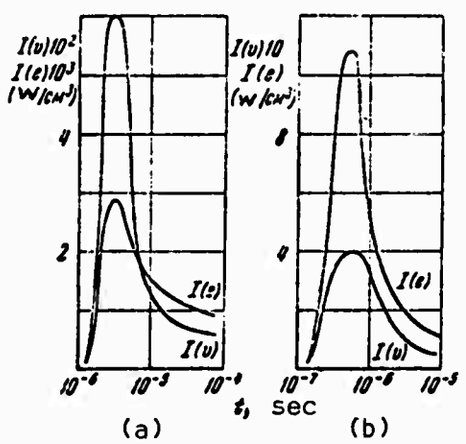

Figure 1. Radiation intensity from first negative band of N_2^+ behind a shock wave.

a - 6 km/sec; b - 8 km/sec

PLASMA-INDUCED SURFACE EFFECTS

Afanas'yev, N. V., S. N. Kapel'yan, V. A. Morozov, and L. P. Filippov. Electrode damage from flare components of an arc discharge. Inzhenerno-fizicheskiy zhurnal, v. 27, no. 1, 1969, 43-49.

Experiments are described on erosion characteristics of local flares generated at electrode surfaces during a powerful arc discharge. The effect was obtained by triggering high-energy capacitive discharges (20—900j, 200μsec) between several types and orientations of metal electrodes, and observing microphotos of the erosion effect. Erosion damage was found to occur in two discrete stages: up to some critical thermal flux density q_{cr}, ordinary surface evaporation occurs, and beyond q_{cr}, a complete flare eruption occurs together with a sharp increase in ejected particle velocities to the order of km/sec. The q_{cr} and other critical parameters of the flare mechanism vary according to electrode metal as well as to electrode polarity, shape, and juxtaposition. The flare is composed of jet vapor filaments which evidently migrate over the electrode surface during discharge; a liquid metal phase is also present at this time. Erosion action of the flare on an aluminum screen inserted between electrodes was also observed and found to have somewhat different characteristics than electrode erosion. Under certain conditions the flare erosion of the screen was more severe than on the electrodes themselves. Measured values of minimum flare velocity, i.e., velocity at the threshold value of q_{cr}, are tabulated. These values agree well with theoretical data obtained by treating the evaporated matter as an ideal gas. The authors note that the mechanism studied in an analog of the action of a pulsed laser on metal.

Kapel'yan, S. N., L. P. Filippov, and E. M. Yudovin. Erosive effects of plasma jets. Zhurnal prikladnoy spektroskopii, v. 11, no. 3, 1969, 396-398.

The experiment reported here is the same one described in detail by Afanas'yev et al (see above) on the effect of plasma flares caused by powerful arc discharges between

metal electrodes. Electrode metals studied were Pb, Zn, Al, Fe, Cu, and W, as well as aluminum grids placed between electrodes. Capacitive discharges of 20-900j at 200μsec durations were used to generate the flares. In the present work, the authors center attention on the combined erosion and depositing actions of ejected metal on the aluminum screen. A special channeling device was used which permitted variation in the relative levels of vapor and liquid phase in the flare material, hence their effect on the target screen. Results show that deposits on the screen from the liquid phase increase with discharge pulse energy up to about 600j, after which erosive action tends to predominate, as shown in Figure 1. For pulse energies above 800j there is a net erosive loss from the screen. Deposits up to 1 mm thick were obtained on the test screen; on this basis the authors suggest their technique as a possibly useful one for plating aluminum and other metals.

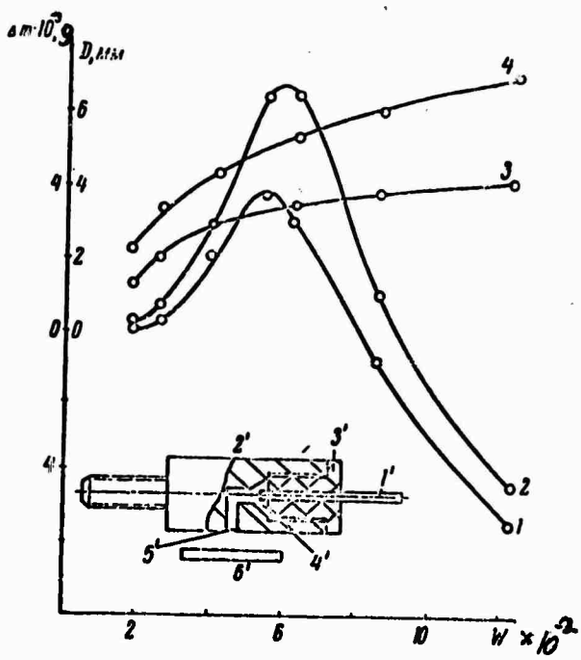

Fig. 1. Jet plasma effect on aluminum grid.
Plating (erosion) using copper (1) and tin (2) electrodes; pit diameters using copper (3) and tin (4) electrodes.

Dustov, I.K., and M.A. Sultanov. Study of the destructive mechanisms in certain polymers from the effect of plasma jets. Zhurnal prikladnoy mekhaniki i tekhnicheskoy fiziki, no. 3, 1969, 151-153.

The destructive action of pulsed plasma jets on a variety of sheet polymer specimens is described. The plasma was generated by pulse discharge from a capacitor bank, between electrodes in a high-pressure capillary; the apparatus and

method were those described in an earlier paper (Sultanov, M. A. AN TadzhSSR. Doklady, no. 11, 1967). Discharge capacity was 300 μf and charge level was 1.5-2kv. The resulting plasma pulse had a periodic decaying waveform with a half-period of about 100 μsec. Plasma temperature was on the order of 10,000°K and propagation velocity was 7-10km/sec. This particular jet type of propagation was sought, since on its striking a target surface the slowdown energy transfer can cause local surface temperatures estimated at up to 50,000°K. Impact tests were made on 50—300 μ thick membranes of several polymers including polystyrene, high-pressure polyethylene, lavsan, kapron, teflon, and others. The destruction effects were photographed and their mechanisms analyzed. Damage could be generally divided into surface and interior effects, both often occurring together in a specimen. Microphotographs illustrating the damage types are included. The authors also establish that the damage sustained is a function of target opacity to incident jet radiation, as asserted by previous authors. This was shown by adding a clear plexiglass overlay to the polymer target surface, and repeating the tests at even higher discharge levels; similar damage occurred to the polymers although the plexiglass cover was practically undamaged.

Dustov, I. K., B. N. Narzullayev, and M. A. Sultanov. Effect of supersonic plasma jets on polymer membranes. IN: AN TadzhSSR. Doklady, v. 12, no. 3, 1969, 19-21.

The experimental results described here of supersonic plasma damage to various polymer targets refer to the same tests reported by Dustov and Sultanov in the foregoing article (Zhurnal prikladnoy mekhaniki i tekhnicheskoy fiziki, no. 3 1969, 151-153). Plasmas generated by high-voltage capacitive discharge between orthogonal electrodes were directed against a number of interposed polymer membranes, and the resulting destruction patterns were photographed. Figure 1 shows the electrodes and target configuration. With the target located approximately 16mm from the plasma source electrode, the

arriving wave front attained velocities on the order of 10km/sec. It was generally noted that oriented polymers such as polystyrene tended to show a striated damage pattern, whereas disoriented types such as teflon showed a more chaotic damage pattern. Sample microphotographs of surface damage at 270X magnification are included.

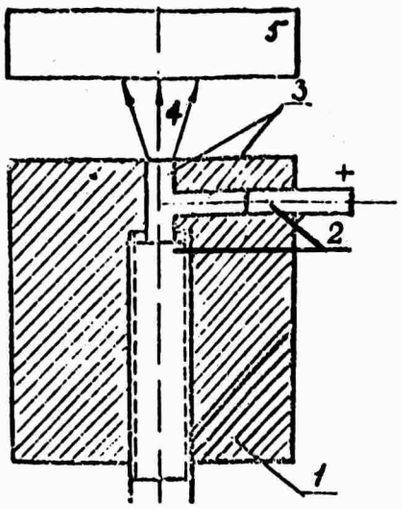

Fig. 1. Plasma generation.
1-Dielectric block;
2-Electrode channels;
3-Plasma discharge channel;
4-Flare;
5-Support for test specimen

Pokrovskaya, L. M., and N. I. Plokhikh. Study of the erosive effects of a plasma jet. Zhurnal prikladnoy spektroskopii, v. 11, no. 3, 1969, 408-412.

Destructive effects of a plasma jet on a wide variety of metals, semiconductors and dielectrics are described. The plasma was generated by capacitive discharge between metal rod electrodes. Capacity was 16,500μf, charged to 200V, and developing 1380a discharge pulses of approximately 14μsec duration and pulse energies up to 190 joules. Tests were done in air at atmospheric pressure. The generated plasma was constricted by a textolite collar to increase its power density before striking a target specimen. The geometry of the eroded areas and other relevant data for all tests specimens are tabulated. In general, the plasma jets caused heaviest damage to metals and semiconductors, less to crystalline and friable dielectrics, and practically none to plastic specimens. The extent of pitting in the metal and semiconductor target surfaces was found to be inversely proportional to fusion temperature, but directly proportional to thermal conductivity. The relatively small amount of damage sustained by dielectrics was most evident in high thermal conductivity specimens such as potassium bromide, glass and mica. Sample photos are given of erosion damage in lead, tungsten germanium and

potassium bromide specimens. As indicated by other authors, the neglible damage sustained by plastics such as paraffin and polyethylene suggests their possible application as protective coatings for more susceptible materials.

Karasev, A. B., and T. V. Kondranin. Damage in graphite subjected to a low-temperature plasma stream in air. Zhurnal prikladnoy spektroskopii v. 11, no. 3, 1969. 403-407.

An analysis is given of a hypothetical supersonic gas flow around a sphere. In the model assumed a detached shock wave is formed, behind which gas temperatures may attain the order of 20,000°K. Expressions are derived which define heat transfer in the so-called viscous shock layer between the shock wave and obstacle. With some simplified assumptions, these reduced to a system of ordinary differential equations which were solved by computer, using the method of successive approximations. The problem was attacked in two steps; in the first, calculations were made on the assumption that optical properties of the gas flow and vaporized impact material in the vicinity of the stagnation point were independent of wavelength, over a wide range of temperatures and pressures. Next, a calculation was made for the hypothetical flow of a low-temperature air plasma around a graphite sphere, with realistic optical behavior taken into account. It is assumed that graphite destruction occurs both by chemical reaction, resulting in CO and CN generation, and by evaporation of surface material in the form of C, C_2, and C_3. The example assumes a sphere radius of one meter and a surface temperature of 3×10^3K. Spectral characteristics of the shock layer are also calculated and analyzed.

An'shakov, A. G., G. Yu. Dautov, Yu. S. Dudnikov, I. S. Mazuraytis, and M. I. Sazonov. Experimental development of a production plasmotron. Fizika i khimiya obrabotki materialov, no. 1, 1969. 27-32.

Tests on an improved production prototype plasmotron in the 150-400 kw range are described. The plasmotron design was simplified as much as possible, resulting in the single-envelope geometry shown in Figure 1. This configuration is

claimed to improve deficiencies in existing models such as drooping volt-ampere characteristic, nonlinear increase in plasma temperature with increase in electrode current, and excessive overheating and erosion of electrodes. Electrode shielding and stabilization of arc position are obtained by peripheral injection of argon gas at G and G' as indicated in the figure. Use of shaped insert 3 and stepped anode 2 also contribute to improved arc stability and controllability. Dimensions given for tests models include: d_1, 0.7-0.85 cm; d_2, 2cm; d_3, 3.8cm; l_2, 24-37cm; and l_3, 12.5-16cm. Arc currents of 700a can be sustained with pure argon flows of G=25-46 g/sec and G'=2-2.5 g/sec; the plasmotron working medium is a 38% air-62% oxygen mixture. Operating characteristics and electrode erosion rates for operation up to 4.5 hours are given for several design variants. The prototype is judged to be a satisfactory design for providing extended plasmotron performance in the 150-400kw range in an aggressive gas medium.

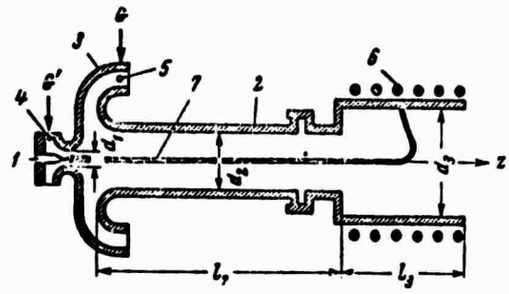

1-cathode;
2-anode;
3-beam forming insert;
4, 5-isolators;
6-solenoid;
7-arc

Fig. 1. Section of plasmotron

LASER SIMULATION AND RELATED EFFECTS

Krol', V. M.; and I. V. Nemchinov. Self-similar motion of a radiation-heated gas behind an absorption inducing shock wave front. Prikladnaya matematika i mekhanika, v. 33, no. 1, 1969, 20-29

A theoretical analysis is given of the motion and heating of a gas behind an absorption wave, propagating by a purely hydrodynamic mechanism. The general case considered assumes a local breakdown caused by an optical beam in gas, sufficiently intense to generate a shock wave at the boundary of the breakdown region; ionization occurring at the shock wavefront provides an absorption region for the incident radiation. In particular, the case of gas motion is examined when the radiation is incident at some discrete distance from the shock wavefront, causing a detonation wave. The analysis is made on the further assumption of a stepwise variation in applied radiation intensity. In this case, the detonation wave velocity also varies in a stepwise fashion, hence the problem can be treated on a self-similar basis.

Arifov, T. U.; G. A. Askar'yan, and N. M. Tarasova. Ionization of gases by the ultraviolet radiation emitted by a substance heated in the focus of a laser beam. Zhurnal eksperimental'noy i teoreticheskoy fiziki, v. 56, no. 2, 1969, 516-521.

The ionizing effect of ultraviolet radiation produced by interaction of a focused laser beam with a target is experimentally investigated. It is found that heating of a substance in the focus of a laser beam produces an ionizing flash of ultraviolet radiation. A ruby laser pulse with approximately 1.5j energy and 30 nsec duration was used for these experiments. Its beam was focused on a target in a chamber with variable pressure ranging from 10^{-6} to 1 torr. In a first series of experiments the ionizing effect of target emission was studied using plasma formed by photoionization in front of the target. A 14 cm lens was used to focus the laser beam; a diagnostic microwave beam (λ = 1 cm) was allowed to pass 4 cm away from the target. The experimental data confirmed the theoretical prediction that about 10% of the laser emission is converted to vacuum ultraviolet. The targets were aluminum, titanium, molybdenum and lead in air or hydrogen. In other experiments metal spherical mirrors were used to focus laser and u-v emission on targets and to separate the target plasma from the region of photoionization.

The total number of reflected ultraviolet quanta was lower by an order than the initial u-v radiation in the first part of the experiment. A third series of experiments was performed to measure directly the ultraviolet flash, using a luminophor with a photomultiplier. Various means of filtering and purifying the ionizing radiation are described in detail. The tests show that output of ultraviolet radiation increases nearly proportionally with laser radiation power. Numerous application possibilities of this phenomenon are discussed.

Afanas'yev, Yu. V.; E. M. Belenov; O. N. Krokhin; and I. A. Poluektov. Avalanche ionization of gas in optical breakdown over a wide range of flux densities. Zhurnal eksperimental'noy i teoreticheskoy fiziki, v. 57, no. 2, 1969, 580-584.

Reference is made to a previous work by Afanas'yev et al. (Zhurnal eksperimental'noy i teoreticheskoy fiziki, v. 56, no. 1, 1969, 256-263) where it was shown that for laser radiation densities of $q = cE_0^2/8\pi \leqslant 10^{15}$ w/cm^2 (c - velocity of light, E_0 - field amplitude), avalanche ionization causes an optical breakdown of gas. The process is related to radiation flux density through the characteristic parameter $\beta_0 \cong \gamma_{in} I_i/\alpha$, where γ_{in} is the frequency of nonelastic collisions of an electron with a neutral atom; I_i is the ionization potential of gas atoms; $\alpha = 1/3\, \varepsilon_0 \gamma_{eff}$, where γ_{eff} is the frequency of elastic collisions of electrons with atoms, and $\varepsilon_0 = e^2E_0^2/2m\omega^2$ is the effective energy of electron oscillations in the field of a light wave with a frequency ω. Previously only the limiting cases of β_0 ($\beta_0 \to 0$ and $\beta_0 \to \infty$) have been considered. In the present article the theory of optical breakdown of gases is developed for arbitrary values of β_0. By solving the kinetic equation the family of time-dependent energy distribution functions $f_{\beta_0}(\varepsilon, t)$ is obtained and a universal curve representing the β_0 dependence of the avalanche development constant γ is constructed. The function $\gamma = \gamma(\beta_0)$ in extreme cases of $\beta_0 \to 0$ and $\beta_0 \to \infty$ coincides with previously obtained values, and reaches its maximum at $\beta_0 = 0.25$.

Generalov, N. A., G. I. Kozlov, and Yu. P. Rayzer. "Bleaching" effect of a plasma caused by laser pulses. Zhurnal eksperimental'noy i teoreticheskoy fiziki, v. 56, no. 3, 1969, 789-791.

The authors investigate the absorption coefficient of a plasma to laser irradiation as a function of laser intensity, and show that at a relatively low intensity level there is a definite peaking in the transmitted light. An experiment was done with a xenon plasma generated in a shock tube, with the laser pulse synchronized to pass diametrically across the plasma at varying distances behind the reflected shock wavefront. The laser was a Q-switched ruby developing 50 ns pulses up to 20 Mw, focused to a parallel beam when intersecting the plasma. Plasma temperature was calculated to be 11,000°K. Experimental data show a definite "bleaching" range for incident levels around 10^2--10^3 Mw/cm^2. A contributing factor to the bleaching effect is suggested to be laser photoionization of atoms in upper levels, thus reducing their population. For a sufficiently large increase in pulse intensity, previously unexcited atoms become ionized, which increases absorption and ends the bleaching effect.

Bulov, A; and B. F. Ponomarenko. A method for studying dynamic stresses caused by laser radiation. Pribory i tekhnika eksperimenta, no. 1, 1969, 179.

The stress pattern developed in a plastic target by laser radiation has been photographed and analyzed. A ruby laser generating one millisecond pulses of 5-7j was focused onto the end of an ED 6 epoxy rod having a cross-section of 6 x 15mm^2. A portion of the laser beam was split off and redirected by prisms to provide cross-illumination of the specimen at the point of interest. Photochronograph recordings were made, triggered about 300 microseconds after the start of the laser pulse to insure observation of a spike-free pulse interval. The resulting photograph was typically an inclined light and dark striped pattern of nearly a constant stripe width, indicating a uniform pressure generation during the pulse action. Test records also indicate that stress wave velocities up to 1580 m/sec were generated.

Gorbenko, B. Z.; Yu. A. Drozhbin; S. D. Kaytmazov; A. A. Medvedev; A. M. Prokhorov; and A. M. Tolmachov. Optical air breakdown induced by ultrashort pulses and studied by means of a photochronograph with an image converter. AN SSSR. Doklady, v. 187, no. 4, 1969, 772-774.

In a previous paper by Kaytmazov et al (DAN SSSR, v. 180, 1968, 1092) the average propagation velocity of a spherical shock wave in plasma was determined. The present experiment was designed to investigate the dynamics of spark development in detail and to determine the maximum velocity of the shock wave. The records made by a FER-2 photochronograph from the screen of a UMI-92 image converter tube were used for this purpose. A triggering spark gap fired by the laser beam itself was included in the circuit. This reduced the time lag between the arrival of the radiation pulse and the beginning of the display to 10-15 n sec, thus permitting observation of the initial phase of optical breakdown in the air. The block diagram of the setup is shown in Fig. 1. A neodymium laser was used to generate a series of ultrashort pulses down to 10^{-12} sec, with a pulse train period of 13 n sec and energy of 2 j. Photochronograms are included which show that the bright region of the breakdown moves for an interval of 1 n sec in the direction of the laser beam with a velocity of 10^8 cm/sec; in the initial stage of the breakdown the velocity reaches the order of 3×10^8 cm/sec. The authors stress the complex nature of this phenomenon, and propose to discuss it in a later paper.

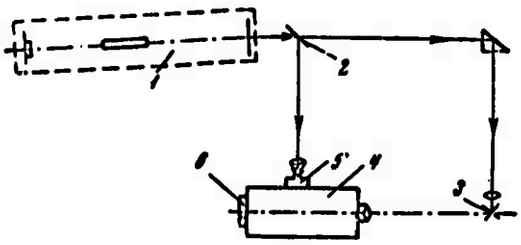

Fig. 1 - Air breakdown experiment

1 - laser; 2 - mirror with reflection coefficient R=10%; 3 - arc in the focus of the lens; 4 - photochronograph; 5 - spark gap trigger; 6 - camera.

Bykovskiy, Yu. A., A. G. Dudoladov, N. N. Degtyarenko, V. F. Yelesin, Yu. P. Kozyrev, and I. N. Nikolayev. Angular distribution of matter evaporated by a laser beam. Zhurnal eksperimentalnoy i teoreticheskoy fiziki, v. 56, no. 6, 1969, 1819-1822.

The authors note that for the case of laser-evaporated material subsequently deposited on an external substrate, measurement of the film thickness is difficult since it is typically on the order of 100°A or less. An experiment to overcome this problem is described in which a radioactive target was used. The measured radioactivity of the deposited layer was then taken as proportional to its depth. The target was a β -active Tl^{204} wafer placed at the center of a spherical shell, and irradiated by a ruby laser operating in both free-running and Q-switched modes. The angle of the target plane to the optical beam axis was varied from 30 to 90 degrees. Data show that the angular distribution density of the deposited film varied in a random fashion. Results further indicate that the bulk of the deposited matter was evaporated in the form of microscopic fragments; in addition, a substantial amount of fragments collected at the bottom of the spherical shell.

Bykovskiy, Yu. A., N. N. Degtyarenko, V. I. Dymovich, V. F. Yelesin, Yu. P. Kozyrev, B. I. Nikolayev, S. V. Ryzhikh, and S. M. Sil'nov. Energy distribution of ions formed by the interaction of a giant laser pulse with a solid target. Zhurnal tekhnicheskoy fiziki, v. 39, no. 9, 1969, 1694-1696.

The energy spectra of ions formed from impingement of a laser beam on a metallic target are described and analyzed. A Q-switched ruby laser was used which generated 40 Mw pulses of 20 ns duration, focused on an approximately 0.5mm^2 area of the metal target which was placed in a time-of-flight mass spectrometer. The ion path from target to detector was 450 cm; the test was run at 10^{-6} torr. Target materials included Al, Co, Mn, Nb, Cd, Mo, and W; however, the data presented for aluminum were a typical of all tested metals. The energy spectrum of singly-charged ions showed a dual peak: a main one at energies of approximately kT_o and a secondary peak at considerably higher energies. From the main peak, laser plasma temperature could be determined. Energy spectra up to quintuply-charged ions are given, and the electron-ion energy exchange mechanism resulting in the higher energy states is discussed.

Afanas'yev, Yu. V.; N. G. Basov; O. N. Krokhin; N. V. Morachevskiy; and G. V. Sklizkov. Investigation of gas-dynamic processes occurring in the evaporation of laser-irradiated solid substances. Zhurnal tekhnicheskoy fiziki, v. 39, no. 5, 1969, 844-905.

Gasdynamic parameters of evaporation processes of opaque materials irradiated by a low density (10^6 - 10^8 w/cm^2) laser radiation are measured. The specific impulse occurring in laser irradiation of various materials has been measured by a free-running neodymium glass laser with a maximum radiation energy of 800 j and pulse length of 1.5×10^{-3} sec. Radiation was focused on the target by a 30 cm lens. The condition $h < d$ was satisfied (h - depth of a crater, and d - diameter of the focused spot) for a "plane case" model. The measurement results are presented in Fig. 1 and 2.

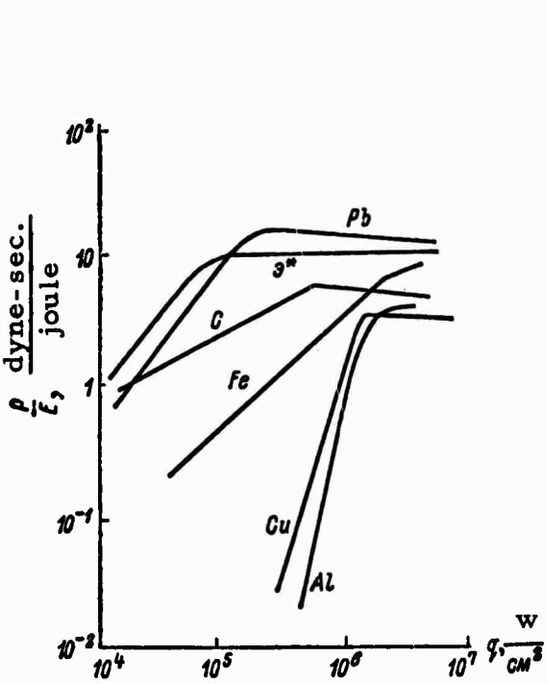

Fig. 1. Specific impulse P/E as a function of incident power density q.

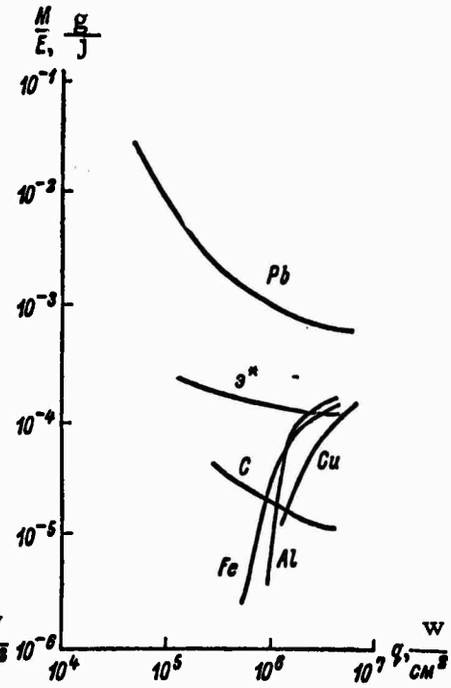

Fig. 2. Ejected mass per unit energy M/E as a function of incident power density q.

To record and measure the velocity of the shock wave created by expansion of the irradiated and vaporized material a form of Schlieren shadow photography was developed and successfully employed, as shown in Fig. 3.

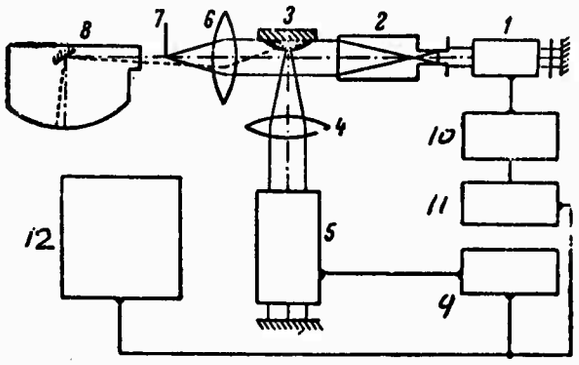

Fig. 3 - Experimental setup for a high-speed shadow photograph.

1 - ruby laser, operating in a regular giant pulse mode;
2 - collimator;
3 - target;
4 - lens focusing Nd laser radiation onto the target;
5 - Nd glass laser;
6 - Schlieren lens;
7 - optical knife edge;
8 - high speed photorecording camera;
9 - pump source for Nd laser;
10 - pump source for ruby laser;
11 - delay;
12 - control unit.

The measured velocity of the shock wave was about 400 m/sec. The overall reflected laser energy per pulse R was measured by the method described by Basov et al (ZhTF,v. 38, no. 1, 1968, 1973), and is presented in Table 1, where it is compared with the reflection coefficient R_o for a weak flux.

Table 1

Material	Energy, Joules	Rad. pwr density, w/cm^2	R, %	R_0, %
Steel	50	$8 \cdot 10^5$	40	63
	500	$6 \cdot 10^6$	30—45	63
Aluminum	50	$8 \cdot 10^5$	46	93
	500	$6 \cdot 10^6$	50—60	93
Copper	50	$8 \cdot 10^5$	65	90

Measured values of specific impulse P/E are similarly compared with values calculated by the formula proposed by Afanas'yev et al (ZhETF, v. 52, 1967, 966) in Table 2.

Table 2

Material	Range of flux $\times 10^6$, w/cm^2	$\frac{P}{E}$, $\frac{\text{dyne sec}}{\text{joule}}$ (exper.)	$\frac{P}{E}$, (theory)	$\frac{P(1-R)}{E}$ (theory)
Steel	1.2 ÷ 3.3	8.2	15.9	9.5
Carbon	0.13 ÷ 3.1	5.7	4.9	4.2
Lead	0.1 ÷ 4.3	15.7	43.0	—
Ebonite	0.8 ÷ 3.2	11.3	—	—
Aluminum	1.2 ÷ 3.5	4.25	13.5	6.1
Copper	4.15 ÷ 4.5	4.1	17.0	6.0

In Table 3 a similar comparison is presented for the ejected mass.

Table 3

Material	Flux density, w/cm^2	$\frac{M}{E} \cdot 10^{-5}$, $\frac{g}{joule}$ (exper.)	$\frac{M}{E} \cdot 10^{-5}$, $\frac{g}{joule}$ (theory)
Steel	1.1 ÷ 3.3	10.5	10.8
Carbon	2.2 ÷ 3.1	1.32	1.25
Lead	0.22 ÷ 4.3	1[illegible]	79.6
Ebonite	0.9 ÷ 3.2	1[illegible]	--
Aluminum	1.2 ÷ 3.5	15.8	9.0
Copper	4.15 ÷ 4.2	13.7	14.0

The disagreement between theoretical and experimental figures is discussed.

Stankevich, Yu. L. On the feasibility of stimulated amplification of characteristic X-ray emission. Akademiya nauk SSSR, Doklady, v. 191, no. 4, 1970, 805-806.

Referring to the possibility of creating population inversions at x-ray wavelengths by the ejection of electrons from the inner atomic shells, as proposed by Duguay and Renzepis (Applied Physics Letters, v. 10, 1967, no. 12, June 15, 1967, 350-352), the author points out that under certain conditions the necessary rise times of the pumping powers may be lower than those estimated by the above authors. He suggests that at densities close

to the solid state, a quasi-stationary population inversion with a multiple utilization of each atom may be created, resulting in a sharp increase of the inverted state lifetime and decrease of the required rise time of the pump pulse. He shows that the sustaining condition for the quasi-stationary population inversion of two electron states in the atom is satisfied for the transitions $1s\frac{1}{2} \rightarrow 2p_1$ (Line $K_{\alpha 2}$) in atoms of elements with $Z \lesssim 47$ and $1s\frac{1}{2} \rightarrow 2p\frac{2}{3/2}$ (Line $K_{\alpha 1}$) for $Z \lesssim 36$. The author estimates that at a solid state density of the laser material the inverted state may be preserved up to temperatures ~ 30 — 100 ev. By further comparing the cross section of the stimulated emission with the absorption cross section of the resonant photons of the higher level electron shells, it is shown that amplification is feasible if approximately (2 — 3) x 10^{-3} of the total number of atoms are in the excited state simultaneously.

Buzukov, A. A.; Yu. A. Popov; and V. S. Teslenko. Experimental study of an explosive process induced by focusing single-pulsed laser radiation in water. Zh. prikl. mekh. i tekh. fiz., no. 5, 1969, 17-24

A detailed experimental study is described of explosive phenomena induced by focusing a laser pulse in distilled water. A ruby laser focused by a 20-30 mm lens was used in two series of tests. In the first step, 0.5j pulses at 50-60 nsec duration were applied, during which time shock wave propagation from the focal point was recorded by an array of barium titanate pressure sensors. In the second step, 30 nsec pulses at 1.5j were applied, while shock wave pressure variation was measured as a function of its position relative to the optical axis and the focal point; in this case tourmaline crystal sensors were used. A detailed study of the high speed photographs shows that shortly after applying the laser pulse, excitation centers develop along the optical axis in the beam focus region, and continue to form for a time following pulse termination. Minute vapor bubbles first form at the focal point and propagate radially from the optical axis. After several microseconds the bubbles grow to form cavitation regions along the axis, with diameters on the order of several millimeters. Maximum cavity size can be calculated from $E_r = 4/3\pi r_m^3 P_0$ where E_r is kinetic energy of the displaced water, r_m is maximum cavity radius, and P_0 is the local hydrostatic pressure. Test data show that the opticohydrodynamic coefficient, i.e. the fraction of incident pulse energy converted to mechanical displacement

of the medium, is at least 7%. Other factors treated include the index η_k, which defines the energy absorption in radial motion of the water owing to pulsation of the generated bubbles. When the laser focus point is near the surface, a plume forms above the explosive region, as for a near-surface concentrated explosive charge. Figure 1 shows the test method; Figure 2 gives shadow photograph sequences taken at 62,500 frames/sec, showing cavity pulsation and plume effects. Figure 3 is a Schlieren photograph showing typical initial stages of cavity development, shock wave and reflected surface wave. The test results verify that the focused laser pulse duplicates the hydrodynamic effects of a chemical or electrical discharge explosion in water.

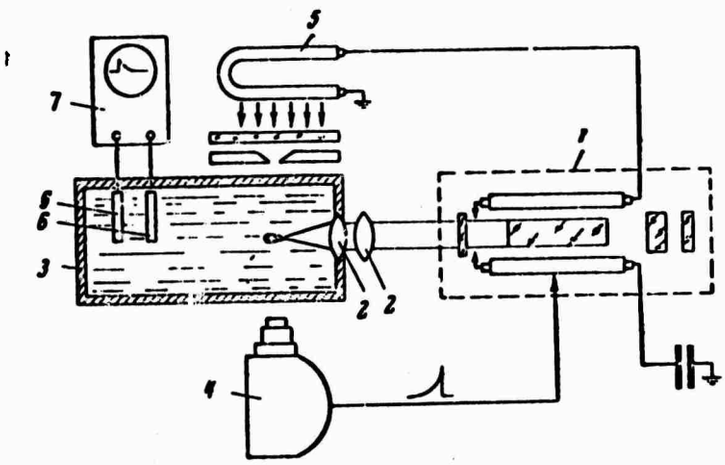

Fig. 1. Laser explosion test.
1 - ruby laser; 2 - focusing lenses; 3 - water vessel; 4 - SFR-IM high-speed camera; 5 - backlight; 6 - pressure sensors; 7 - oscilloscope

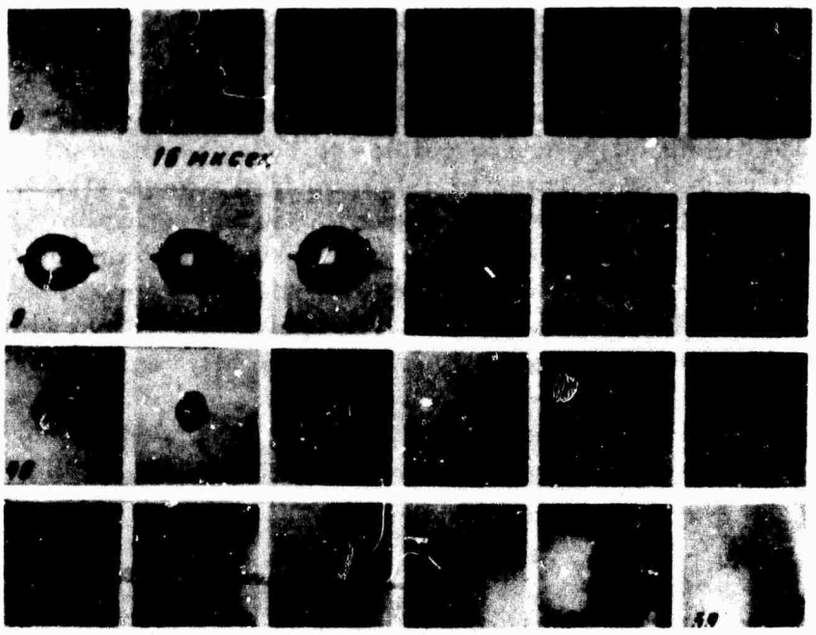

Фиг. 2а

Fig. 2. Explosion cavity formation.

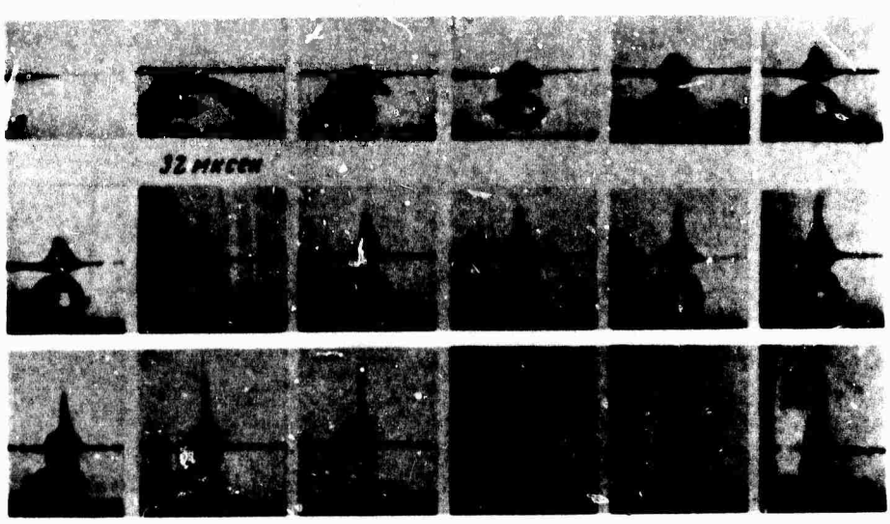

Фиг. 2б

Fig. 3. Plume formation from near-surface explosion.

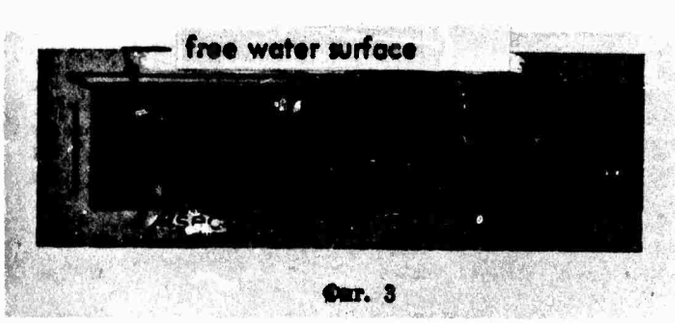

Фиг. 3

Fig. 4. Wave propagation near surface.

DEFORMATION OF MATERIALS

Aleksandrov, A. Ya., M. Kh. Akhmetzyanov, G. N. Albaut, and V. N. Baryshnikov. Polarized optical studies of large deformations. Zhurnal prikladnoy mekhaniki i tekhnicheskoy fiziki, no. 5, 1969, 89-99.

Several experiments are described in which elastic and plastic deformations in stressed materials are evaluated by means of a piezooptical polyurethane coating. The type used, identified as SKU-6 polyurethane, is transparent and can withstand elongations up to 100% of normal dimensions without exceeding its plastic limit; it also exhibits a distinct optical interference pattern when illuminated with polarized light. Experiments were made on tensile loading of narrow SKU-6 strips, approximating a one-dimensional strain, and various two-dimensional forms; the loading method is not specified. In a second part of the test, SKU-6 coatings were bonded to various metal specimens, including steel and copper, for optical observation of tension and compression stress patterns. Graphs and photos are included illustrating the elastooptical effects observed. Theoretical strain expressions are developed and shown to correlate well with test results; however, it is emphasized that these formulas depend largely on the physical parameters of the stressed material, and so must be rederived to suit any given case.

Blekherman, M. Kh., and V. L. Indenbom. Configuration of atomic planes bordering a crack, based on a modified Peierls-Nabarro model. Zhurnal prikladnoy mekhaniki i tekhnicheskoy fiziki, no. 1, 1970, 96-102.

An approach to analysis of crack propagation at the microscopic level is proposed. This is defined as investigating propagation mechanisms in terms of interactions with existing dislocations, vacancies, and other defects already present in the material structure. The method thus involves treating crack propagation on a small enough scale that it may be considered in terms of atomic planes which are sufficiently separated so that their interaction has a distinctly nonlinear character. The treatment is then developed in terms of a modified Peierls-Nabarro model, in which assumed local initial and boundary conditions are taken

into account. With certain simplifying assumptions this method is shown to yield maximum stress levels in the surface region bounding the crack, as well as an approximate description of crack configuration. The analysis is also claimed to be valid for analyzing the motion of large-scale dislocations in the stressed material.

V'yukov, L. A., Yu. N. Lokhov, and Yu. D. Fiveyskiy. On the theory of damage to optically transparent dielectrics from giant laser pulses. Fizika i khimiya obrabotki materialov, no. 4, 1969, 3-9.

Damage stresses caused by giant laser pulses in a transparent dielectric are analyzed theoretically, with the object of defining tolerable power densities. It is suggested that behind the shock wave propagating through the dielectric a phonon oscillation is excited within the lattice, causing intense local heating. The associated thermoelastic stresses can be high enough to cause breakdown of the crystal structure. Calculations show the possibility of local temperatures up to the order of 1,000°K and pressures up to 10^5 atm, or sufficient to break atomic bonds within a lattice. The stressed matter is partially converted to a highly compressed gas, in which sonic velocity is 1.5-2 times greater than in the surrounding dielectric, as reported in original experiments by Belikova et al (ZhETF, v. 54, no. 37, 1968). Expressions are derived for maximum beam intensity in terms of dielectric capabilities. The calculations assume a homogeneous defect-free crystal structure, hence represent an upper limit to realistically usable pulse power levels in ruby and other dielectrics.

Brekhovskikh, V. F., N. N. Rykalin, and A. A. Uglov. The possible effect of gas content in metals on the reaction zone of a laser beam. AN SSSR. Doklady, v. 190, no. 5, 1970, 1059-1062.

Theoretical and experimental data are given on the cratering effects of a laser beam on copper. A GOS-30Nd glass laser was used in a free-running mode, generating one μsec pulses varying from 2 to 7 joules. Focusing lenses were included to vary radiation intensity of the specimen surface. At the lower intensity levels, a noticeable difference in crater formation was

seen between photos of porous and monolithic specimens; crater diameters in porous specimens were up to twice as large. Porous specimens also tended to have local deep pits within a crater, apparently associated with entrained gas and solid impurities. Theoretical crater dimensions, as determined from an idealized gasdynamic model of the destruction process, were found to be much smaller than those produced experimentally. This discrepancy emphasizes the need for taking porosity and impurities into account when estimating a laser-produced cratering effect. The authors suggest extending their study to powdered metals, for which little laser damage research has been reported to date.

Shestopalov, L. M., B. A. Sidorov, N. I. Alekseyev, I. N. Zimkin, and M. I. Stepanov. Effect of laser radiation on metals. AN SSSR. Izvestiya. Metally, no. 2, 1969, 96-104.

Comparative effects of pulsed laser radiation on 28 pure metals are described. A He-Ne laser was used at one millisecond pulses, developing intensities up to 10^5 w/cm^2 on target surfaces. Incident radiation was defocused to a spot of several millimeters diameter in order to clearly reveal damage patterns. Tests were done in a 10^{-4} torr vacuum. Specimens were examined microscopically after irradiation and were also tested for hardness and strength properties. Tabulated data are given listing local melting characteristics, surface hardness, and other parameters as functions of laser beam intensity. Susceptibility to laser damage is found to depend on the reflective properties of the target metal surface, as well as on enthalpy of the metal at the fusion point, and on heat transfer properties from the surface layer. For several metals, e.g., steel, iron, chromium and titanium, an increase in surface microhardness resulted from laser irradiation. This tempering effect is thought to depend on the amount of variable-solubility entrained impurities, and on the presence of allotropic transitions in the test metals.

Akimov, A. I., and L. I. Mirkin. Certain relationships governing the effects of laser pulses on pure metals. Akademiya nauk SSSR. Doklady, v. 183, no. 3, 1968, 562-564.

Cratering effects of pulsed laser radiation on 28 chemically pure elements, principally metals, are described. The radiation source was a free-running ruby laser generating 1 ms pulses with energies up to 7 joules; incident power density was up to 10^5 w/cm^2. Target configurations ranged from thin foil to bulk material. For low melting-point metals, the irradiation generated approximately hemispherical clouds of luminescent vaporized surface material, within which were intense filaments of vapor rising from the crater interior surface. In higher melting-point metals, the filament effect became more diffused. Graphical data are given showing the almost linear relation between crater dimensions and incident light energy; crater size is also shown to have a definite correlation with the position of the metal in the Periodic Table. In many cases, the characteristic dimension h of the crater could be related to incident energy E by the approximate expression $h = AE^B$, where A and B are empirical constants. Examples given for Al, Cu, and W are: A = 0.47, 0.32, 0.24 and B = 0.57, 0.57, and 0.52, respectively. Boundary phenomena around the crater rim are also discussed. Since crater size varied almost linearly with pulse energy, it was possible to extrapolate back to find the threshold energy density required to start cratering action. Two such values given are 7j/mm^2 for aluminum and 12j/mm^2 for copper.

Akimov, A. I., and L. I. Mirkin. Structural effects and surface erosion in metals irradiated by 10^{-8} second laser pulses. Fizika i khimiya obrabotki materialov, no. 2, 1969, 11-18.

The authors report experimental results of laser damage to a variety of materials, most of which were metals. In the first part of the test, giant ruby laser pulses were directed onto 20 pure chemical elements, at 10^{-8} sec. duration and energies of 0.5 to 1 joule. In a second part of the test, various metallic compounds were irradiated, e.g., steels with differing carbon contents, using a neodymium glass laser developing up to 10 j pulses. In the ruby tests, the relatively low radiated power was insufficient to cause surface cratering except in the lowest melting-point elements, such as sulfur. Even in this case, crater depth did not exceed 10 microns. Data for the high-power portion of the test include crater surface profiles, x-ray analysis, and microphotos of the crystal lattice in the irradiated regions. The

x-ray analysis showed evidence of increased defect density in crystal lattices after irradiation, although this effect was less pronounced than has been observed with 10^{-3} sec. pulses having identical energy content. The observed damage phenomena are in accord with a proposed model of giant laser pulse action, in which a plasma is generated at the impact point and diverges through the surrounding region.

Mirkin, L. I. Plastic deformation of metals from the action of 10^{-8} second laser pulses. Akademiya nauk SSSR. Doklady, v. 189, no. 3, 1969, 528-531.

This article is a continuation of the studies by the author and co-workers (Akimov and Mirkin, Fizika i khimiya obrabotki materialov, no. 2, 1969, 11-18) on effects of short powerful laser pulses on a metal surface. In the present test, Q-switched laser pulses up to 35j at 10^{-8} second duration were applied to specimens of low-carbon steel. Crater formation, evaporation phenomena and dislocations in the neighboring crystal lattice were recorded and analyzed. At a 35j pulse level, craters were produced up to 0.9mm in diameter and 0.5mm deep, surrounded by solidified ejecta over an area 5mm in diameter. The resulting alterations in local crystal structure could be identified in 3 general zones, examples of which are given by microphotographs. A comparison with effects of 10^{-3} sec. laser pulses shows qualitatively similar cratering action, but more pronounced deformation in the case of the shorter pulses owing to sharper temperature gradients. A further comparison with mechanical impact effects shows that cratering action of a 20g mass with 4km/sec. impact velocity was an order of magnitude greater than for the 10^{-8} sec. laser pulses. The occurrence of twinning as a function of crater geometry is cited as a typical example of deformations caused by short laser pulses. From the experimental data, a qualitative model of shock wave propagation through the target area is suggested, showing the similarity to damage effects from a point explosive charge.

Akimov, A. I.; and L. I. Mirkin. Relationships governing metal damage from pulsed laser radiation. Fizika i khimiya obrabotki materialov, no. 1, 1969, 7-16.

This article is a more detailed treatment of pulsed ruby laser damage to a number of pure chemical elements, described by the authors in an earlier report herein .
In the present case, more data is given on the relations between crater dimensions and laser energy density for the target chemical elements, as well as for the relative flare geometries generated at the impact area. For a given laser radiation level, there was found to be a characteristic flare geometry for each of the elements tested. Photos of flares and craters for several irradiated metals are included. Figure 1 shows crater depths and diameters as functions of pulse energy for several of the tested metals. It was noted that in foil specimens, the crater diameters tended to be less than in bulk specimens, which indicates the relative difference in outflow of molten metal during the cratering process.

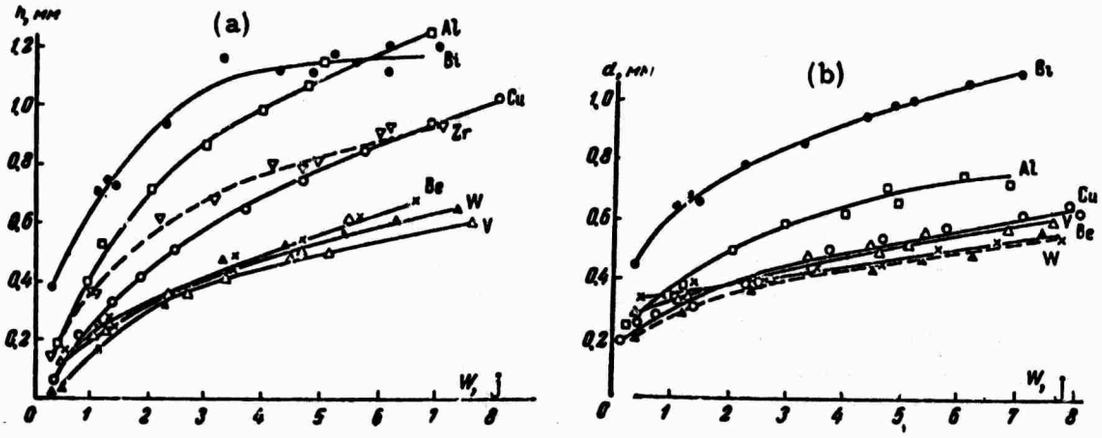

Figure 1. Crater dimensions vs. laser pulse energy. (a) - depth; (b) - diameter

Grebenkin, G. G., and A. A. Kaminskiy. The development of transve- . cracks at holes in compressed bodies. Mekhanika tverdogo tela, no. 2, 1969, 172-178.

The development of equilibrium transverse shear cracks which radiate from the boundary of a curvilinear hole are investigated, for the case of a body under compression. The theoretical treatment assumes a simplified model, i.e., one in which the cracks are separate from each other. An

approximate method is suggested for obtaining the function representing the boundary of an arbitrary aperture with two arbitrary cracks symmetrically opposed. Stress conditions are examined near the curve boundary, assuming straight line cracks developed in a thin elastic plate subjected to steady-state compression and tension loading. The critical loads resulting in shear crack formation are determined for the case of two identical cracks radiating from a square aperture in a thin plate under compression.

Mikhaylov, A. M. Extension of the beam approach to problems of crack theory. Zhurnal prikladnoy mekhaniki i tekhnicheskoy fiziki, no. 3, 1969, 171-174.

This article is an extension of an earlier work by the author, in which crack propagation along a rod is examined. It is assumed that the behavior of the rod is adequately described by the beam theory of Bernoulli-Euler. The latter approach is first extended to a two-dimensional case, namely for propagation of a crack along the median plane of a thin plate. This type of problem can be experimentally analyzed by the destruction of laminated materials, or by stripping two bonded sheets apart. The beam model for determining crack generation is next extended to include the effect of transverse force on bending, and also the rotational inertia of transverse cross sections of the bar. It is shown that these factors set the conditions for the limiting velocity of crack propagation. The cited equations were obtained by using the principle of least action, which greatly simplifies the treatment.

Galin, L. A., Ya. B. Fridman, G. P. Cherepanov, Ye. M. Morozov, and V. Z. Parton. Conditions at crack terminations. IN: Akademiya nauk SSSR. Doklady, v. 187, no. 4, 1969, 754-757.

The authors note that conditions at the terminations of stress cracks in solids must be arrived at through a separate analysis which does not follow from expressions for crack motion and configuration. Solutions to this problem for elastic bodies can be obtained by using the concept of the Irwin condition for brittle or quasi-brittle destruction. A general expression for limit stresses at a crack termination is thus obtained, followed by separate qualitative analyses for the specific cases of elastic and elasto-plastic materials.

Morozov, Ye. M. The variational principle in the mechanics of destruction. IN: Akademiya nauk SSSR. Doklady, v. 184, no. 6, 1969, 1308-1311.

A possible solution to the problem of defining crack propagation is suggested. The approach is free of the usual constraint that cracks are assumed to propagate in straight line segments, hence is more generally applicable. The problem is attacked by treating a sequence of arbitrarily small elements of the stressed material, each containing a segment of a crack, according to elasticity theory. This yields a class of functions which can be solved by the variational principle. Starting with the energy balance for an arbitrary crack, the author examines specific cases of propagation along fixed and variable trajectories, and shows that the method permits prediction of crack termination location for a given load condition. Results are in agreement with the Griffith-Irwin theory.

Morozov, Ye. M. Energy conditions for crack propagation in elastoplastic bodies. IN: Akademiya nauk SSSR. Dok'ady, v. 187, no. 1, 1969, 57-60.

Energy balance criteria are proposed as a method for solving the problem of crack propagation in an ideal elastoplastic body. The analysis is restricted to small areas symmetrically opposed at the ends of an existing crack, at which concentrated plastic deformations are assumed to occur nonlinearly as a function of applied stress. The energy balance condition can then be expressed in terms of the energy increment required for an incremental degree of plastic deformation. Graphical solutions are included showing limit stresses thus obtained for crack propagation in thin sheet materials having assumed strength and elasticity properties.

Cherepanov, G. P. Crack propagation in viscous materials. Mekhanika tverdogo tela, no. 1, 1969, 122-127.

Expressions are derived which define idealized crack propagation in a variety of materials. The stressed region in question is limited to a differential area bounding the termination of an existing crack; symmetrical linear propagation under constant

load is assumed. In the most general case, the increase in crack length l will be a function of applied stress N, elapsed time t, and temperature T_0, or $dl = \varphi_1 dN + \varphi_2 dt + \varphi_3 T_0$. In the cases actually treated, the destruction process is assumed to be either isothermic or adiabatic, so that the third term drops out and the problem reduces to finding values for φ_1 and φ_2. This is done for several combinations of assumed elastic, plastic and viscous materials, as well as for brittle matter. Using a modification of the Neyber concept, the author also arrives at an expression for rate of crack growth for the assumed model.

Martynyuk, P. A., and V. F. Tarasov. Constant velocity crack propagation. Zhurnal prikladnoy mekhaniki i tekhnicheskoy fiziki, no. 3, 1969, 168-171.

A rigorous solution is given to the planar self-similar problem of Broberg for constant velocity crack propagation. The model assumes a steady-state tensile stress applied to the material, and also a finite region in the vicinity of a crack termination within which shear stress magnitude and velocity can be quantitatively expressed. Formulas are derived which define crack propagation velocity in terms of applied stress and developed shear stress, for which sample graphical solutions are given. The analysis confirms the findings of Barenblatt et al (Prikladnaya matematika i mekhanika, no. 2, 1962) that for a given material, there exists a minimum threshold for crack propagation velocity.

Novozhilov, V. V. On the theory of equilibrium cracks in elastic bodies. Prikladnaya matematika i mekhanika, no. 5, 1969, 797-812.

This article is an expansion and refinement of the author's previous theoretical work on crack propagation in elastic material (Prikladnaya matematika i mekhanika, no. 2, 1969). The analysis is made on the basis of atomic interactions, and treats crack formation in elastic bodies as a nontrivial form of equilibrium deformation, i.e., crack formation is considered as a large-scale

instability in the trivial equilibrium state. The resulting treatment leads to a refinement of the criteria for brittle destruction in the vicinity of crack terminations. Using the model postulated by Griffiths, the author also obtains an approximate method for evaluating the load capacity of a material subject to equilibrium cracks.

Palatnik, L. S., T. M. Ravitskaya, and I. M. Lyubarskiy. On the mechanism of forming secondary structures from impulse loading of steel. IN: Akademiya nauk SSSR. Doklady, v. 191, no. 3, 1970, 568-571.

A brief summary is given of experimental observations on the formation of local secondary structures in steel. Specimens of high-carbon austenitic steel were subjected to shock loads up to 180 kgm, after which cross-sections of the specimen were examined by x-ray analysis, electron microscopy and micro-hardness tests to determine the changes in local structure. Results indicate that local surface or subsurface regions of increased micro-hardness are generated by this type of shock stress; this can occur at sonic or even supersonic rates. Sample microphotographs are included typifying several such formations.

Kaminskiy, A. A., and Ya. Ya. Rushchitskiy. Applicability of the Volterra principle in studying crack propagation in inherently elastic media. Prikladnaya mekhanika, v. 5, no. 4, 1969, 102-108.

The problem of equilibrium crack propagation in a linear inherently plastic medium is examined. In particular, the necessary conditions are set forth which permit the use of the Volterra principle for determining propagation parameters at the crack terminations. The model assumes an existing crack under tensile loads which are symmetrical but functions of both crack length and time. Illustrative examples are given to verify the applicability of the Volterra principle for the elastic medium case.

HIGH-PRESSURE RESEARCH

Anikina, L. D., G. I. Berdichevskiy, V. I. Mali, and T. M. Sobolenko. The interaction of copper and molybdenum under explosive loads. Fizika goreniya i vzryva, no. 1, 1970, 120-122.

An explosively compressed mixture of Mo-Cu was investigated by x-radiation. The samples for investigation were made from powder pressed into caps made of tsepon (sic) varnish. The composition of the crystals in the Mo-Cu mixture zone was studied with a microprobe. It was determined that 3-5% Cu is found in the molybdenum, but in the copper molybdenum practically was not present. According to the literature, solubility has not been established either in the solid or in the liquid phase for the system Mo-Cu. The solid solution of Cu-Mo obtained hence can be explained only by the events related to a shock wavefront.

Bakanova, A. A., I. P. Dudoladov, and Yu. N. Sutulov. Electron transitions in hafnium europium and ytterbium under high pressures. Fizika tverdogo tela, no. 7, 1969, 1881-1884.

Dynamic compressibility properties of Eu, Yb and Hf have been determined under shock wave loading from 100 kbar to 3-4 Mbar. The compression wave was generated in an explosive test apparatus, using different amounts of charge; target specimens were mounted on grids placed in the shock wave path. Tabulated and graphical data are given for parameters of interest, including mass and wave velocities, compression factor and density for several shock pressure levels. One characteristic common to all three elements is a slope discontinuity in the D-U curves, indicating a discrete jump in compression rate at some critical pressure. The effect was most pronounced in Eu, where the critical point occurred at 380 kbar. The phenomenon is believed to be associated with transition of electrons from external s-levels to internal d-levels. The authors compare their findings with other shock compression data for similar trivalent rare earth elements.

Seryakov, K. I. Condensation on the wall of a shock tube during the propagation of a shock wave in vapor. Fizika goreniya i vzryva, no. 1, 1970, 48-54.

In this article, the process of film and drop condensation of water vapor on the surface of glass observation windows is investigated. Results are presented for the measurement of film thickness, and for computing this thickness from a formula derived in the article. The examination conducted and the analysis of the related experimental work show that when planning any investigation in shock tubes filled with vapor, and in the interpretation of the results, special attention must be paid to possible condensation of the vapor. In a number of cases, striving for the "pure" experiment, i.e., for the complete elimination of gas impurity from the vapor under study, can lead to the loss of a homogeneous sample. On the contrary, the presence of such an impurity can ensure the success of the experiment, as was the case in working with mercury and iodine vapors.

Deribas, A. A., and A. M. Staver. Shock compression of a mixture of TiO_2+$BaCO_3$ powders. Fizika goreniya i vzryvov, no. 1, 1970, 122-123.

A mixture of powders of TiO_2 (29%) + $BaCO_3$ (71%) was subjected to impact compression in cylindrical molds. After detonation of the 150- and 200- gram charges of hexogene, the mixture became a monolithic cylindrical briquette with a diameter of 2 to 4 mm, which had a yellowish-green color. The physical properties of the compressed mixture were studied, particularly its piezoelectrical properties. The dielectric losses, dielectric constant, and electrical resistance were measured. The experiments described show, that during shock compression of a mixture of TiO_2 and $BaCO_3$ powders there occurs the synthesis of barium titanate, which is widely used in transducers for measuring the pressure in shock waves. In several cases, the ferreolectric effect was established without subsequent polarization, which may attest to the ordering of the polar axes of the individual crystals of $BaTiO_3$ resulting in conjunction with the synthesis. This ordering is evidently the net effect of a large number of electrical moments, which have similar direction or primary orientation in a single direction as a result of the passage of the shock wave through the $BaTiO_3$ sample. These investigations show that in certain materials, the polarization effect can be sustained after unloading.

SOIL MECHANICS

Lyakhov, G. M. Determining viscous properties of soil. Zhurnal prikladnoy mekhaniki i tekhnicheskoy fiziki, no. 4, 1968, 68-71.

An experiment is described whose object was to evaluate the quantitative effect of soil viscosity on propagation of a compression shock wave through it. The test was performed using dry sand of average grain size confined in a 24 cm. diameter smooth-walled cylinder, subjected to an air shock wave as indicated in Figure 1. In one part of the test the sand specimen received both incident and reflected shock loading from the shock tube and wall; in a second part, the cover aluminum disc was subjected to direct shock loading. In both cases, the specimen density was approximately 1.55g/cm^3; moisture content was 3-10% and maximum compression wave velocity was 80-100 m/sec. Data were taken to establish the relationship between load level and displacement or deformation in the sand specimen. In all cases, the deformation peak lagged the loading peak, verifying the presence of viscous drag in the specimen. A more detailed viscosity mechanism is suggested, broken down in terms of elastic and plastic deformation caused by the shock wave. For the experiment described, the approximate value for soil viscosity index was found to be $\eta = 3 \times 10^4$kg/μsec.

Fig. 1. Soil viscosity experiment. 1-aluminum disk; 2--5-pressure sensors. Arrow shows shock wave path.

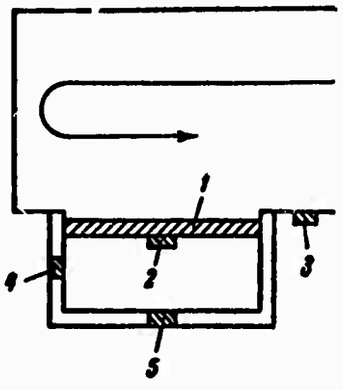

Nikolayevskiy, V. N. Hydrodynamic analysis of shock curves in heterogeneous mixtures of materials. Zhurnal prikladnoy mekhaniki i tekhnicheskoy fiziki, no. 3, 1969, 82-88.

Equations of state are derived for high-pressure shock transfer through a heterogeneous mixture of materials. A hydrodynamic

approach is used based on a model of two mutually permeable complex media which are assumed to be initially in the liquid phase, in which case phase pressures are equal. Compression of individual phases is shown to deviate from a Hugoniot adiabatic curve, as has been previously observed for the case of shock transfer through open-pore media. Using the general expressions first derived, the author briefly considers the porous media case, where the open pore regions may be considered as the second "phase" of the system. The anomalously high temperatures arising from shock transfer in this case can be accounted for on the basis of the proposed non-Hugoniot adiabatic model.

Smirnov. V. V. On the resistance of rock to crack propagation. Fiziko-tekhnicheskiye problemy razrabotki poleznykh iskopayemykh, no. 1, 1969, 58-62.

An analysis of crack resistance of rock to shock loads is presented in terms of modulus of cohesion and of surface stress concentration caused by the applied load. Test data were obtained using a pyramid-shaped diamond to apply concentrated loads to test specimens of siderite, conglomerate, sandstone and plastic. Crack size and propagation rate were observed as functions of load and test specimen parameters. Each type of rock specimen is shown to have a characteristic value of the constant B (kg/mm), defined as the force needed to propagate a crack over a unit distance per unit specimen width. For rock with clearly granular structure, this constant takes the general form:

$$B = B_0 + kd^{1/2}, \qquad (1)$$

where B is a constant determined by mineral content, d is mean grain diameter, and k is a constant with the dimensions of modulus of cohesion. As Eq. 1 shows, increased grain size requires greater force for crack propagation, owing to increased resistance to plastic deformation. From further analysis based on applied stress concentration and known elastic moduli, it is shown that the effective surface energy density in rock is proportional to B and can be found experimentally. Finally, if the elastic modulus E is known, it follows that the relative modulus of cohesion K_0 can be determined from $K_0 = (EB_0)^{\frac{1}{2}}$.

Rykov, G. V. Effect of deformation rate on compressibility and shear of clay and sandy soils under short-term loads. Zhurnal prikladnoy mekhaniki i tekhnicheskoy fiziki, no. 3, 1969, 155-160.

Experimental data from several cited authors are analyzed to show the effect of deformation rate on compressibility and shear of several types of soil. Short-term shock loads only were considered, applied either by mechanical impact in a cylinder and piston, or by explosives. Soils tested included several varieties of clay, loam and sand. A quasistatic loading was assumed as an approximation for calculation purposes, in which wave effects in the soil samples were neglected. Under the measured conditions of compressibility and shock wave velocity, this assumption was shown to be not over $\pm$15% in error. Graphical data are given which compare the time characteristics of load stress and deformation for several soil types at different specific weights and moisture content. The data established a definite correlation between compressibility and deformation rates, or viscosity, for clay and sandy soils. A similar analysis with respect to shear in the specimen as a function of deformation rate shows a much weaker correlation; it follows that to a first approximation, viscosity effects can be neglected when shear alone is to be considered.

Kolkov, O. S., V. I. Kulikov, A. M. Tikhomirov, and A. F. Shatsukevich. Effect of static pressure on the motion of sandy soil following an explosion. Zhurnal prikladnoy mekhaniki i tekhnicheskoy fiziki, no. 3, 1969, 165-167.

Laboratory experiments are reported on comparative displacement velocities of loose and compacted dry sandy soil following an internal explosion. Figure 1 shows the test vessel and sensor configuration; to obtain a compacted specimen, air was exhausted from rubber shell 5, giving a uniform surface pressure of about 1 kg/cm^2. Data from TNT and electrical detonations developing up to 8.5 kj were used for comparison; particle velocity behind the shock wave was detected by the motion of inductive pickup 3, moving through an applied external magnetic field. At sufficient radial distances from the detonation point, the arrival times of velocity maxima were found to be a nearly linear function of radial distance, over the limits observed. Arrival velocity

was greater for compacted than loose soil specimens. In compacted soil tests, there was no substantive difference in effects from chemical and electrical explosions, which verifies the usefulness of the latter for tests of this type. The results presented agree well with cited previous reports on the subject.

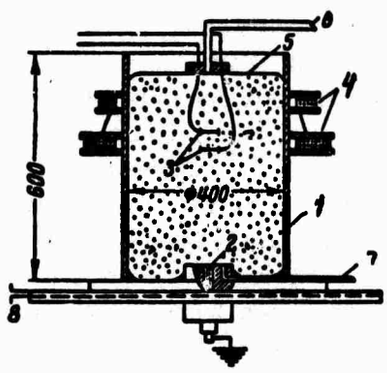

Fig. 1. Explosion test vessel. 1-brass shell; 2-charge holder; 3-velocity sensor; 4-field coils; 5-rubber liner; 6-exhaust port; 7, 8-leads. Dimensions in mm.

Vovk, A. A., V. I. Kononenko, I. A. Luchko, and V. A. Plaksiy. Study of shock wave parameters from detonation of horizontal cylindrical charges in loam. Zhurnal prikladnoy mekhaniki i tekhnicheskoy fiziki, no. 3, 1969, 161-164.

Results of shallow underground explosion tests in loam are described. Cylindrical charges were buried at depths ranging up to about 1 meter, with pressure and velocity sensors positioned around the charge in boreholes in a horizontal plane bisecting the charge cylinder. Inductive velocity pickups with constant magnetic fields were used. The main object of the test was to correlate shock pressure amplitude and propagation velocity with the physical parameters at hand, i.e., size and depth of charge, radial distance from charge axis, and existing soil parameters. The latter included mean grain size, specific weight, and soil moisture content. Over the range of depths and charge sizes tested, stress magnitudes and propagation rates were generally related to charge size and depth by an exponential function. Tabulated results are given with empirical values for the constants of this function, which in turn depend on test conditions. The data show that shock stresses tended to increase with greater charge depth; it is hence concluded that all tests were done near enough to the surface that a strictly confined explosion did not occur.

Alekseyenko, V. D., and G. V. Rykov. Experimental data on stress wave parameters from underground and contact explosions in soil. Zhurnal prikladnoy mekhaniki i tekhnicheskoy fiziki, no. 4, 1968, 65-67.

The authors report on comparative experiments on underground and contact explosions in clay and sandy soils. The objective was to derive a quantitative relation between the energy disseminated in an underground test and that fraction of contact explosion energy which also disseminates underground. The analysis is based on the premise that in a contact explosion, the underground stress parameters which are developed within a certain angular limit of the vertical axis of symmetry will be qualitatively the same as for an equivalent underground explosion. From previously reported data, this region of equivalence holds over a solid angle up to 30° off the axis of symmetry. With this assumption, the problem reduces to determining the fraction of energy from a contact explosion which will be absorbed into the soil, as determined by charge size and soil parameters. From experimental data, an empirical expression for this fraction is derived, expressed in terms of measured radial and axial stres maxima in the soil. The technique thus permits the effects of a contact explosion to be translated to those of an underground explosion, and vice versa, under identical soil conditions.

Mosinets, V. N. Conditions for brittle and plastic destruction of rock by an explosion. IN: Mel'nikov, N. V., ed. Problema razrusheniya gornykh porod vzryvom (The problem of rock destruction by an explosion). Moskva, Izd-vo nedra, 1967, 77-100.

A detailed summary is presented of current theory on the factors which govern crack propagation in rock. From experimental data of several cited authors, it is shown that crack propagation generally can be treated in three discrete time intervals, i.e., an initial interval following start of stress in which cracks propagate relatively slowly; a second brief interval with a rapid increase in propagation rate; and a final period during which crack propagation rate levels off at some steady-state value. The second acceleration period is relatively so short it may be neglected, resulting in the simplified two-step model suggested by Smecal. The comparative degrees of brittle cracking and plastic deformation are functions

of load stress gradient as well as of inherent rock characteristics. It is noted that many types of rock can exhibit either kind of destruction or a combination of both, depending on the magnitude of the stress gradient. For a given gradient, the corresponding destruction type will then depend on rock structural factors, including dynamic compressibility, acoustic hardness and Poisson ratio of the rock in question. Sample data are given illustrating destruction mechanisms in several types of rock, for the particular case of explosion stresses. It is concluded that in the case of explosions, a differentiation between brittle and plastic destruction will only appear within a limited proximity to the explosive charge; the author gives this limit as about fifty charge radii. Beyond this active zone, plastic deformation becomes the dominant form of destruction.

Lyakhov, G. M. Experimental study of shock compression curves in soil and rock. IN: Mel'nikov, N. V., ed. Problema razrusheniya gornykh porod vzryvom (The problem of rock destruction by an explosion). Moskva, Izd-vo nedra, 1967. 57-68.

A general anlaysis is given of the factors governing shock stress propagation in rock, followed by examples of experimental data. The author considers the effect of directivity and rate of shock wave propagation, in addition to its magnitude. The model used assumes a shock wave propagating spherically through rock media which are divided into the following categories: linear elastic; nonlinear elastic, in which the stress-strain curves for loading and unloading are dissimilar; and combined elastic/plastic, which behaves as elastic for small loads and as plastic for large loads. In any case of explosion-generated stress propagation through a solid medium, the problem is further complicated by the fact that the type of reaction to stress is not constant, but is also a function of radial distance from the explosion source. Comparative test data are listed for local stress levels developed as functions of explosive charge size and radial distance from it. Media cited include water-bearing and dry soil, water, and granite. It is concluded that in rock there is in general, a difference in the effect of static and dynamic (e.g., shock) loading; in particular, additional deformation can occur behind an explosive shock wave as a function of both stress magnitude and duration of application.

Rodionov, V. N., V. M. Tsvetkov, and P. V. Speranskiy. Studies on the effect of strength in explosions in solids. IN: Mel'nikov, N. V., ed. Problema razrusheniya gornykh porod vzryvom (The problem of rock destruction by an explosion). Moskva, Izd-vo nedra, 1967, 15-21.

Laboratory explosion tests are described whose object was to determine explosive effectiveness in terms of a constant A, defined as the ratio of explosive cavity size to charge weight. This factor varies by several orders of magnitude, depending on the strength of the solid medium. One specimen used was rock salt, chosen because it retains its elastic properties even in relatively small masses, and also because it normally is almost crack-free. A second propagation medium used was sodium tiosulfate ($Na_2S_2O_3 5H_2O$), chosen for its small grain size and its workability under laboratory conditions. In all cases the specimen size was made large enough so that the explosion cavity would have time to form before the shock wave reached the specimen boundaries, so that for these particular test purposes the specimen could be considered infinitely large. From data of previous authors, this required a cube about 250 mm on an edge for rock salt, based on a one gram explosive charge. Specimens were also confined in a metal shell to preserve stress pattern formations for subsequent observation. Spherical charges of TEN were used, varying from 0.2 to 2.4 g and up to 15mm in diameter, centrally placed in the specimen. Cross-sectional photos of specimens after explosion are shown, illustrating the cavity geometry. Relationships derived from test data show that approximately half of the explosive energy is absorbed in cavity formation.

Pokrovskiy, G. I. A generalized method for calculating stresses from explosions in rock. IN: Mel'nikov, N. V., ed. Problema razrusheniya gornykh porod vzryvom (The problem of rock destruction by an explosion). Moskva, Izd-vo nedra, 1967. 5-14.

The author notes that in spite of the wide existing variety of rock characteristics, their behavior in transmitting shock wave stress maxima from explosions are quite similar. It follows that a generalized expression could be derived for predicting energy

absorption in rock media as a function of radial distance from the detonation point, irrespective of rock types. The author does this in terms of relative excess energy at the shock wave front; since it does not allow for energy dissipated in crack propagation, the derived expression must be considered as an upper limit to stress maxima in the rock. Experimental validation was obtained from detonation of TNT and other explosive charges in rock, including granite and marble. Figure 1 shows a composite graph of the author's and other experimental data, together with the theoretically derived curve. While there was a wide divergence of results for different rock and explosive types, the experimental mean was found to be close to theoretical curve 4, particularly in the range below the crush-resistance limit of the rock. The general expression derived is also claimed to be adaptable for explosion stress calculations in liquid or gaseous media.

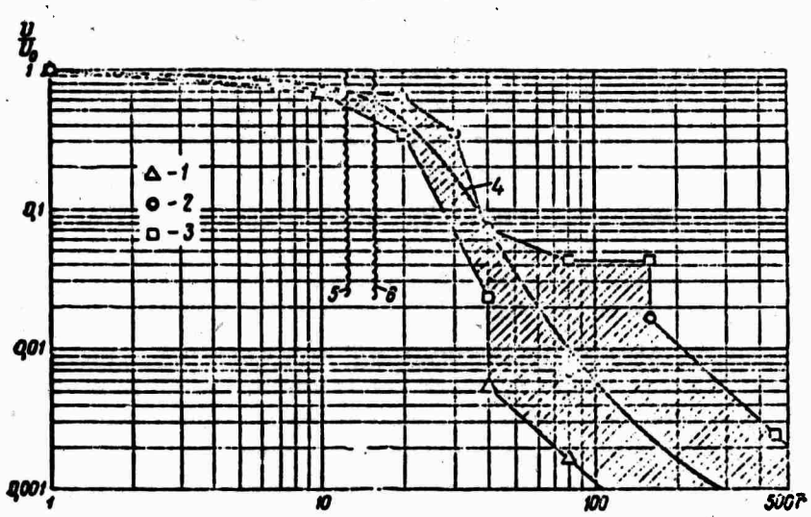

Fig. 1. Fraction of energy retained in shock wave. 1-TEN in marble; 2-TEN in granite; 3-TNT in granite; 4-theoretical; 5, 6-crush limits for granite and marble.

Vovk, A. A., G. V. Rykov, V. G. Kravets, V. A. Plaksiy, and I. A. Luchko. Experimental study of compressibility of loam from explosions. Prikladnaya mekhanika, v. 5, no. 4, 1969, 132-135.

Experiments on explosive compressibility of loam are described, from which expressions are derived defining radial and tangential stresses as functions of test parameters. The latter include charge size and depth, radial distance from the charge, and soil constants. The soil region tested had a nominal density of 1690 kg/m^3 and a moisture content of 11-15%; concentrated explosive charges from 2 to 250 n were used. Deformation was detected by a buried strain gauge array, and was also measured by

relative radioactivity levels in core samples before and after an explosion. Graphs of radial and tangential stress maxima are shown as a function of radial distance from the charge center. Calculated soil deformation on the basis of shock wave parameters was found to be appreciably less than that actually measured. This is explained by the fact that the calculated method does not take into account the entire active stress time, i.e., unloading stress is not accounted for. The tests also verify the accuracy of the radioactive measurement method for determining density in the compacted region. A similar approach is concluded to be feasible for explosion stress analysis in clay or sandy soils.

Krivtsov, V. A. Determining the cavity radius from an underground explosion, in the presence of residual pressure from explosion products. IN: AN UkrSSR. Institut geotekhnicheskoy mekhaniki. Vzryv v poristykh i dispersnykh sredakh (Explosions in porous and dispersed media). Kiev, Izd-vo naukova dumka, 1969. 28-33.

Expressions are derived for calculating cavity radius from confined explosions, for the idealized case in which the pressure generated by explosion products is maintained for an indefinite length of time. Examples of spherical, cylindrical and planar charges are given, with typical parameters of TNT assumed, i.e., ρ_0 equals 1.6g/cm^3, and detonation rate equals 7 km/sec. For a spherical charge it is thus calculated that cavity radius will be 11.0 (r_o) where r_o is charge radius. For a cylindrical TNT charge, cavity radius is similarly calculated to be 35.6 (r_o); and for a planar charge, 1260 (r_o) in which case r_o is defined as half the plane width. In the latter case, the planar area is assumed sufficiently larger than plane thickness that edge effects may be neglected. Comparisons made with experimental data on various soils show that the predicted values overestimate actual cavity radius by 20 to 35%, owing to disregard of energy dissipation in cracks, pores, etc. However, tests of confined explosions in clay soil have shown that residual cavity pressure will remain practically constant for periods on the order of a month.

Kazakov, N. N. Pressure and mass velocity in the shock zone of an explosion. IN: AN UkrSSR. Institut geotekhnicheskoy mekhaniki. Vzryv v poristykh i dispersnykh sredakh (Explosions in porous and dispersed media). Kiev, Izd-vo naukova dumka, 1969, 45-52.

On the basis of a mathematical model previously suggested by the author, a number of computer-generated graphical solutions are given which relate explosion product and shock wave velocities to elapsed time following a confined explosion. A soil with nominal 100 mm diameter porosity is assumed, and theoretical results are given for charges of both no. 6 ammonite and igdanite. As an example of the utility of the method presented, the author superimposes pressure-vs.-time and pressure-vs.-cavity radius curves, and shows that the time for a cavity to attain a given radius can be readily determined from them. For one cited case assuming an ammonite charge, it is shown that 17 μsec following detonation the cavity will have reached a diameter of 120 mm. Similar time and distance relationships are developed for explosion product and shock wave front velocities. From tabulated data for igdanite explosions, values of instantaneous particle velocity are shown in Table 1 as functions of elapsed time and radial distance from the charge center. Solutions were obtained on a Ural-2 computer, using a program designed by the author.

Table 1

V (R, t)

t, μsec	R, mm						
	80	105	209	316	401	504	613
10,7	513	276	—	—	—	—	—
30,5	261	159	80	—	—	—	—
51	198	116	59	39	—	—	—
67	147	99	50	33	26	—	—
87	122	86	43	29	22,6	18	—
108	104	76	38	25	20	16	13

Vovk, A. K., G. I. Cherniy, V. G. Kravets, V. A. Plaksiy, L. I. Demeshchuk, I. A. Luchko, I. I. Denisyuk. Study of the compressibility of loam from a confined explosion. IN: AN UkrSSR. Institut geotekhnicheskoy mekhaniki. Vzryv v poristykh i dispersnykh sredakh (Explosions in porous and dispersed media). Kiev, Izd-vo naukova dumka, 1969, 64-70.

(This article describes the same tests reported by Vovk et al on page herein.)

Akutin, G. K., A. G. Smirnov, V. A. Plaksiy, and I. A. Luchko. Effective zone of a cylindrical explosive charge in a compressible medium. IN: AN UkrSSR. Institut geotekhnicheskoy mekhaniki. Vzryv v poristykh i dispersnykh sredakh (Explosions in porous and dispersed media). Kiev, Izd-vo naukova dumka, 1969, 70-81.

The authors assert that analysis of soil displacement from explosions in terms of plastic deformation is more realistic than the classical model, in which displacement occurs as for an ideal incompressible liquid. A plastic deformation model for explosions of cylindrical charges in soft soil is therefore proposed and developed, with the simplifying assumption that displacement occurs only radially and at the shock wave front. Expressions for wave front propagation, cavity development, deformation at the wave front, and stress vs. radial distance from detonation point are derived. All variables in these equations are referred to coordinates of the shock wave front. The expression for wave front motion is integro-differential, which requires a computer for its rigorous solution. Some approaches to simpler approximate solutions are suggested, using empirical constants of known soil types. It is emphasized that the solutions presented, although for idealized conditions, are more generally useful than a set of existing empirical expressions defining the same explosion parameters. This is because the empirical solutions are strictly applicable only to their particular combination of explosion test parameters, and might not be readily extrapolated to other situations.

Pechkovskiy, V. I., and G. S. Kal'chik. Radial crack formation in the elastic compression region, caused by an explosion. IN: AN UkrSSR. Institut geotekhnicheskoy mekhaniki. Vzryv v poristykh i dispersnykh sredakh (Explosions in porous and dispersed media). Kiev, Izd-vo naukova dumka, 1969, 81-85.

Some mechanics of crack formation from explosions in solids are briefly examined. A two-stage destruction process is assumed, in which an initial elastic compression occurs prior to any destructive effects, followed by displacement and radial crack formation. The authors mainly consider the first period, and give a quantitative analysis of stress propagation and plastic deformation occurring during this interval. From expressions

for wave propagation velocity it is concluded that under high compression loads soil can be treated as a slightly compressible medium when the dimensions of the unstressed medium are large compared to any propagation wave length ($d/\lambda \gg 1$). Experimental studies have also shown that the destruction threshold for explosion-stressed solids, in particular soils, depends strongly on granular formation and contact conditions at particle boundaries, in addition to the nominal bulk physical properties of the material itself.

Krivtsov V. A., and R. K. Zinov'yev. Questions on measuring pore pressure from explosions in dry sand. IN: AN UkrSSR. Institut geotekhnicheskoy mekhaniki. Vzryv v poristykh i dispersnykh sredakh (Explosions in porous and dispersed media). Kiev, Izd-vo naukova dumka, 1969. 97-103.

It is shown that for the case of confined explosions in soil, if the relative change in pore gas pressure can be determined, the soil porosity and a number of deformation parameters can be deduced. The theoretical model assumes no escape of gas or liquid from pores during detonation, so the increase in density occurs solely as a result of gas compression in the pores. A test method developed by the authors is described in which specially mounted strain gauges are used to record the increase in pore gas pressure following a confined explosion. Tests were done in river sand with a specific weight of 1.6g/cm^3, moisture content of 2,35% by volume, and a porosity of 0.41. The explosive was TNT, in 0.2 kg charges. At each monitoring point around the charge, besides the pore pressure gauge there was a second gauge for registering total shock pressure. Monitor points were located radially up to 70 cm from the charge location. Figure 1 gives a comparison of net and pore pressures vs. radial distance; it is seen that pore pressure is relatively insensitive to distance. Oscillograph wave forms of the amplified pressure pulses showed almost identical wave forms, which indicates that the pore pressure sensors were providing a faithful reproduction of the differential pressure pulse.

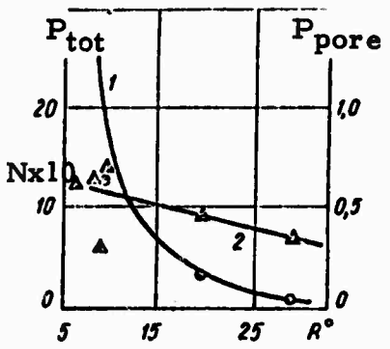

Fig. 1. Net normal pressure (curve 1) and pore pressure (curve 2) vs. distance.

Gundarev, K. A., and A. V. Mikhalyuk. The relation between strength properties and deformation of loams in the effective zone of an explosion. IN: AN UkrSSR. Institut geotekhnicheskoy mekhaniki. Vzryv v poristykh i dispersnykh sredakh (Explosions in porous and dispersed media). Kiev, Izd-vo naukova dumka, 1969, 112-118.

Experimental results are given for confined explosion tests in loam having the following measured characteristics: specific weight, 2.67 g/cm^3; moisture content, 16-18% by weight; cohesion, 5 newton /cm^2; and internal coefficient of friction tgφ = 0.56. Tests were done with 25 kg TNT charges buried 2.5 m deep. Following detonation, core samples from the effective zone were taken and analyzed by standard methods. The main parameters of interest were the effect of the explosion on soil cohesion and internal friction, as deduced from the core samples. Figure 1 shows the behavior of these parameters as functions of radial distance from the charge. Examination showed that cohesion at the cavity walls had approximately doubled. Patterns of mutually perpendicular cracks were also observed on the cavity walls, the cracks being up to 80 mm wide and extending in some cases out to 15-18 charge radii. From test data the authors derive empirical expressions for cohesion and tgφ in terms of radial distance, and discuss the limitations on applying these formulas in practice.

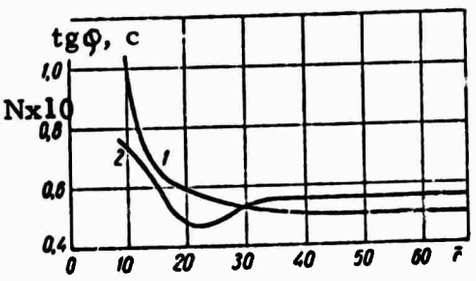

Fig. 1. Cohesion (1) and friction (2) vs. distance, after explosions in loam.

Mikhalyuk, A. V. Determination of cavity dimensions and compaction region from explosions in soil, with viscous properties taken into account. IN: AN UkrSSR. Institut geotekhnicheskoy mekhaniki. Vzryv v poristykh i dispersnykh sredakh (Explosions in porous and dispersed media). Kiev, Izd-vo naukova dumka, 1969, 124-130.

Expressions are derived for calculating the cavity size and the range of non-reversible deformation from confined explosions in soil. Using laboratory results from uniaxial compression tests on clay soils, the author develops a mathematical explosion model which takes into account the elastic, plastic and viscous properties of the medium. The analysis considers the two cases of cylindrical and spherical charges. Calculated values of deformation vs. radial distance, based on the derived formulas, are shown to agree well with field data from confined explosions in clay soil of 1,85 g/cm^3 specific weight. Expressions are also derived for calculating cavity radius in terms of the given test conditions. It is emphasized that soil viscosity is an important factor in determining explosion effects, and must be included in a realistic model.

Skobeyev, A. M. Measuring soil compressibility. Zhurnal prikladnoy mekhaniki i tekhnicheskoy fiziki, no. 1, 1970, 111-113.

A discussion is given on a method for studying dynamic compressibility of soil, using a laboratory device previously described by Mel'nikov et al (PMTF, no. 2, 1965). The device consists of a vertical cylinder in the bottom of which a soil specimen is placed. The specimen is statically compressed by an elastic piston, which is in turn driven periodically by a drop hammer. Recordings are made during a test of piston and sample displacement as functions of time. The process is treated as quasi-static, in which deformation is defined simply as the relation of displacement to original specimen height. Since shock waves can occur, the test process will not always be quasi-static; the limits of applicability of the quasi-static model must therefore be established when using the described test method.

Pluzhnik. V. I., V. I. Kononenko, and P. A. Parshukov. Field equipment for measuring explosion waves in soils. IN: AN UkrSSR.

Institut geotekhnicheskoy mekhaniki. Vzryv v poristykh i dispersnykh sredakh (Explosions in porous and dispersed media). Kiev, Izd-vo naukova dumka, 1969. 118-124.

A combined synchronizing and gating unit is described which was designed for use with serially-produced H-010 and H-700 light beam oscillographs. The objective was to improve the fidelity and reliability of recording wave forms from explosion tests in soil. The circuitry described in particular compensates for variations in the photosensitive tape transport speed, and prevents recording on start-up until the tape has reached nominal speed, thus avoiding time distortion in the signal trace. The unit is ruggedized to insure reliable performance under severe field conditions.

PARTICLE BEAMS

Krasovitskiy, V. B. Non-linear radial self-focusing of a modulated electron beam in a plasma. Zhurnal eksperimental'noy i teoreticheskoy fiziki. Pis'ma v redaktsiyu, v. 9, 1969, 679-683.

Some conditions for determining plasma parameters by means of a modulated electron beam are considered. The author assumes a dense periodically pulsed beam passing through the plasma, with a modulation frequency close to plasma frequency, i. e. $|\omega_M - \omega_p| \ll \omega_p$. Within the plasma the beam configuration is thus a train of disk-shaped pulses of variable diameter and spacing, depending on the applied modulation conditions. Limiting ratios of disk size vs. space are examined, in particular the case where disk radius $r \ll l$. Under this condition, the generated radial field component E_r substantially exceeds the longitudinal component E_z, causing self-focusing of the beam pulse. Equilibrium conditions for the self-focusing phenomenon are investigated, and an expression for electron density within a pulse packet is derived in terms of beam geometry. It is shown that within the limits discussed, the self-focusing beam method is useful for determining approximate values of dielectric constant and other plasma parameters.

Savchenko, O. Ya. Obtaining an ion beam by passing a neutral particle beam through a helium gas target. Zhurnal tekhnicheskoy fiziki, no. 2, 1970, 305-309.

An improved use of helium as a stripping agent for generating an ion beam is described. The technique is an adaptation of the pulsed arc method developed earlier for generating a proton beam, reported by the author and others (Dimov et al, Zhurnal tekhnicheskoy fiziki, v. 38, 1968, 997). An improved discharge tube geometry has been introduced as shown in Figure 1, which permits stable beam generation over an increased range of ion current densities. The advantage is gained by using two overlapping discharge tubes having wider diameters than the previous model, with helium introduced in the second tube for stripping. Sample experimental data given for production of H^+ beams at 14 kev ion energy and 100 μsec pulses

show that currents up to 1a are attainable, compared to 150 ma maximum for N^+. The improved discharge tube geometry also results in an output beam divergence estimated at not over 0.02 radian.

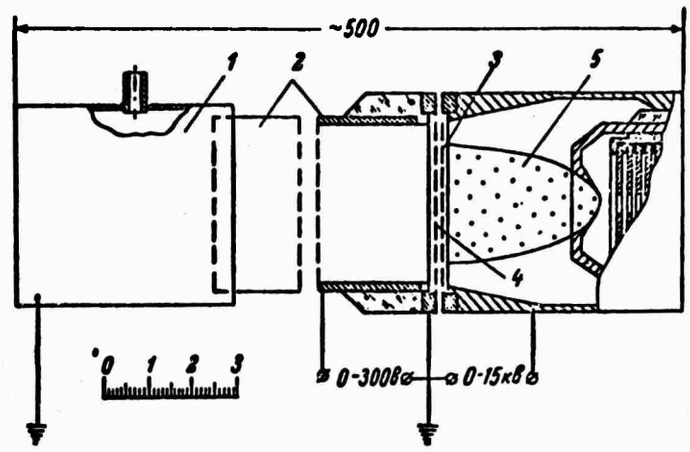

Fig. 1. Helium target ion source. 1-first tube; 2-second tube; 3, 4-grids; 5-plasma. Dimensions in mm.

Beylis, I. I., V. I. Rakhovskiy, L. G. Tkachev, and M. Ya. Smelyanskiy. Study of energy losses in a powerful electron beam. Zhurnal tekhnicheskoy fiziki, no. 9, 1969, 1650-1657.

The authors examine the principle loss mechanisms which occur during electron beam heating of metals in vacuo. The operating ranges treated are 10-20a beam currents, at 20-40kv energies. The two types of losses which are considered most important are from inelastic rebound of incident electrons from the target metal surface, and from kinetic energy loss to residual particles in the electron beam path. Test data show that the loss from incident electron rebound is sufficiently greater than secondary emission loss from the target surface that the latter may be ignored in a heat balance equation. Measured primary reflection losses varied from 8% for titanium up to 19% for tantalum. Transit losses to residual matter in the vacuum vessel were also measured, and found to be negligible at pressures lower than 10^{-5} torr; these losses become measurable at 10^{-4} torr, and jump abruptly to 20-25% at 10^{-3} torr. At higher pressures, the transit losses become the major loss factor; in practice, chamber vacuum should therefore be maintained at the order of 10^{-4} torr or less.

MISCELLANEOUS

Yakovlev, A. T. On calculating critical conditions when deriving equations of state for real gases. Teplofizika vysokikh temperatur, no. 1, 1969, 180-181.

The author briefly examines the possibility of analytically defining the critical conditions for P, V and T in equations of state, while still observing the statistical variability of these parameters near a phase change region. The treatment is a refinement of the Lagrange method for determining unknown coefficients, using the method of least squares. The solution of the derived expression can be obtained on an M-20 computer, using a standard subprogram for a linearized approximation. It is concluded that the proposed approach permits introduction of critical conditions into equations of state without distorting their inherent statistical behavior.

Vasserman, A. A.; Ya. Z. Kazavchinskiy; and O. S. Kalenov. Generalized form of equations of state, based on elementary functions. Akademiya nauk SSSR. Doklady, v. 186, no. 6, 1969, 1291-1294.

It is shown that the general equation of state Z=pV/RT, expressed as a series of elementary functions of the variables V and T, can be directly derived from the single-valued form of the equation proposed by Maier and Bogolyubov. The proof is given, showing the correspondence of elementary functions in the latter's expression to temperature and volume variables. Strictly speaking, the equivalence of the two solutions holds only at low or moderate particle densities; however, experimental data have shown that for practical purposes the equivalence is maintained for values of V_{cr}/V up to 3.

Lanyi, J.; and I. Rakoczy. Study of pressure waves generated by an underwater explosion. Geofizikai kozlemenyek, v. 18, no. 3, 1969, 97-102 (Hungary).

Pressure recordings of underwater explosions in the Drava River, conducted by the Eotvos Lorant Geophysical Laboratory in 1967, are presented and analyzed. TNT charges varying from 0.2 to 30 kg and spaced at intervals from 50 to 880 meters were placed near the river bottom at depths up to 6 meters. Pressure wave propagation from the detonated charges were recorded by piezo sensors placed about one meter below the surface, and displayed on an oscilloscope. As indicated by Fig. 1, the pressure variation with distance can be expressed by $P(r)=A/r^B$,

where A and B are constants. The relation of pressure to charge weight is shown in Fig. 2 for three distances from charge origin. This relation can be expressed as $P(r, Q) = DQ^n/r^B$; experimental values for the constants are given as B = 0.9727; D = 272; and n = 0.3294. The authors assert that their apparatus and technique are also applicable to atmospheric explosions.

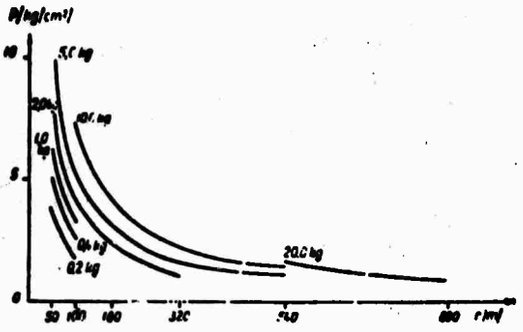

Fig. 1. Pressure vs. distance for various charge sizes.

Fig. 2. Pressure vs. charge size at various recording ranges.

Shefter, G. M. Effect of viscosity and heat conductivity on the propagation of sound impulses in an inhomogeneous moving medium. Prikladnaya matematika i mekhanika, v. 33, no. 1, 1969, 162-168.

Approximate equations of short wave propagation in a moving, inhomogeneous, viscous and heat-conducting medium are derived. These equations include the principal nonlinear and dissipative terms, and make possible the description of the two-dimensional structure within the wave. Two limiting cases of the problem on propagation of sound impulses are considered. A rigorous solution is obtained for the case when the influence of the dissipative terms is vanishingly small, i.e., when the medium can be assumed perfect. This solution in turn yields expressions for the decay of weak shock waves in a moving inhomogenous nonviscous gas with zero heat conductivity. These laws have been investigated earlier, but are obtained here for the first time as the result of a straightforward solution of first approximation equations describing the gas flow within the wave. Asymptotic forms of the sound impulses and the laws of decay over very long periods of time are principally governed by the dissipative terms, and nonlinear terms are not essential at this stage.

Romashin, A. G. Thermal conductivity of transparent materials. Teplofizika vysokikh temperatur, no. 4, 1969, 659-665.

Experimental findings are given on the temperature dependence of thermal conductivity in transparent sitalls, quartz glass and ceramics having porosities of 1.5; 12, and 28% respectively, over a temperature range of 300 to 1200°K. From a comparison of the temperature dependencies, the photon thermal conductivity was determined, and a comparison was made between experimental and computed data based on an idealized Stefan-Boltzmann model. Calculations were made with heat flux penetration taken into account. The analysis includes a comparative evaluation of internal photon and phonon thermal conductivity. In addition to corroborating the theoretical findings, the results agree well with known data on the sharp temperature gradients which can occur in transparent thin films of the glass and sitall types. The author emphasizes that these temperature jumps must be accounted for in any calculation of stationary or nonstationary thermal stress, since they can be the limiting factor in determining thin-film structural integrity.

Gadion, V. N. A velocity-measurement method and camera-system triggering equipment for photographing "glowing" models in aeroballistic studies. Zhurnal nauchnoy i prikladnoy fotografii i kinematografii, v. 15, no. 4, 1970, 246-249.

Following a brief review of problems involved in using photomultipliers in triggering the measurement sequences in aeroballistic ranges, the author describes an improved system in which spurious triggering effects are eliminated, e.g., muzzle-flash, gas glow behind the bow wave due to impurities, etc. The modifications were made on a range which uses a light-gas gun launcher providing model velocities of 2300--5000m/sec. With a timing accuracy of 0.1 μsec and base-length measurement accuracy of 0.1 mm, model-velocity measurement accuracy is said to reach within 0.1 to 0.3%.

Baum, F. A.; N. S. Sanasaryan; and V. D. Kroshchenko. Effect of hydrostatic pressure on parameters of an underwater explosion. IN: Mel'nikov, N. V., ed. Problema razrusheniya gornykh porod vzryvom (The problem of rock destruction by an explosion). Moskva, Izd-vo nedra, 1967. 69-76.

Experimental results of underwater explosions tests are described, for the case where explosive charges are detonated in water which is under initial static pressure. Tests were done in a 350mm diameter autoclave using spherical and cylindrical charges of TEN explosive in tap water. Static pressures up to 400 atm were initially applied by compressing the

air layer above the water surface. Spherical charges were 0.72g and 10mm in diameter; cylindrical charges, 1.7g and 6mm in diameter by 36mm long. Explosions were observed through plexiglass viewports and recorded with an SFR camera operating at 7,500 rpm when studying pulsations of the vapor cavity, and 45,000 rpm when recording shock wave propagation. The main object was to evaluate the effect of applied static pressure P_0 on maximum growth rate and size of the explosion cavity, as well as on the pressure behavior of the shock wave front over the interval $1 < R/R_0 < 15$ where R_0 = charge radius and R = distance from charge center. It was found that $R_{max} \sim P^{-1/3}$, whereas $T_{max} \sim P^{-5/6}$, in agreement with theory. Pressure P at the shockwave front is given by

$$\Delta P = \Delta P_0 \left(\frac{R_0}{R}\right)^k \left(\frac{P_0}{B} + 1\right)^{1-\frac{k}{\nu}},$$

where k takes on various values depending on wave profile and distance; $\nu = 2$ for a cylindrical wave and 3 for a spherical wave; and B is a constant in the equation of state for water. Figure 1 shows $R/R_0(t)$ at 4 static pressures; Figure 2 is the shock adiabatic curve for 1 atm and 400 atm applied loads, and shows the negligible effect of static pressure on shock wave parameters.

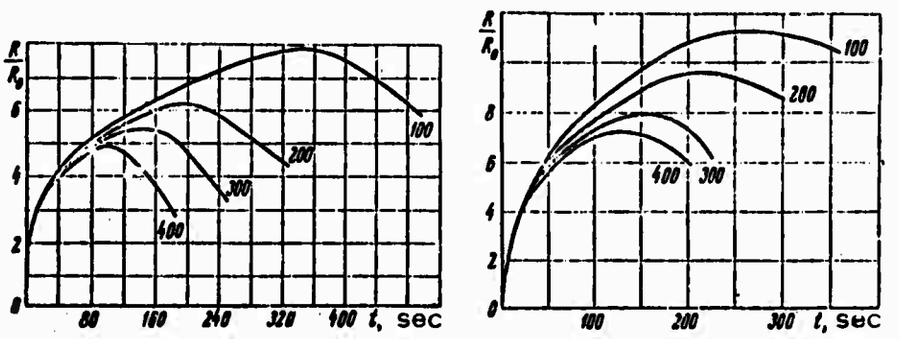

Fig. 1. $R/R_0(t)$ for (a) cylindrical and (b) spherical charges.

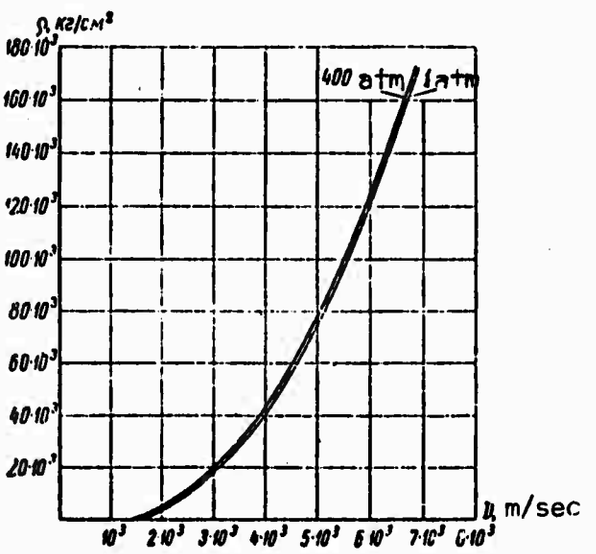

Fig. 2. Shock adiabat in water at 1 and 400 atm loads.

Kolosov, M. A.; A. V. Sokolov; L. V. Fedorova; and P. A. Shirey. Absolute attenuation factor of laser radiation intensity in water fogs as a function of droplet size. AN SSSR. Doklady, v. 188, no. 6, 1969, 1277-1280.

The optical transparency of fog to a laser beam has been measured and correlated with the microphysical characteristics of fog. Experiments were performed in an artificial fog chamber (height = 18m, diameter = 15m) at facilities of the Institute for Applied Geophysics. The fog was generated by adiabatic expansion after preliminary increase of the air pressure to 1.5 atm. Laser sources with wavelengths = 0.63, 1.15, and 3.39 microns were used. A special "aerosol meter" was developed for this purpose by the Institute of Radioengineering and Electronics at the Academy of Sciences, USSR. In combination with photoelectric sensors developed by the Institute of Applied Geophysics, this instrument automatically measures the spectrum of droplet radii in a range from 0.5 to 14 microns, and their absolute concentration with a resolution of 2200 particles/cm^3. Comparison of the experimentally measured attenuation factor exp at = 0.63 micron with values calculated from the single scattering theory $_{calc}$ is shown in Fig. 1.

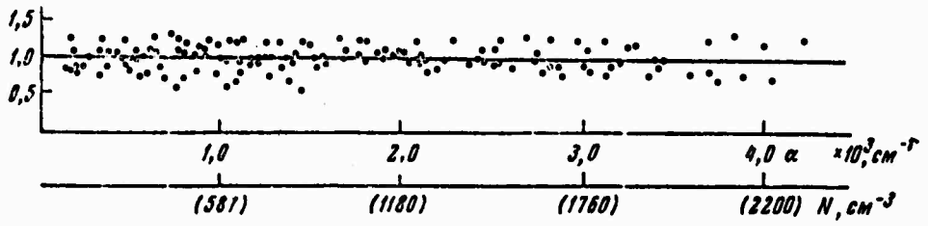

Fig. 1. Calculated vs. measured attenuation factor for laser propagation in fog.

The basic factor determining attenuation is found to be droplet concentration N, as shown in Figure 2 at $\lambda = 3.39\mu$, for $D_2 = 8.5 \pm 1\mu$, and $D_2 = 10.0 \pm 1\mu$, where D_2 is rms droplet diameter.

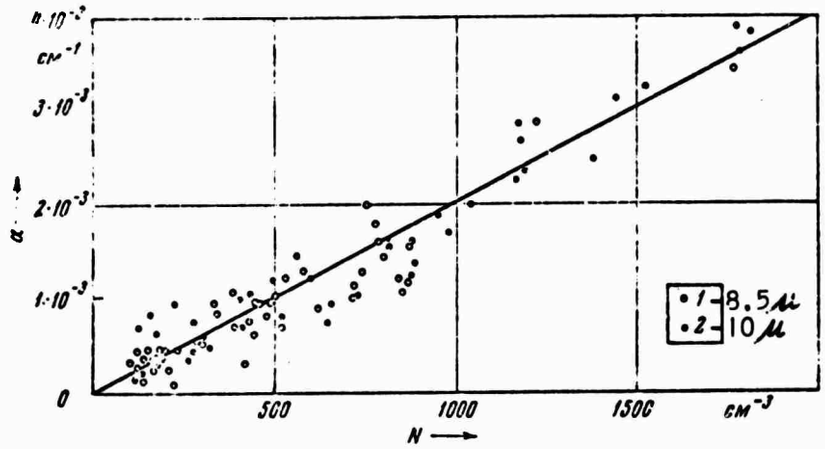

Fig. 2. Attenuation vs. droplet concentration.

It is concluded that satisfactory coincidence of theoretical and experimental data supports the theory of single scattering, i.e. attenuation of coherent radiation in the 0.63 to 3.39μ range is similar in behavior to attenuation of noncoherent radiation from ordinary thermal sources.

Tatarskiy, V. I. Light propagation in a medium with random inhomogeneities of refractive index in an approximation of a Markovian random process. Zhurnal eksperimental'noy i teoreticheskoy fiziki, v. 56, no. 6, 1969, 2106-2117.

A theory of strong fluctuations in the intensity of light propagating in a turbulent medium is developed. It is based on a rigorous solution of the parabolic equation which is assumed to describe with sufficient accuracy the propagation of light through a medium having random inhomogeneities in refractive index. Other assumptions are that fluctuation in dielectric constant present a Gaussian random field, and are delta-correlated in the wave propagation direction. Rigorous closed equations are derived for the field mean value and for the mutual coherence function, and their solutions are considered for some simple cases. It is shown that the expression for the coherence function coincides with formulas obtained earlier by a first approximation to perturbation theory. It is also shown that for arbitrary initial conditions, the solution for the mean field value contains a factor corresponding to the solution of the diffraction problem in the absence of fluctuations. For the assumed model of the medium, the characteristic field functional satisfies an equation of the Fokker-Planck type. It follows from these properties that exact closed equations can be obtained for field moments of arbitrary order. Based on the foregoing qualifications, an equation for field intensity fluctuations is derived which is valid for both strong and weak fluctuations. This theoretical approach can also be readily extended to the case where fluctuations in dielectric constant are a known function of distance along the propagation path.

Koval'chuk, B. M.; V. V. Kremnev; and G. A. Mesyats. Avalanche discharge in gas, and generation of nanosecond and sub-nanosecond high current pulses. AN SSSR. Doklady, v. 191, no. 1, 1970, 76-78.

Two variants of capacitive dischargers are described which avoid the usual inductive limitations of high current pulse generators, and are thus capable of producing kiloampere discharges in the subnanosecond

range. The method depends on developing an electron avalanche following the initial breakdown of the air gap between charged electrodes, as shown in Fig. 1. Avalanching is begun by u-v photoionization or particle irradiation of the air gap. Examples of current waveforms are given in Fig. 2, showing that for the configuration of Fig. 1 (b) a 3 ka pulse is generated at less than 0.2 nsec. The amplitude and shortness of the pulse are ultimately limited by capacitor geometry, and are given by

$$i_a \approx 0{,}5\pi\varepsilon_0 C_0 E_K D\sqrt{\varepsilon_r}, \quad t_n = D\sqrt{\varepsilon_r}/2C_0, \qquad (1)$$

in which ε_0 = air dielectric constant; ε_r = capacitor dielectric constant; C_0 = capacity; E_K = field gradient in the capacitor dielectric; and D = capacitor diameter. The theoretical limits for the design of Fig. 1 (a), for example, are accordingly 40,000 a and 5 nsec.

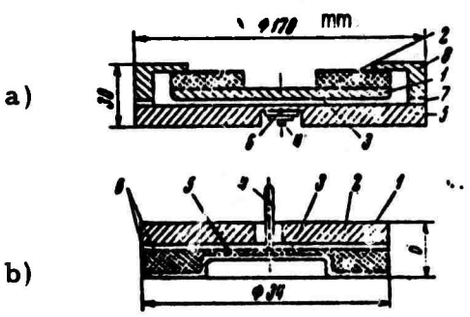

Fig. 1. Avalanche pulse discharger. a) 1, 5- electrodes; 2 - capacitor, 6200 μf; 3-3 mm air gap; 4-2kv ignition electrode; 6-titanate starter element; 7-shunt; 8-case

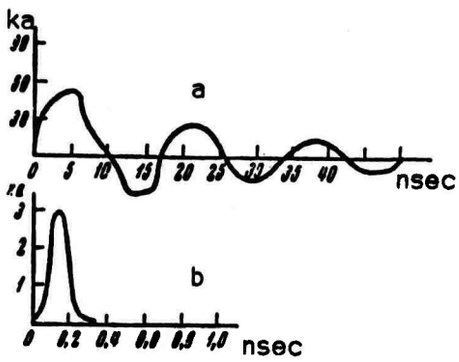

Fig. 2. Current waveforms a) for Fig. 1 (a); b) for Fig. 1 (b).

Belozerov, A. N.; and R. I. Soloukhin. Seventh International Symposium on Shock Tubes. (Toronto, June 23-26, 1969). Fizika goreniya i vzvryva, no. 1, 1970, 131-137.

The Seventh International Symposium on Shock Tubes was organized by a section of the American Physical Society jointly with the University of Toronto Institute for Aerospace Studies, held in Toronto, Canada, in 1969. In the six sessions of the symposium, 40 reports were presented on the following areas of shock-tube technology and the physical and chemical applications of shock tubes:

1. Deviations from ideal flows in shock tubes.
2. Shock tubes with highly enthalpic sources of driver gas (arc heating, piston compression).

3. The application of explosives in shock tube research.
4. Electric discharge shock tubes and their application in plasma physics.
5. The kinetics of molecular and chemical processes in shock waves.
6. Methods of measuring and obtaining fundamental data in shock tube experiments.

The titles of 12 more were also announced, but they were not accepted for presentation because of the fact that the program was already overloaded. These included research on investigating strong (ionizing) waves, research on double diaphragm shock tubes, on obtaining cesium plasma in shock tubes, and on the spectroscopy and mass-spectrometry of high temperature gases obtained by means of shock tubes.

Lavren'tyev, M. A.; R. I. Soloukhin; and M. Ye. Topchiyan. Second International Colloquium on the Gasdynamics of Explosions and Reactive Systems (Novosibirsk, August 24-29, 1969). Fizika goreniya i vzryva, no. 1, 1970, 137-141.

The main theme of this colloquium was the study of problems in the gas dynamics of explosions. Attention was particularly devoted to analysis of nonstationary flow phenomena in a gas, for cases where the determining factor is the rate of homogeneous liberation of energy in a compressed medium. The structure of shock and detonation waves in various media was examined, as were the role of shock waves and the kinetics of chemical reactions during combustion in supersonic flows. The correlation between the type of detonation process and the method of energy liberation in the medium was also treated. The colloquium included a special section on the gas dynamics of reactive systems, which dealt principally with analysis of flows under conditions of rapid combustion of heterogeneous systems, mainly as applicable to combustion of rocket fuels. Theoretical and experimental work of a general nature were presented, including some results of applied research.

III. STUDIES

HYPERSONIC GAS FLOW AROUND A BLUNT BODY (COMPREHENSIVE STUDY)

A group of Soviet mathematicians from the Computer Center of the Academy of Sciences USSR and from the Ioffe Physico-Technical Institute in Leningrad under the leadership of O. M. Belotserkovskiy has for the past decade been developing numerical algorithms for the computation of hypersonic gas flow problems. Their most pertinent papers published during this time are listed as references (1-27). This work was initiated when academician A. A. Dorodnitsyn, the director of the Computer Center since 1955, presented a paper at the Third All-Union Mathematical Conference in 1956 (28) on a direct method of integral relations for solving problems of hypersonic gas flow about axisymmetric blunt bodies. Dorodnitsyn's method introduces an approximation of a function with respect to one variable. Partial differential equations are then substituted by a system of ordinary differential equations which can be solved by well-known numerical means.

The bulk of the present review is based on the two most recent papers (1) and (2) on the subject, while the remaining sources serve to establish the necessary perspective and background. A summary of the early publications (4-27) is provided in (3). A great importance is attributed to the choice of an appropriate coordinate system for the interpretation of the equations, their solution, and the automatic numerical calculations. Three computation outlines have been developed, each accordingly using a slightly different body-oriented orthogonal system of coordinates. They are presented below in a two-dimensional form.

Outline 1. (5, 8, 10, 12, 14, 16, 18, 19, 24, 26). The initial system of equations is converted into an (S, n) coordinate system, where S is arc-length measured along the body contour, and n is normal to S. The system is shown in Fig. 1. The body contour equation is n=0. S=0 is the equation of the body center line (axis of symmetry), and the equation of the detached shock wave is $n=\varepsilon$, where ε denotes the shock wave detachment distance. The integration region is outlined by the body center line, body contour line, shock wave, and the limiting characteristic S (n), or the closing ray S=S* may be chosen. The integration region is subdivided into N curvilinear strips (N is degree of approximation) by lines between the body contour (n=0), and shock wave ($n=\varepsilon$). The functions and integrals themselves are presented by interpolation polynomials across the shock layer, with the interpolation points on the strip boundaries. This outline is useful for flow computation at high Mach numbers, when the shock layer is relatively thin and its parameters vary smoothly across the layer. It is suitable for flow computation about extremely blunt bodies (8, 15, 16), also for bodies with a broken contour line (12) or broken contour curvature (14).

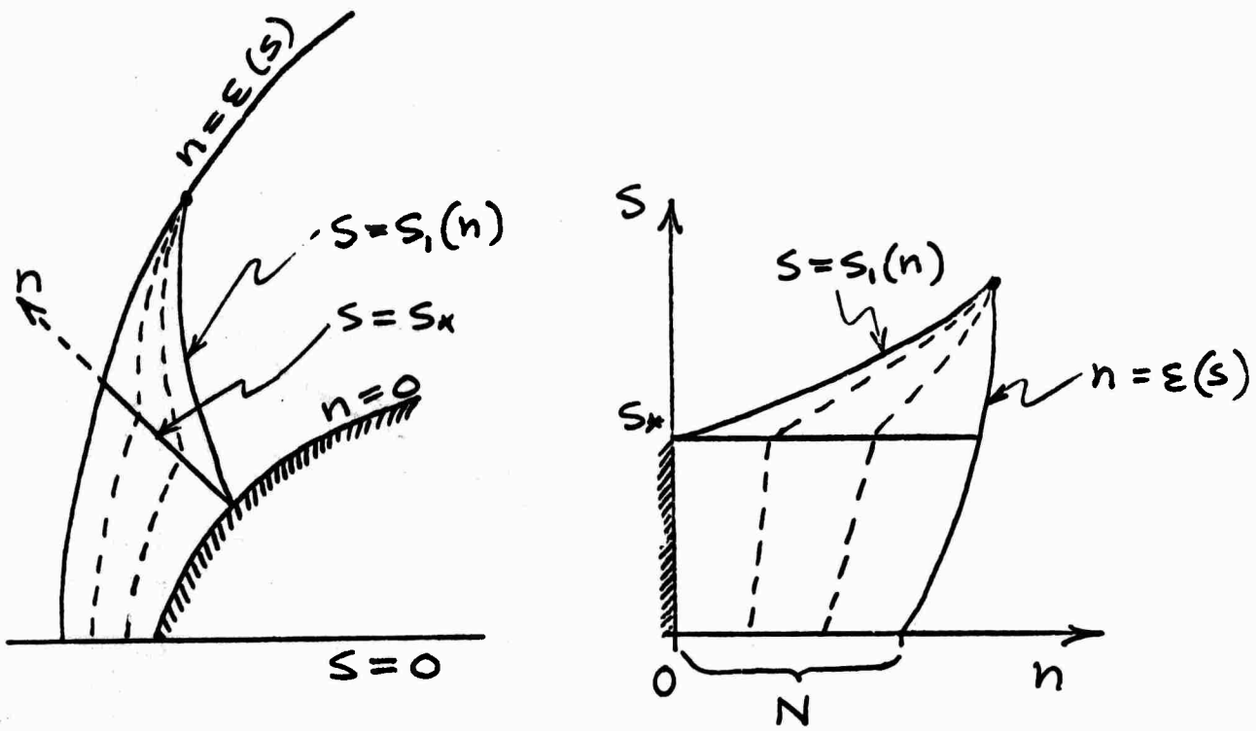

Fig. 1. Coordinate Notation, Outline 1

Outline II. (5-7, 11, 13, 17-19). The coordinate system S and $\xi = n/\varepsilon$ (S) is used, where S, n, and ε are the same as in Outline I. The body contour equation is $\xi = 0$, and $\xi = 1$ indicates the detached shock wave with S_1 (ξ) the limiting characteristic. The integration region is subdivided into N curvilinear strips by the lines $\eta = S/S_1$, (ξ) = const, between the body center line s=0 and the boundary characteristic $S = S_1$ (ξ). The functions are approximated along the shock layer by polynomials in S with a symmetry at S=0 taken into account. The method in this outline is advantageous in cases of large variation in flow parameters across the shock layer, such as in bodies with a smooth contour curvature at low Mach numbers, or at nonequilibrium flow when parameters change abruptly across the shock layer. In such cases Outline II yields good accuracy even for rough approximations (7, 13, 17). In addition, Outline II generally requires less computer time than Outline I.

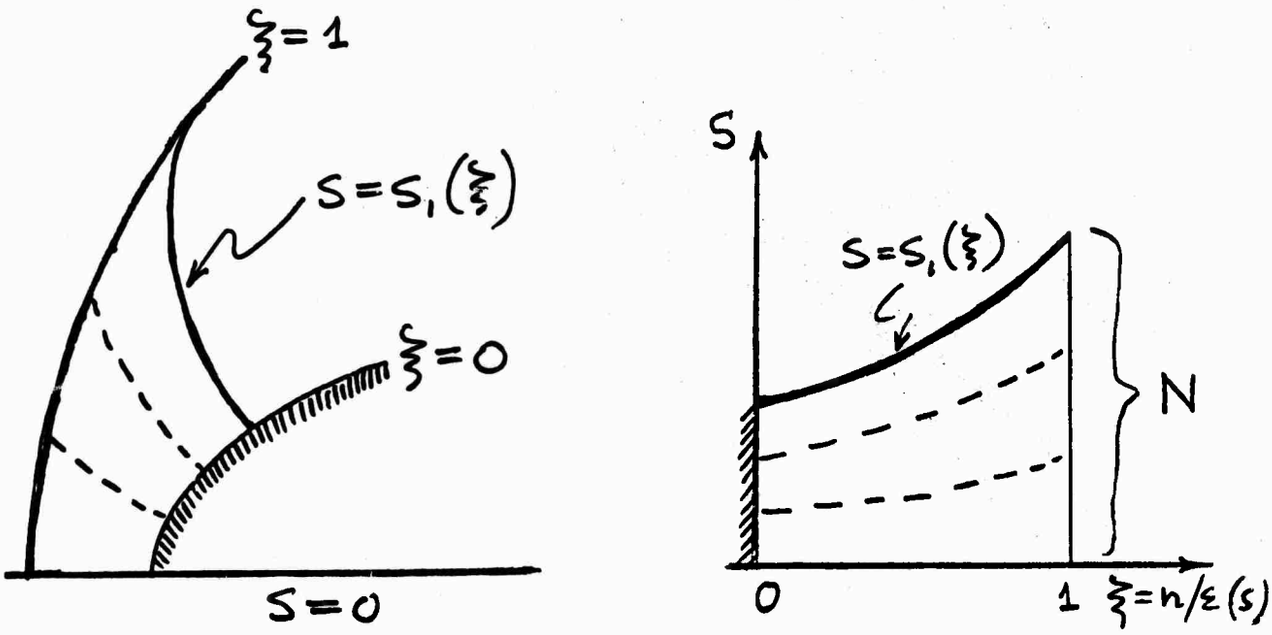

Fig. 2. Coordinate notation, Outline II

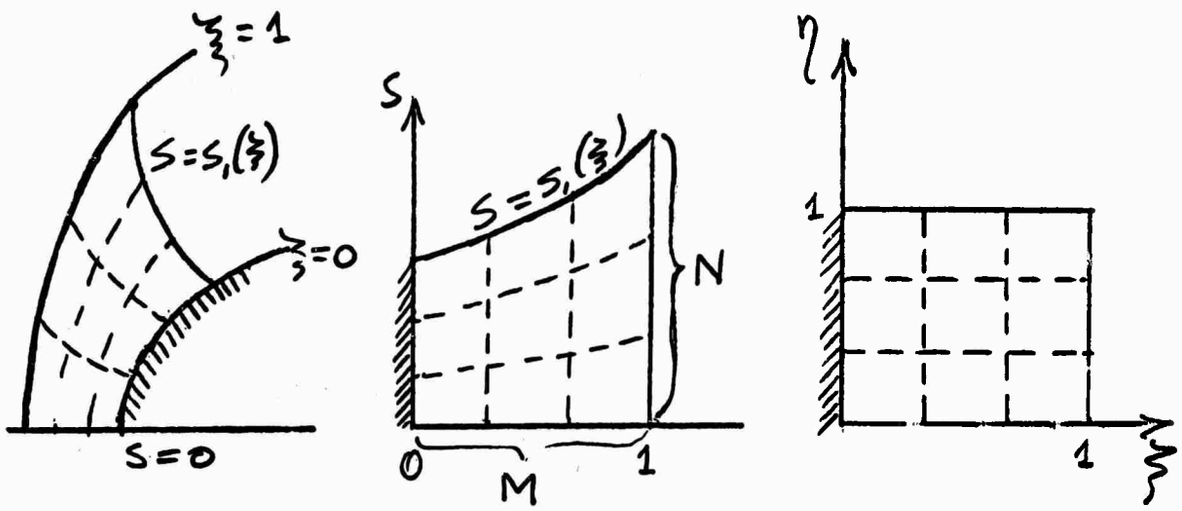

Fig. 3. Coordinate notation, Outline III

Outline III (5, 9, 19) utilizes finite difference presentations on a selected computational grid in both directions with coordinates $\xi = n/\varepsilon$ (S) and $\eta = S/S_1$ (ξ), and the body surface equation $\xi = 0$, shock wave $\xi = 1$, and limiting characteristic $\eta = 1$ (Fig. 3). The resulting nonlinear equations are solved by numerical iteration methods and give values of unknown parameters at nodal points of the grid. This outline requires less computation in the case of viscous flows.

The choice of the outline to be used is based on the considerations of the most accurate function description for the least amount of approximation points.

Both reviewed papers (1) and (2) employ the following system of gas-dynamic equations for inviscid, thermally nonconductive, thermodynamically balanced gas flow:

$$\frac{d\bar{w}}{dt} = -\frac{1}{\rho}\operatorname{grad} p, \tag{1}$$

$$\operatorname{div}(\rho\bar{w}) = 0, \tag{2}$$

$$\rho\frac{dh(p,T)}{dt} + \rho\bar{w}\frac{d\bar{w}}{dt} + \int_0^\infty k'_\nu\left(4\pi B_\nu - \int_\Omega I_\nu\, d\Omega\right)d\nu = 0, \tag{3}$$

$$\frac{dI_\nu}{dr} = k_\nu'(B_\nu - I_\nu), \qquad B_\nu = \frac{2h\nu^3}{c^2}\frac{1}{\exp(h\nu/kT) - 1}, \tag{4}$$

$$p = \frac{\rho RT}{\mu(p,T)}. \tag{5}$$

where $\bar{w}$ - velocity vector,
p - pressure,
ρ - density,
T - temperature,
h - enthalpy,
μ - molecular weight,
R - universal gas constant,
I_ν - radiation intensity,
K - Boltzmann's constant
h - Planck's constant
r - direction of radiation transfer
$d\Omega$ - elementary solid angle,
ν - frequency,
c - velocity of light,
$k'_\nu = k_\nu \left(1-\exp\left\{-h\nu/KT\right\}\right)$ - absorption coefficient with the stimulated emission taken into account.

The radiative energy transfer equation (4) is replaced by the system of differential equations

$$\operatorname{div} H_\nu = -k_\nu'(I_{\nu 0} - 4\pi B_\nu), \tag{6}$$

$$\operatorname{grad} I_{\nu 0} = -3k_\nu' H_\nu. \tag{7}$$

where $H_\nu = \int I_\nu \Omega d\Omega$ is radiant energy flux.

In (1) the subsequent procedure is described in some detail. The frequency range ν is subdivided into n intervals, assuming absorption coefficient is constant within each interval. This permits one to substitute summation for integration in the energy equation, so that the energy equation can be approximated by

$$\rho \frac{dh(\rho_1 T)}{dt} + \rho w \frac{dw}{dt} + \sum_{k=1}^{n} [k_\nu'(4\pi B_\nu - I_{\nu 0})]_k \Delta\nu_k = 0. \tag{9}$$

Thus a closed system of differential equations (1), (2), (5), (7), and (9) with the unknown functions $\bar{w}$, ρ, p, T, I_{ν_0}, and H_ν, is obtained. It is valid for multidimensional flows of spectrally emitting and absorbing gas at any thickness of the shock layer.

Outline II is used in (1) for further computation and all above equations are converted into a closed system of partial differential equations (10), (11), (12), (13), and (14), in a nondimensional form in the S and $\xi = n/\varepsilon(S)$ system of coordinates. (Numbers refer to the original paper). These and subsequent equations are not reproduced here. The second approximation (N=2) of Outline II is used to construct the approximation system of ordinary differential equations producing 12 + 8n equations for the same number of unknowns (n-number of intervals). This system is solved for the derivatives of the desired functions, producing a system of equations suitable for numerical integration (15). The system consists

of 12 equations to determine derivatives of gasdynamic functions and 8n equations to determine derivatives of functions $H_\nu S_i^{(K)}$, $H_\nu z_i^{(K)}$, and $I_\nu o_i^{(K)}$ (K = 1, 2, ... n), which characterize radiation transfer. Gasdynamic boundary conditions are taken to be the same as in (7). The approximate boundary conditions (16), (17), and (18) were assigned for emission.

Some results of calculations are presented in (1), while more detailed data, analysis and comparision with other calculations are given in (2).

Calculations were made for an assumed hypersonic flow around a sphere of a radius R = 1m by a radiating and absorbing gas at $M_\infty = 33$, $P_\infty = .0029$ atm, and $T_\infty = 257^\circ K$. Variations of temperature T and density ρ along the boundaries of the strips S=0, $S=S_1$ and $S=0.5S_1$ in the shock layer are presented in figures 4 and 5 by solid lines.

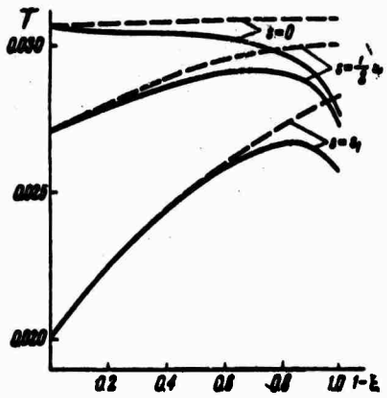

Fig. 4. Temperature variation T(S)

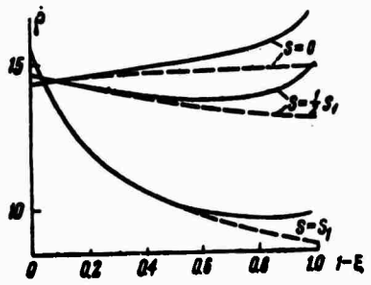

Fig. 5. Density variation ρ (S)

Dashed lines show the same variations in the absence of radiative transfer. It can be seen that taking into account spectral radiation leads to a temperature decrease and a density increase in the shock layer. Computations provide sufficient data to plot the magnitude of radiation energy flux $\tilde{H}_\nu$ on the body surface and at any point of the shock layer. As an example, a $H_{\nu\xi}$ variation along S=0 for various ν is shown in Fig. 6. The radiative thermal flux at the stagnation point of the body surface and its frequency characteristic is shown in Fig. 7 by a solid line. The dashed line shows the flux in absence of energy losses. The components $H_{\nu\xi}$ and $H_{\nu S}$ of the radiative energy flux at $S_2 = 0.5S_1$ for two different ν are presented in Fig. 8.

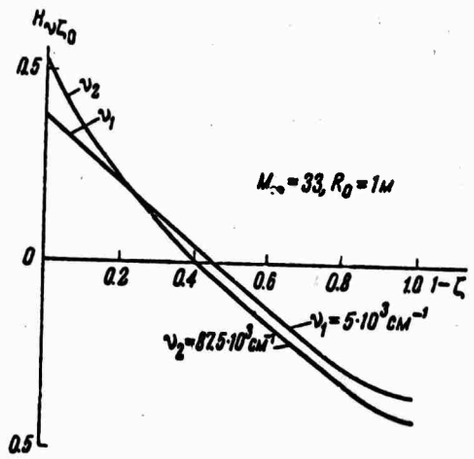

Fig. 6. Energy variation, $H_{\nu\xi}$ (S)

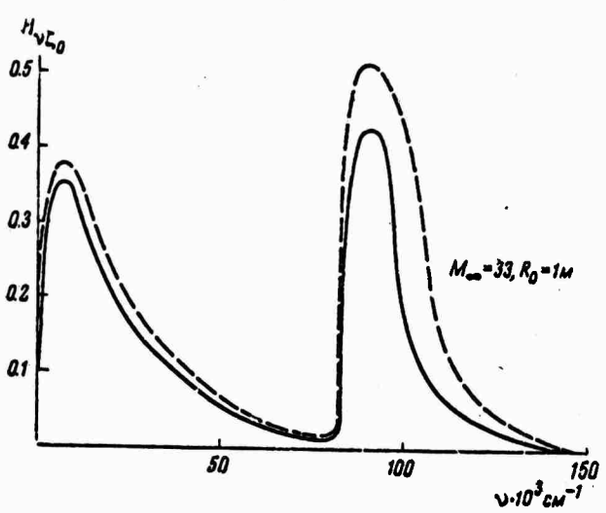

Fig. 7. Flux variation vs. frequency

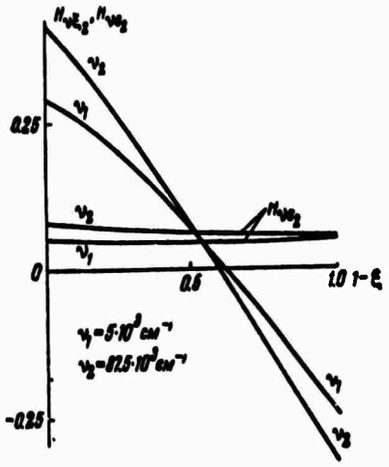

Fig. 8. H_ν (S) at two frequencies

The second paper (2) takes radiative energy transfers in a shock layer into account in a more general way, and for a variety of cases. However, this is done with less computational details than in (1). Computations have been performed by Outline I and by two variants of Outline II. Initial numerical data are the same as in (1) (R_0= 1m, M_∞= 33, P_∞ = .0029 atm, and T_∞= 257°K. Calculation results as presented in (2) follow.

The temperature variation along the body center line S=0 from the shock wave toward the body as calculated by Outline II in a second approximation (N=2) is presented in Fig. 9.

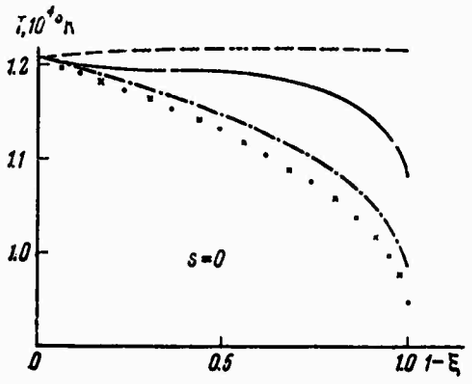

Fig. 9. Temperature profile along S=0.

The curves shown differ depending on how the radiation losses are taken into account: dashed line - no radiation losses; solid line - spectral radiation and absorption taken into account; dot-dash line - spectral radiation taken into account, using data from Biberman et al (Kosmicheskiye issledovaniya, v. 2, no. 3, 1964, 441-454); the dotted curve presents calculated results using the data of Kivel (J. Aeronaut. Sci., v. 28, no. 2, 1961, 96-102), and the crosses present calculated results obtained by a variant of Outline II using integration of the energy equation. The same data for the line of the boundary characteristic S_1, and for S=1/2S, are presented in Figures 10 and 11.

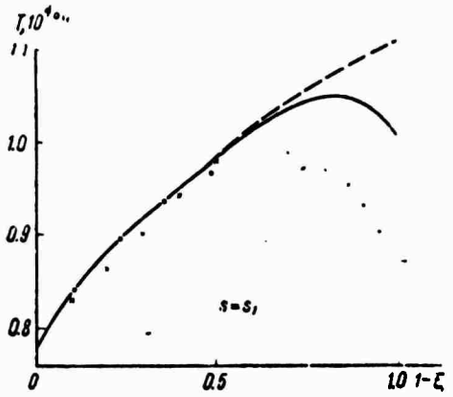

Fig. 10.T(S) at S_1

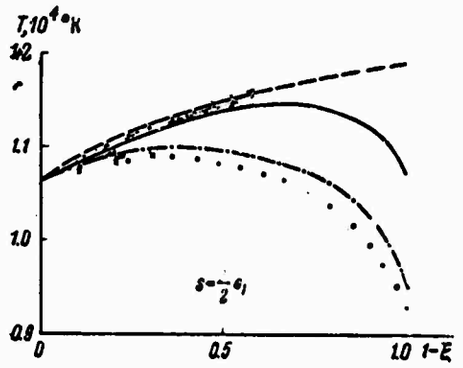

Fig. 11. T(S) at $\frac{S_1}{2}$

Density variations in the shock layer are presented on the same lines and with the same assumptions about radiation behavior in Figures 12, 13, and 14.

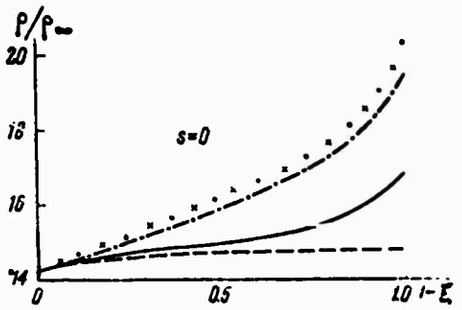

Fig. 12. Density variation, S=0

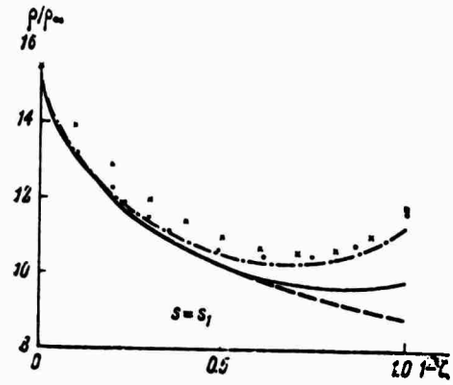

Fig. 13. Density variation, $S=S_1$

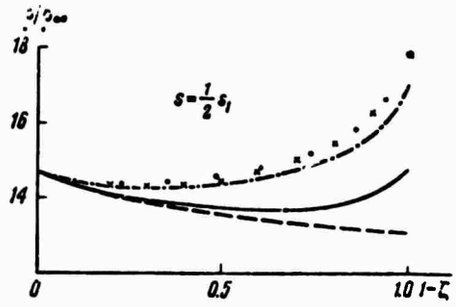

Fig. 14. Density variation, $S=\frac{S_1}{2}$

It can be seen that in all cases the temperature in the shock layer decreases, while the density increases. Calculations also show that pressure in a shock layer practically does not change, while velocity diminishes slightly near the body surface because of radiation. This leads to the important conclusion that radiation affects thermal flux arriving at the body surface but does not influence its aerodynamic characteristics. Temperature decrease and density increase in the shock layer lead to a decrease in shock wave detachment (Figure 15) and subsequently to a decrease of radiative thermal flux.

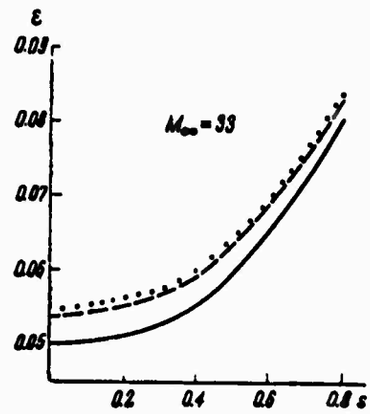

Fig. 15. Shock wave detachment, $\varepsilon(S)$

— $E \neq 0$, $R_0 = 1$ м;
– – – $E \neq 0$, $R_0 = 0.1$ м;
. . . $E = 0$

Temperature and density variations in a shock layer of a 91% N_2 + 9% CO_2 gas mixture are shown in Figures 16 and 17 (M_∞=40, P_∞ =.005, T_∞ =300°K, R_0 =1m).

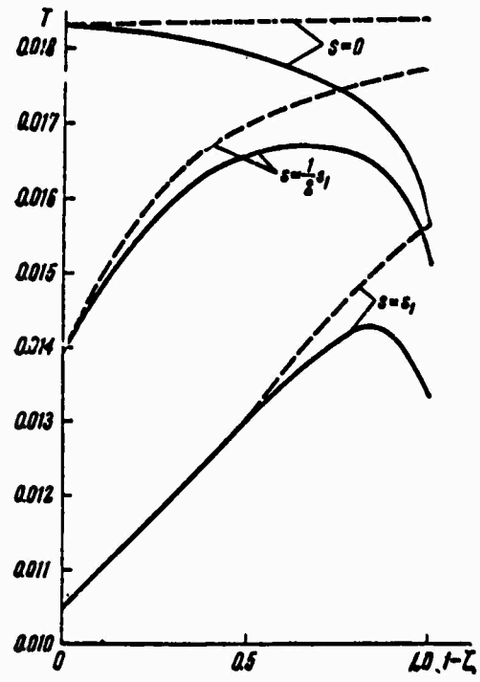

Fig. 16. Temperature variation in CO_2-N_2 shock wave.

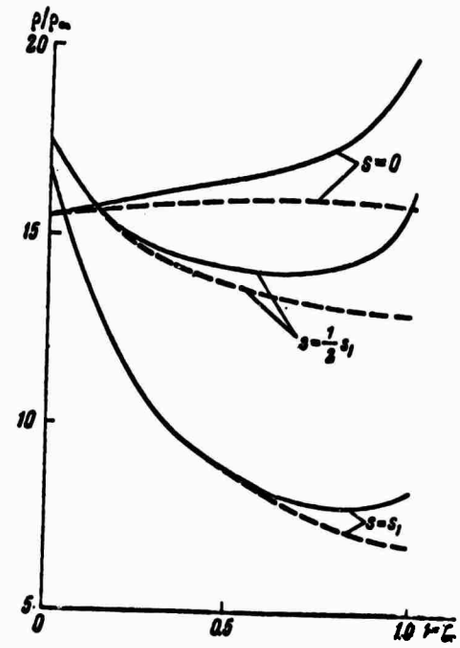

Fig. 17. Density variation in CO_2-N_2 shock wave.

T and ρ variations in a shock layer on a side of a cone are presented in Figure 18, which shows that taking radiation into account leads to a temperature decrease and density increase only in a narrow zone near the cone surface.

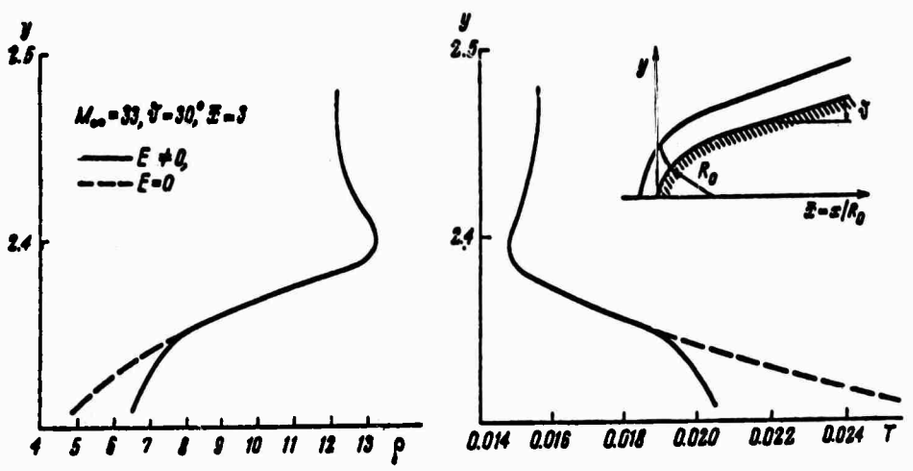

Fig. 18. Variation in T and ρ in a conical shock wave.

REFERENCES

1. Lebedev, V. I.; and V. N. Fomin. Hypersonic gas flow around blunt bodies with spectral absorption and emission taken into account. Zhurnal vychislitel'noy matematiki i matematicheskoy fiziki, v. 9, no. 3, 1969, 655-663.

2. Belotserkovskiy, O. M.; and V. N. Fomin. Calculation of radiative gas flows in a shock layer. Ibid., v. 9, no. 2, 1969, 397-412.

3. Belotserkovskiy, O.M., ed. Obtekaniye zatuplenykh tel sverkzukovym potokom gaza. Teoreticheskiye i eksperimental'nyye issledovaniya (Hypersonic gas flow around blunt bodies. Theoretical and experimental studies). 2nd ed., rev. and enl., Moskva, Izd-vo Vychislitel'nyy tsentr, 1967. 400p. (SERIES NOTE: Akademiya nauk. Vyychislitel'nyy tsentr. Trudy)

4. Fomin, V. N.; and N. P. Shulishnina. Hypersonic gas flow around blunt cones with radiation taken into account. Zhurnal vycheslitel'noy matematiki i matematicheskoy fiziki, v. 7, no. 4, 1967, 933-937.

5. Belotserkovskiy, O. M.; A Bulekbayev; and V. G. Grudnitskiy. Numerical algorithms of integral relations for computation of mixed gas flows. Ibid., v. 6, no. 6, 1966, 1064-1081.

6. Belotserkovskiy, O. M.; Ye. S. Sedova; and F. V. Shugayev. Hypersonic flow around axisymmetric blunt bodies with a sharply bent surface. Ibid., v. 6, no. 5 1966, 930-934.

7. Fomin, V. N. Hypersonic gas flow past blunt bodies with radiation taken into account. Ibid., v. 6, no. 4, 1966, 714-726.

8. Lun'kin, Yu. P.; and F. D. Popov. Effect of non-equilibrium dissociation on hypersonic gas flow past blunt bodies. Zhurnal tekhnicheskoy fiziki, v. 36, no. 4, 1966, 661-671.

9. Popov, F. D. One computational outline for the method of integral relations in a problem of hypersonic flow around blunt bodies. Ibid., v. 36, no. 2, 1966, 239-245.

10. Tolstykh, A. I. Numerical computation of hypersonic viscous gas flow around blunt bodies. Zhurnal vychislitel'noy matematiki i matematicheskoy fiziki, v. 6, no. 1, 1966, 113-120.

11. Golomazov, M. M. Computation of three-dimensional hypersonic flows around blunt bodies. AN SSSR. Vychislitel'niy tsentr. Report. Moscow, 1965.

12. Ivanov, V. F. Computation of hypersonic flow around blunt bodies with a sharply bent contour. AN SSSR. Report on All-Union conference on computational mathematics, January 22-26, 1965. Moscow, 1965.

13. Dushin, V. K.; and Yu. P. Lun'kin. Hypersonic non-equilibrium dissociating air flow about a blunt body. Zhurnal tekhnicheskoy fiziki, v. 35, no. 8, 1965, 1461-1470.

14. Golomazov, M. M. Computation of hypersonic flow past blunt bodies with a broken contour curvature. AN SSSR. Vychislitel'niy tsentr. Report. Moscow, 1964.

15. Lun'kin, Yu. P.; and F. D. Popov. Effect of non-equilibrium dissociation on hypersonic flow around blunt bodies. Zhurnal vycheslitel'noy matematiki i matematicheskoy fiziki, v. 4, no. 5, 1964, 896-904.

16. Belotserkovskiy, O. M.; M. M. Golomazov; and N. P. Shulishnina. Calculation of an equilibrium dissociating gas flow around blunt bodies with a detached shock wave. Ibid., v. 4, no. 2, 1964, 306-316.

17. Belotserkovskiy, O. M.; and V. K. Dushin. Non-equilibrium hypersonic gas flow past blunt bodies. Ibid., v. 4, no. 1, 1964, 61-77.

18. Belotserkovskiy, O. M. Ideal and real axisymmetric hypersonic gas flow about blunt bodies. Ibid., v. 2, no. 6, 1962, 1062-1085.

19. Belotserkovskiy, O. M.; and P. I. Chushkin. Numerical method of integral relations. Ibid., v. 2, no. 5, 1962, 731-759.

20. Belotserkovskiy, O. M. Flow computation of axisymmetric bodies with a detached shock wave (calculation formulas and flow field tables). AN SSSR. Vychislitel'niy tsentr. Moscow, 1961.

21. Chuskin, P. I.; and N. P. Shulishnina. Tables of hypersonic flow about blunt coves. AN SSSR. Vychislitel'niy tsentr. Moscow, 1961.

22. Chushkin, P. I. Blunt bodies of simple shape in a hypersonic gas flow. Prikladnaya matematika i mekhanika, v. 24, no. 5, 1960, 927-930.

23. Belotserkovskiy, O. M. Flow computation of axisymmetric bodies with a detached shock wave, using a digital computer. Ibid., v. 24, no. 3, 1960, 511-517.

24. Belotserkovskiy, O. M. Flow computation of a circular cylinder with the detached shock wave. IN: AN SSSR. Sbornik. Vychislitel'naya matematika, no. 3. Moscow, 1958, 149-185.

25. Belotserkovskiy, O. M. Flow past a symmetric profile with a detached shock wave. Prikladnaya matematika i mekhanika, v. 22, no. 2, 1958, 206-219.

26. Belotserkovskiy, O. M. Flow around a circular cylinder with a detached shock wave. AN SSSR. Doklady, v. 113, no. 3, 1957, 509-512.

27. Chushkin, P. I. Calculation of some sonic gas flows. Prikladnaya matematika i mekhanika, v. 21, no. 3, 1957, 353-360.

28. Dorodnitsyn, A. A. A method for numerical solution of some nonlinear aerohydrodynamic problems. IN: Akademiya nauk SSSR. Trudy tretoy vsesoyuznoy matematicheskoy konferentsii. T. 3, Moskva, 1956 (Proceedings of the Third All-Union Mathematical Conference. V. 3, Moscow, 1956). Moscow, 1959. 447-453.

ELECTRICAL EXPLOSION IN VACUUM (COMPREHENSIVE STUDY)

In cooperation with colleagues at the Institute of Semiconductor Physics (Siberian Branch, USSR Academy of Sciences) in Novosibirsk, V. I. Petrosyan and E. I. Dagman have been studying the electrical explosion of metallic and semiconductor materials in vacuo since 1964. In an effort to develop an efficient method for producing uniformly deposited thin films, they have been carrying out extensive experimental and theoretical research on this subject. The three recent papers reviewed below represent the results of their research on the efficiency of vaporization by electrical explosion of metals and semiconductors in ambient pressures on the order of 10^{-5} torr. In /1/, droplet formation from explosion of Ag, InSb and Ge specimens in vacuo is investigated experimentally as a function of energy injection rate. In /2/, the vaporization efficiency of an electrical explosion is studied theoretically, while in /3/ the apparatus and experimental technique are described.

Experiment

Experiments were performed over a wide range of stored energies up to about 100 kj, and at discharge times from 4 to 140 μsec. Explosion efficiency was judged by the relative content of droplets in a 40x100 mm^2 film, deposited on a glass plate 10 cm away from the exploded specimen. For this purpose a series of microphotographs spaced at 2 to 4 mm intervals were made with a 90X MII-7 microscope, with the droplets in each frame being counted. Thickness distribution of the film was determined photometrically; its mass and total droplet weight were calculated, and relative droplet content in the film was determined. Detailed test data are tabulated, presenting the following as functions of charge voltage, stored energy, discharge time, and specimen length and cross section:

total surface density of droplets

maximum film thickness

percent weight of droplets

relative droplet content by size

The data indicate that an increase in discharge power, achieved only by shortening the discharge time, may reduce droplet formation. This reduction is significant for Ag, less for InSb and least for Ge.

Additional experiments were conducted using the modified method of "characteristic patterns" attributed to Conn (W. M. Conn, "Conference on Extremely High Temperatures," John Wiley and Sons, New York, 1950). The exploding specimen was supported by two glass plates, which also served as symmetrical precipitation plates and provided a permanent record of explosive effects. The "characteristic patterns" obtained show that during a "slow" discharge on the order of 50 μsec, a wide shunting plasma column is generated, leaving barely enough energy to attain vaporization temperature. It is concluded that to achieve efficient vaporization while avoiding droplet formation in the deposited film, the explosion interval should be 1 μsec or less /1/.

Experimental Apparatus

The basic components of the experimental apparatus are a vacuum chamber, an explosion chamber and a current-pulse generator consisting of a capacitor, transmission line, spark-gap trigger, power supply, and charging and firing controls. The two possible modes have the following characteristics:

	1	2
Stored energy, kj	100	10
Charging voltage, kv	5-7	50
Discharge time, μsec	40-140	4-10
Capacitor type	1M5-150	1M50-2.5
Capacitor inductance, μh	---	2×10^{-2}

The adjustable spark gap is shown in Fig. 1. Its inductance is 0.08 μh,

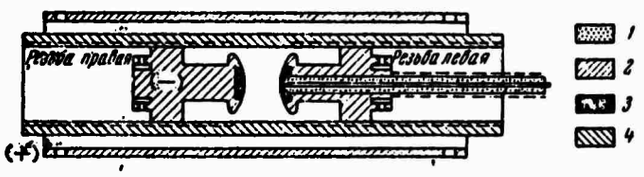

Fig. 1 Spark gap trigger
1- type RK cable; 2- duralumin tube; 3- stainless steel; 4- vinyl tube

and the discharge time is 20 nsec. Fig. 2 shows the explosion chamber, whose advantages include: 1) axial symmetry, required for electrodynamic stability of specimen and discharge; 2) convenient mounting, good electrical contact and mechanical security of fragile specimens; 3) adjustability of one electrode, assuring good contact for high currents by means of a bellows; 4) adaptability to a variety of specimen dimensions. A specimen is butted up against the electrodes, and

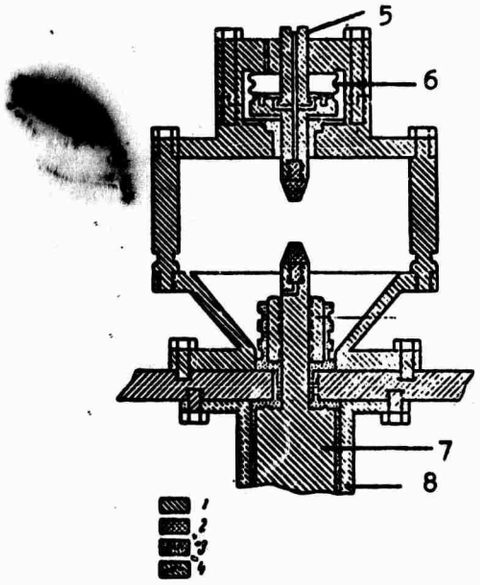

Fig. 2. Explosion chamber 1- stainless steel; 2- Mo or W; 3- Teflon; 4- brass; 5- adjusting screw; 6- bellows; 7- high voltage electrode; 8- shunt

supported from the sides by glass plates (Fig. 3) when "characteristic patterns" are to be recorded. Provision is also made for electrical preheat of semiconductor specimens at 350v, to reach a desired conductivity before the explosion is triggered.

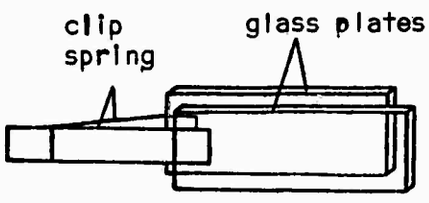

Fig. 3. Specimen holder

Theory

In the theoretical phase of the research /2/, the authors analyze explosion efficiency, defined as the ratio of evaporated mass to initial mass of the specimen, as a function of its parameters and physical characteristics. An analytic model given for the explosion is as follows. The expansion velocity of the discharge channel in vacuo is approximately 10^5 cm/sec, and within the order of microseconds a shunting arc develops on the surface of the evaporated layer. Thus the discharge currents splits into two components I_l and I_v, passing through the liquified specimen and through the vapor respectively. A differential equation is then obtained which takes into account the resistances of both branches and the energy distribution. This equation, together with the equations for thermal balance of the plasma and the balance of gas-kinetic and magnetic pressures, forms a system which is adequate for determining the power required for vaporization, depending on specimen parameters (l, r_0) and characteristics of the exploding material (λ, σ_l, m, ρ). Here l and r_0 are the length and initial radius of the specimen; λ is the heat of vaporization; ρ is density of the liquified specimen material; σ_l is its conductivity near the boiling point, and m is the atomic mass of the test material.

Since the system can be solved only by numerical methods, the following approximate solution was obtained after some simplifying assumptions, for the differential evaporation time of a specimen, Δt:

$$\Delta t \cong \frac{2\rho\lambda(r_0^2 - r_l^2)}{\sigma_l \left[\frac{r_0^2}{l^2} V_0^2 + \alpha \frac{r_l^2 \delta \sqrt{\delta (r_0^2 - r_l^2)\rho}}{(\delta^2 - r_l^2)^2 \sqrt{m}}\right]}$$

where $\alpha = 10^8$. It can be seen that evaporation time decreases with a decrease in the dimensions of the region occupied by the plasma (δ). Since $\delta \cong r_0 + \bar{v}\Delta t$ for a given applied power, it can be kept small by reducing the energy injection time. It also follows that explosion efficiency is higher for materials with lower heat of evaporation and higher conductivity. For specimens with less favorable characteristics, the explosion efficiency can be improved and the energy injection time reduced by increasing the field intensity V_0/l. Experimental and theoretical results of efficiency characteristics for the three materials tested are given in Fig. 4.

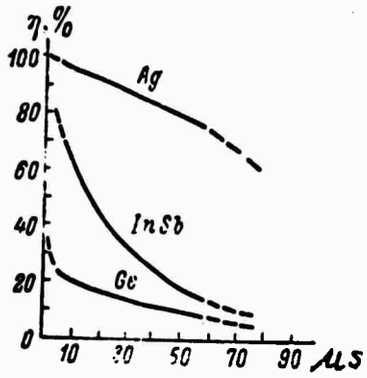

Fig. 4 Efficiency vs. injection time

REFERENCES

1. Petrosyan, V. I.; E. I. Dagman; D. S. Aleksenko; and P. A. Skripkina. Some specific features of electrical explosion of metal and semiconductor specimens in vacuo. Zhurnal tekhnicheskoy fiziki, v. 39, no. 11, 1969, 2076-2083.

2. Petrosyan, V. I.; and E. I. Dagman. Theory of electrical explosion in vacuo. II. Ibid., v. 39, no. 11, 1969, 2084-2091.

3. Petrosyan, V. I.; E. I. Dagman; and V. N. Surganov. Experimental apparatus for the study of electrical explosions. Pribory i tekhnika eksperimenta, no. 5, 1968, 152-156.